Doctoral Thesis

Modeling Flood-Induced Human Displacement Risk Under Global Change

Cumulative Dissertation
for the degree of
doctor rerum naturalium
(Dr. rer. nat.)
in the research discipline Natural Hazards

submitted to the Faculty of Science
at the University of Potsdam

prepared at the Potsdam Institute for Climate Impact Research (PIK)

by

Benedikt Mester

Defended on September 5th, 2023

First Supervisor: Prof. Dr. Anders Levermann
Second Supervisor: Prof. Dr. Oliver Korup

First Reviewer: Prof. Dr. Anders Levermann
Second Reviewer: Prof. Dr. Dieter Gerten
Independent Reviewer: Prof. Dr. JCJH Aerts

Examination board members:
Prof. Dr. JCJH Aerts
Prof. Dr. Dieter Gerten
Prof. Dr. Oliver Korup
Prof. Dr. Anders Levermann
Prof. Dr. Bruno Merz
Prof. Dr. Annegret Thieken

Published online on the
Publication Server of the University of Potsdam:
https://doi.org/10.25932/publishup-60929
https://nbn-resolving.org/urn:nbn:de:kobv:517-opus4-609293

Declaration of originality

I, Benedikt Mester, hereby declare that, to the best of my knowledge, this work does not bear resemblance to any other work in whole or in part and has been completed by myself. I did not use any other sources and means than specified. Furthermore, this work has not been previously submitted to any university. All sources have been referred to and this work gives adequate credit to others for their work. I, in no way, claim to have created this information myself.

Location and Date	Benedikt Mester

The greatest teacher, failure is.

- Yoda, The Last Yedi

Acknowledgements

Many people have supported me on my way to this PhD. The road has been bumpy at times; tough reviews, pandemic work settings, or never-ending code debugging, just to name a few. Still, I am grateful for every experience I have had, the good and the bad, with the former outnumbering the latter. I have had the opportunity to work on societally and environmentally relevant projects and connect with inspiring people who have motivated me to follow my path. Although numerous people have accompanied me over the years, I would like to highlight in the following the ones who have supported me the most.

First and foremost, I am very grateful to my mentor and daily supervisor Dr. Jacob Schewe for his excellent guidance during my PhD. With his deep technical and methodological understanding, it was always a pleasure to collaborate, discuss and work out new projects with him. Jacob helped me stay focused and on track in times of uncertainty; likewise, he provided me with a safe and encouraging work environment in which I could unleash my creativity and enthusiasm. His guidance has supported my work in many ways; I could not have asked for a better mentor for my PhD.

Next, I would like to thank Dr. Katja Frieler, who has been an outstanding leader of Research Department 3 at PIK. Her leadership of ISIMIP has produced unprecedented research output from which I have also benefited. Katja's comments and ideas have always been appreciated and helped steer our manuscripts in the right direction.

I would also like to thank my two main supervisors, Prof. Anders Levermann and Prof. Oliver Korup, for their guidance and contribution to my research, and for giving me the opportunity to pursue a PhD at PIK and the University of Potsdam. Their achievements inspired me, and I could always count on their support in pursuing my PhD.

Without my great colleagues at PIK, my PhD would have been much more difficult and only half as much fun. My special thanks go to Jan Volkholz and Sven Willner, the two "wranglers" of CaMa-Flood, and Thomas Vogt, who provided me with tons of simulation results that served as input for my daily work and publications. I really enjoyed working with the senior scientists Christian Otto, Matthias Mengel and Stefanie Heinicke, who helped me a lot with their experience. It was always very comforting to talk with Inga Sauer, share frustrations and develop new projects. My warmest thanks go to Karim Zantout for proofreading this thesis. I would also like to thank the members of my Future Lab, namely Barbora Šedová, Sidney Michelini, Lucas Kluge, Lisa Binder, Sarah Lohr, and also former members Rania Zaatour, Albano Rikani, and Theresa Falkendal, for their input, feedback, and in-depth discussions, but also for all the fun activities.

A special thanks also goes to Prof. Dai Yamazaki, the developer of CaMa-Flood. I had the privilege to spend a short-term research visit at his lab in Japan, which was one of the most interesting experiences in my life.

I am grateful to the European Union's Horizon 2020 project RECEIPT for funding and research support, and its members for fruitful and transnational collaboration despite restricted traveling times.

My thanks include all the other people I have not mentioned here, including the administrative staff, the caretakers, and the cleaning service at PIK.

Furthermore, I would like to thank my family and non-academia friends for their support over the years.

Finally, my deepest thanks go to my partner, friend, and love of my life Laura. You have backed me up countless times and believed in me at all times. On top of this, during the very last part of this thesis, we were blessed to welcome our newborn Taro.

Summary

Extreme flooding displaces an average of 12 million people every year. Marginalized populations in low-income countries are in particular at high risk, but also industrialized countries are susceptible to displacement and its inherent societal impacts. The risk of being displaced results from a complex interaction of flood hazard, population exposed in the floodplains, and socio-economic vulnerability. Ongoing global warming changes the intensity, frequency, and duration of flood hazards, undermining existing protection measures. Meanwhile, settlements in attractive yet hazardous flood-prone areas have led to a higher degree of population exposure. Finally, the vulnerability to displacement is altered by demographic and social change, shifting economic power, urbanization, and technological development. These risk components have been investigated intensively in the context of loss of life and economic damage, however, only little is known about the risk of displacement under global change.

This thesis aims to improve our understanding of flood-induced displacement risk under global climate change and socio-economic change. This objective is tackled by addressing the following three research questions. First, by focusing on the choice of input data, how well can a global flood modeling chain reproduce flood hazards of historic events that lead to displacement? Second, what are the socio-economic characteristics that shape the vulnerability to displacement? Finally, to what degree has climate change potentially contributed to recent flood-induced displacement events?

To answer the first question, a global flood modeling chain is evaluated by comparing simulated flood extent with satellite-derived inundation information for eight major flood events. A focus is set on the sensitivity to different combinations of the underlying climate reanalysis datasets and global hydrological models which serve as an input for the global hydraulic model. An evaluation scheme of performance scores shows that simulated flood extent is mostly overestimated without the consideration of flood protection and only for a few events dependent on the choice of global hydrological models. Results are more sensitive to the underlying climate forcing, with two datasets differing substantially from a third one. In contrast, the incorporation of flood protection standards results in an underestimation of flood extent, pointing to potential deficiencies in the protection level estimates or the flood frequency distribution within the modeling chain.

Following the analysis of a physical flood hazard model, the socio-economic drivers of vulnerability to displacement are investigated in the next step. For this purpose, a satellite-based, global collection of flood footprints is linked with two disaster inventories to match societal impacts with the corresponding flood hazard. For each event the number of affected population, assets, and critical infrastructure, as well as socio-economic indicators are

computed. The resulting datasets are made publicly available and contain 335 displacement events and 695 mortality/damage events. Based on this new data product, event-specific displacement vulnerabilities are determined and multiple (national) dependencies with the socio-economic predictors are derived. The results suggest that economic prosperity only partially shapes vulnerability to displacement; urbanization, infant mortality rate, the share of elderly, population density and critical infrastructure exhibit a stronger functional relationship, suggesting that higher levels of development are generally associated with lower vulnerability.

Besides examining the contextual drivers of vulnerability, the role of climate change in the context of human displacement is also being explored. An impact attribution approach is applied on the example of Cyclone Idai and associated extreme coastal flooding in Mozambique. A combination of coastal flood modeling and satellite imagery is used to construct factual and counterfactual flood events. This storyline-type attribution method allows investigating the isolated or combined effects of sea level rise and the intensification of cyclone wind speeds on coastal flooding. The results suggest that displacement risk has increased by 3.1 to 3.5% due to the total effects of climate change on coastal flooding, with the effects of increasing wind speed being the dominant factor.

In conclusion, this thesis highlights the potentials and challenges of modeling flood-induced displacement risk. While this work explores the sensitivity of global flood modeling to the choice of input data, new questions arise on how to effectively improve the reproduction of flood return periods and the representation of protection levels. It is also demonstrated that disentangling displacement vulnerabilities is feasible, with the results providing useful information for risk assessments, effective humanitarian aid, and disaster relief. The impact attribution study is a first step in assessing the effects of global warming on displacement risk, leading to new research challenges, e.g., coupling fluvial and coastal flood models or the attribution of other hazard types and displacement events. This thesis is one of the first to address flood-induced displacement risk from a global perspective. The findings motivate for further development of the global flood modeling chain to improve our understanding of displacement vulnerability and the effects of global warming.

Kurzfassung

Durch extreme Überschwemmungen werden jedes Jahr durchschnittlich 12 Millionen Menschen vertrieben. Vor allem marginalisierte Bevölkerungsgruppen in Ländern mit niedrigem Einkommen sind stark gefährdet, aber auch Industrieländer sind anfällig für Vertreibungen und die damit verbundenen gesellschaftlichen Auswirkungen. Das Risiko der Vertreibung ergibt sich aus einer komplexen Wechselwirkung zwischen der Hochwassergefahr, der Exposition der in den Überschwemmungsgebieten lebenden Bevölkerung und der sozioökonomischen Vulnerabilität. Die fortschreitende globale Erderwärmung verändert die Intensität, Häufigkeit und Dauer von Hochwassergefahren und untergräbt die bestehenden Schutzmaßnahmen. Gleichzeitig hat die Besiedlung attraktiver, aber gefährdeter Überschwemmungsgebiete zu einem höheren Maß an Exposition der Bevölkerung geführt. Schließlich wird die Vulnerabilität für Vertreibungen durch den demografischen und sozialen Wandel, die Verlagerung der Wirtschaftskräfte, die Urbanisierung und die technologische Entwicklung verändert. Diese Risikokomponenten wurden im Zusammenhang mit dem Verlust von Menschenleben und wirtschaftlichen Schäden intensiv untersucht, über das Risiko der Vertreibung im Rahmen des globalen Wandels ist jedoch nur wenig bekannt.

Diese Arbeit zielt darauf ab, unser Verständnis des durch Überschwemmungen verursachten Vertreibungsrisikos unter dem Einfluss des globalen Klimawandels und des sozioökonomischen Wandels zu verbessern. Dieses Ziel wird durch die Beantwortung der folgenden drei Forschungsfragen erreicht. Erstens: Wie gut kann eine globale Hochwassermodellierungskette die Hochwassergefahren historischer Ereignisse, die zu Vertreibung geführt haben, reproduzieren, wobei ein Fokus auf die Wahl der Eingangsdaten gelegt wird? Zweitens: Welches sind die sozioökonomischen Merkmale, die die Vulnerabilität für Vertreibung beeinflussen? Und schließlich, inwieweit hat der Klimawandel möglicherweise zu den jüngsten hochwasserbedingten Vertreibungsereignissen beigetragen?

Zur Beantwortung der ersten Frage wird eine globale Hochwassermodellierungskette durch den Vergleich der simulierten Überschwemmungsfläche mit satellitengestützten Überschwemmungsdaten für acht große Hochwasserereignisse überprüft. Der Schwerpunkt liegt dabei auf der Sensitivität gegenüber verschiedenen Kombinationen der zugrunde liegenden Klimareanalysedatensätzen und globalen hydrologischen Modellen, die als Input für das globale Hydraulikmodell dienen. Ein Bewertungsschema von Leistungsindikatoren zeigt, dass die simulierte Überschwemmungsfläche ohne Berücksichtigung des Hochwasserschutzes meist überschätzt wird und nur bei wenigen Ereignissen von der Wahl der globalen hydrologischen Modelle abhängt. Die Ergebnisse sind empfindlicher gegenüber dem zugrunde liegenden Climate Forcing, wobei sich zwei Datensätze erheblich von einem

dritten unterscheiden. Im Gegensatz dazu führt die Einbeziehung von Hochwasserschutznormen zu einer Unterschätzung der Überschwemmungsfläche, was auf mögliche Mängel bei der Schätzung des Schutzniveaus oder der Hochwasserhäufigkeitsverteilung innerhalb der Modellierungskette hinweist.

Nach der Analyse des physikalischen Hochwassergefahrenmodells werden in einem nächsten Schritt die sozioökonomischen Triebkräfte für die Vulnerabilität für Vertreibungen untersucht. Zu diesem Zweck wird eine satellitengestützte, globale Sammlung von Hochwasseüberschwemmungsflächen mit zwei Katastrophendatenbänken verknüpft, um die gesellschaftlichen Auswirkungen mit der entsprechenden Hochwassergefahr zusammenzuführen. Für jedes Ereignis werden die Anzahl der betroffenen Menschen, Vermögenswerte und kritischen Infrastrukturen sowie sozioökonomische Indikatoren berechnet. Die daraus resultierenden Datensätze werden öffentlich zugänglich gemacht und enthalten 335 Vertreibungsereignisse und 695 Todesopfer-/Schadensereignisse. Auf der Grundlage dieses neuen Datenprodukts werden ereignisspezifische Vertreibungsvulnerabilitäten bestimmt und vielfältige (nationale) Abhängigkeiten mit den sozioökonomischen Prädiktoren abgeleitet. Die Ergebnisse deuten darauf hin, dass wirtschaftlicher Wohlstand nur teilweise die Anfälligkeit für Vertreibungen beeinflusst; Urbanisierung, Kindersterblichkeitsrate, der Anteil älterer Menschen, Bevölkerungsdichte und kritische Infrastrukturen weisen eine stärkere funktionale Beziehung auf, was den Schluss zulässt, dass ein höheres Entwicklungsniveau im Allgemeinen mit einer geringeren Vulnerabilität verbunden ist.

Neben der Untersuchung der kontextabhängigen Faktoren der Vulnerabilität wird auch die Rolle des Klimawandels im Zusammenhang mit der Vertreibung von Menschen untersucht. Am Beispiel des Zyklons Idai und den damit verbundenen extremen Küstenüberschwemmungen in Mosambik wird ein Ansatz zur Attribution der Auswirkungen angewandt. Eine Kombination aus Küstenüberflutungsmodellierung und Satellitenbildern wird verwendet, um faktische und kontrafaktische Überschwemmungsereignisse zu konstruieren. Diese Storyline-artige Attributionsmethode ermöglicht die Untersuchung der isolierten oder kombinierten Auswirkungen des Meeresspiegelanstiegs und der Intensivierung der Windgeschwindigkeiten von Zyklonen auf die Küstenüberflutung. Die Ergebnisse deuten darauf hin, dass das Vertreibungsrisiko durch die Gesamtwirkung des Klimawandels auf Küstenüberschwemmungen um 3,1 bis 3,5 % gestiegen ist, wobei die Auswirkungen der zunehmenden Windgeschwindigkeit der dominierende Faktor sind.

Zusammenfassend zeigt diese Arbeit die Potentiale und Herausforderungen der Modellierung von hochwasserbedingten Vertreibungsrisiken auf. Während diese Arbeit die Sensitivität der globalen Hochwassermodellierung in Bezug auf die Wahl der Eingabedaten

untersucht, ergeben sich neue Fragen, wie die Reproduktion von Wiederkehrintervallen und die Darstellung von Schutzniveaus effektiv verbessert werden kann. Die Ergebnisse liefern nützliche Informationen für Risikobewertungen, effektive humanitäre Hilfe und Katastrophenhilfe. Die Studie zur Auswirkungs-Attribution ist ein erster Schritt zur Bewertung der Effekte der globalen Erwärmung auf das Vertreibungsrisiko und führt zu neuen Forschungsherausforderungen, z. B. zur Kopplung von Fluss- und Küstenhochwassermodellen oder zur Untersuchung anderer Gefahrenarten. Diese Arbeit ist eine der ersten, die das durch Überschwemmungen verursachte Vertreibungsrisiko aus einer globalen Perspektive heraus betrachtet. Die Ergebnisse motivieren dazu, die globale Hochwassermodellierungskette weiterzuentwickeln, um unser Verständnis der Vertreibungsvulnerabilität und der Auswirkungen der globalen Erderwärmung zu vertiefen.

Contents

List of Figures

List of Tables

Abbreviations

ARI	Average recurrence interval
CC	Clausius-Clapeyron
DEM	Digital elevation model
DFO	Dartmouth Flood Observatory
FRQ	Future Research Question
GFD	Global Flood Database
GFM	Global flood model
GHM	Global hydrological model
GIDD	Global Internal Displacement Database
GTSM	Global Tide and Surge Model
IDF	Intensity-damage function
IDMC	Internal Displacement Monitoring Centre
IDP	Internally displaced person
IPCC	Intergovernmental Panel on Climate Change
JRC	Joint Research Centre
MERIT	Multi-Error-Removed Improved-Terrain
IOM	Organization for Migration
RICorDE	Rolling HAND Inundation Corrected Depth Estimator
RQ	Research Question
SLR	Sea level rise
SSP	Socioeconomic pathway
SST	Sea surface temperature
TC	Tropical cyclone
UFP	UNOSAT Flood Portal
UN	United Nations
UNOSAT	United Nations Operational Satellite Applications Programme

Chapter 1 Introduction

1.1 Motivation

Over the past millennia, the examples of climate change destabilizing civilizations by causing food shortages, housing destruction, infectious diseases, and civil unrest are numerous (McMichael, 2012). Human mobility, serving as a response to climate stresses and shocks, is considered as an important adaptive strategy within human evolution. (Groth et al., 2020; Warner et al., 2010). Recent human-made climate change, however, is heating up the planet at an unprecedented pace, leading to drastic changes in magnitude, frequency, and timing of weather and climate extremes (Seneviratne et al., 2021, 2012). This process is changing human mobility patterns from more proactive and voluntary flows to forced disaster displacement (Sedova and Kalkuhl, 2020; Thalheimer et al., 2021b). In the early 1990s, the Intergovernmental Panel on Climate Change (IPCC) already warned about the potential impacts of global warming on human settlement and stated that “[t]he gravest effects of climate change may be those on human migration as millions are displaced by shoreline erosion, coastal flooding and severe drought” (IPCC, 1992). 30 years later, the IPCC WGII report states with “high confidence” that climate and weather extremes are increasingly driving displacement in all regions over the world (Cissé et al., 2022). And United Nations secretary-general António Guterres states that “[t]he plight of internally displaced persons is more than a humanitarian issue. It takes an integrated approach – combining development, peacebuilding, human rights, climate action and disaster risk reduction efforts" (UN, 2022).

By today, an average of 21.8 million people are internally displaced by weather and climate extremes every year, more than two and half times the number of conflict-related displacements (Figure 1.1) (IDMC, 2022). Flooding accounts for 54 % of weather-related displacements, making it one of the most dangerous hazards along with tropical cyclones (TCs) and storms (IDMC, 2022). Climate change is affecting fluvial flooding (Berghuijs et al., 2017; Blöschl et al., 2019, 2017), coastal flooding due to TCs (Knutson et al., 2019; Woodruff et al., 2013), and urban (flash) flooding (Fowler et al., 2021; Ye et al., 2017) in various ways, making it of primary concern for displacement risk. Flood risk projected to change within the next decades, with many regions experiencing distinctive increases in societal impacts (Alfieri et al., 2017; Bates et al., 2021; Hirabayashi et al., 2013; Lin et al., 2012; Willner et al., 2018b; Winsemius et al., 2016). Future projections by the World Bank Groundswell Part 2 report postulate an estimate of 216 million internal migrants by 2050 (including non-flood hazards), with “climate migration hotspots” already emerging by 2030 (Clement et al., 2021). Thus, a strong increase in regional flood protection is required to maintain current high-end flood risk for the period 2035 to 2044 and beyond (Willner et al., 2018a; Winsemius et al., 2016). Otherwise, by the end of the 21st century, relative global fluvial flood displacement risk is estimated to increase by 50% (150%) for a strong (weak) climate change mitigation scenario,

assuming current flood protection levels and fixed population size as of 2000 (Kam et al., 2021).

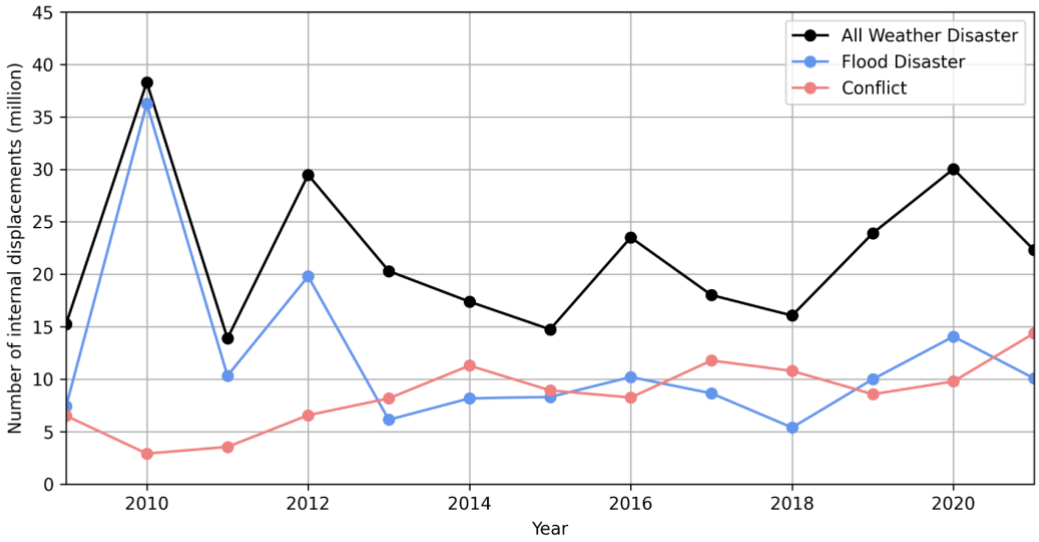

Figure 1.1: Number of internal displacements per year due to all weather-related disasters (black), floods (blue), and conflict (red) (IDMC, 2022).

In the light of these numbers, the broader issue of climate mobility is attracting widespread interest from the public, policymakers, practitioners, and academia (Hoffmann et al., 2020). However, the connection between climate change, extreme events, and associated mobility is often oversimplified, leading to artificially inflated displacement numbers (Gemenne, 2011). The public and scientific discussion is also hampered by an usage of misleading terminologies, such as “climate refugee” or “climate-induced mass migration” (Ayeb-Karlsson et al., 2022). As a consequence, alarmist tones further fuel the debate by framing climate-related mobility as a security threat (Hartmann, 2010). This calls for standardized and transparent methodologies of estimates and predictions of people displaced by environmental changes (Gemenne, 2011). The usage of more appropriate terminologies, e.g., environmental migration or disaster-induced displacement, which depict different motives and destinations of migration, is another important aspect (Dun and Gemenne, 2008). In fact, the correct and distinctive labeling is difficult, as often multiple drivers lead to a migration process (Boas et al., 2019). Conflict, economic opportunities, socio-political crises, and other contextual characteristics may both enhance or suppress migratory responses, making it difficult to single out climate extremes as the primary reason for human mobility (Hoffmann et al., 2020; Schutte et al., 2021; Thalheimer et al., 2021a).

Yet, it would be crucial to understand how climate change may have already contributed to recent displacement events, especially those of high-intensity or even unprecedented magnitude. In recent years, probabilistic attribution methodologies have been developed to assess the impact of global warming in terms of attributable risk (Philip et al., 2020), e.g., for

heavy precipitation (Luu et al., 2021; Oldenborgh et al., 2017). However, these approaches lack a full applicability on extreme events involving complex dynamical processes of the climate system (Shepherd, 2016), e.g., coastal flooding driven by severe TCs. In addition, it is also difficult to depict how the effects of global warming on the physical characteristics of extreme events might translate to changes in the societal impacts (Trenberth et al., 2015), such as human displacement. Access to such information would be particularly important for risk awareness, adaptation financing, or even litigation (Marjanac and Patton, 2018; Shepherd, 2016; Stuart-Smith et al., 2021; Trenberth et al., 2015).

Besides shifts in population size and changing flood hazards due to global warming, displacement risk is also influenced by changes in vulnerability (Cardona et al., 2012; Oppenheimer et al., 2014). In the context of flooding, mortality and the vulnerability of economic assets have been decreasing for most income groups over the past decades (Formetta and Feyen, 2019; Jongman et al., 2015). However, also increases in vulnerability can be found for some world regions and countries (Sauer et al., 2021; Tanoue et al., 2016), which could be explained by socio-physical dynamics, e.g., the “levee effect” (Di Baldassarre et al., 2015). Very few studies examine vulnerability to displacement at the global level to explore its universally applicable mechanisms (Kakinuma et al., 2020); implying that there is a clear lack of scientific evidence for international decision makers on how socio-economic factors shape the susceptibility of being displaced. A solid understanding of vulnerability, however, is necessary to model estimates and projections of displacement risk under current or future climate change, respectively.

Facing these challenging tasks, global flood models (GFMs) are a powerful tool in reproducing historic flood-induced displacement events, investigating the role of climate change or simulating future risk under different socio-economic pathways (Hirabayashi et al., 2013; Kakinuma et al., 2020; Kam et al., 2021). Most global-scale river flood models consist of a cascade of climate-hydrology-hydraulic models and simulate continental-scale rivers (Yamazaki et al., 2011). Coastal flooding due to TCs can be simulated by storm surge models which are based on storm tracks, pressure fields, and sea level information (Mandli and Dawson, 2014). Global models help to understand the mechanisms of flood risk from a broader perspective, as they are not limited to single basins but can be employed to simulate flood hazards and associated societal risk in virtually any place on earth (Ward et al., 2015). Even though these models have been employed for less than two decades, astonishing advancements have been achieved, especially considering the enormous challenges of global-scale data assimilation (Bates et al., 2021, 2018; Yamazaki et al., 2014). Yet, high uncertainties remain in the modeling framework, e.g., the input models, protection standards, or the flood frequency analysis (Ward et al., 2013; Zhou et al., 2021). Alternatively, new satellite-based flood products with global coverage offer unexplored opportunities in modeling flood risk (Tellman et al., 2021) and hence also investigating the mechanisms of displacement. A major challenge that all flood hazard reproduction methods face is the correct representation of the physical flood characteristics, such as extent or depth (Hoch and Trigg, 2019). Another

key point is the incorporation of displacement vulnerability within the societal impact assessment, e.g., in terms of intensity-impact functions as it exists in the form of depth-damage functions for economic loss analyses (Ward et al., 2020). Mostly, simplistic approaches, such as binary step-functions regarding the flood depth (Kam et al., 2021), are assumed, leading to high uncertainties regarding the share of displacements among the exposed population.

In conclusion, flood-induced human displacement is a pressing topic of our time and will increase in severity under future global change. Flood events are affected by climate change in various ways and the population exposed is experiencing socio-economic changes which alter its vulnerability of being displaced. Yet, it is unknown how these processes shape the risk of flood-induced displacement. From this lack of knowledge regarding the underlying mechanisms of displacement, the following **Overarching Research Question** of this thesis emerges:

What is the effect of global climate change and socio-economic change on flood-induced human displacement risk?

Modeling displacement risk is a promising option to answer this question and fill the numerous knowledge gaps, however, a set of challenges is identified. First, existing flood model setups need to be evaluated and new flood data products, e.g., derived from remote sensing, pose promising extensions or even alternatives which need to be incorporated. The assessment and explanation of vulnerability as well as its representation within the modeling chain is of crucial importance. Lastly, climate change is one of the main drivers of future risk, calling for attribution studies on how global warming affects flooding and associated displacement. Advancements on these topics would help to improve our understanding of the mechanisms of human mobility in the context of extreme flooding and assess global displacement risk under future global change.

1.2 Background

The lack of knowledge around the effects of climate change and socio-economic change on flood-induced displacement risk is identified as the main motivation of this thesis. This section provides background information on the topic, methods and datasets used. It also serves as an contextualization of the research work, introducing the topics within a broader scope than laid out within the manuscripts in the subsequent main chapters. The first section gives an insight in the terminology, data sources and associated uncertainties related to flood-induced displacement. This is followed by an overview on the concept of vulnerability, in which the multiple contextual drivers are introduced and findings are presented that go beyond studies

on flooding or displacement. Lastly, it is highlighted how climate change affects flooding in various ways and presents techniques to attribute these changes.

1.2.1 Flood-induced displacement

International organizations and authorities have placed the issue of climate-related human mobility at the core of several legal frameworks, policy initiatives and governance structures, such as the Cancun Adaptation Framework, the Task Force on Displacement, the Global Compact for Migration, or the Sendai Framework for Disaster Risk Reduction (International Organization for Migration, 2019; Oakes et al., 2019; United Nations Office for Disaster Risk Reduction, 2015). While these frameworks cover a broad spectrum of people movement, this thesis addresses the topic of flood-induced displacement which is more closely defined in the following, including reporting uncertainties and data availability. This is an important step in the research question conceptualization as the correct terminology and framing are critical in the context of human mobility (Dun and Gemenne, 2008; Heslin et al., 2019; Hoffmann et al., 2021).

Several definitions of human mobility in the context of climate and environmental change exist. The International Organization for Migration (IOM) distinguishes migration according to the destination (international or internal); the United Nations (UN) additionally categorizes according to the motivation (voluntary or forced) (Heslin et al., 2019). Alternative representations of this binary motivation perspective exist, such as a continuum view from totally voluntary migration to totally forced migration (Hugo, 1996). Yet, a clear classification within this motivation spectrum is difficult due to a complex system of interacting push and pull factors (Obokata et al., 2014; Renaud et al., 2007; Warner et al., 2010).

The form of migration movements can be categorized into adaptive migration, planned relocation, involuntary migration, also described as displacement, and immobility (Cissé et al., 2022; Oakes et al., 2019). Displacement is a widely interpreted term for which no clear unified definition exists; it includes pre-emptive evacuation, temporary displacement or permanent displacement, with potential resettlement in new territory (Gemenne, 2011). Extreme events often result in internally displaced persons (IDPs) (Black et al., 2013). Displacement is a global phenomenon with absolute displacement numbers being particularly high in Asia and sub-Saharan Africa, while relative numbers are largest in small island states (Cissé et al., 2022). Disaster-induced internal displacement is in the focus of this thesis and describes individuals and households forced to leave homes or places of habitual residence due to extreme weather and climate events (OCHA, 2004); human movements are limited to national borders, separating this type from refugees or asylum-seekers (UN, 1951). The term “displacement” used throughout this study refers to disaster-induced internal displacement unless otherwise noted. Following the migration definition by the UN, the motivation of an IDP is the fear of serious harm rather than a voluntary movement (Heslin et al., 2019). In the wake of forced displacement, weather extremes may trigger a humanitarian crisis cascade, resulting in loss

of life, business disruption, uncontrolled urban settlements, which in turn can lead to violence and conflict (Gannon et al., 2018; Ghimire et al., 2015; Trisos et al., 2022). The scope of movement is limited by financial resources (Black et al., 2011), which may partially explain why disaster-induced displacement is mostly internal and international mobility often extends only to neighboring countries (Cardona et al., 2012; Cissé et al., 2022).

Displacement can be further distinguished by its cause in sudden-onset and slow-onset (Dun and Gemenne, 2008). Sea level rise (SLR) and droughts are considered as causes for slow-onset displacement, which often overlap with other socio-economic factors that drive the decision of moving away (Desai et al., 2018). Sudden-onset displacement is the result of livelihood disruption, for example, due to storms, river flooding and wildfires (IDMC and ADB, 2022), leading to both short-term and long-term displacement (Cissé et al., 2022). A special example are TCs that generate coastal flooding, pluvial flooding due to heavy rain, and extreme wind speeds, causing displacement either individually or as multi-hazard events (IDMC, 2021). Coastal and inland flooding by TCs are considered as flood-induced displacement in this work, even though displacement in the context of these hazards may also be considered as storm-induced.

Considering the variety of human mobility and the difficulty to track displaced people, e.g., in terms of return flows or repeated displacement, assessing displacement quantitatively is a challenging task (Hoffmann et al., 2021, 2020). The Global Internal Displacement Database (GIDD), maintained by the Internal Displacement Monitoring Centre (IDMC), is considered as one of the most credible displacement inventories on conflict and disaster. The GIDD exhibits a global coverage and lists all types of weather and climate extreme events. The beginning of data recording dates back to 2008; since then the database has increased in information density over the years, such as the tracking of affected administrative units. Only in recent years, information has been recorded also on the status of the IDPs, e.g., the number of IDPs returned after evacuation or permanently displaced in shelter camps. For most entries only one total number of IDPs is stated per event in the GIDD, which covers all types of displacement, ranging from precautious evacuations in relatively controlled circumstances to severe, multiple and/or long-term displacement (Anzellini et al., 2017). This has far-reaching implications for modeling of displacement. For instance, preventive evacuation and only minor housing damage may result in the same registered number of IDPs as due to the complete destruction of housing. Other disaster databases incorporate even coarser approaches, for example, displaying only the “number of homeless” or directly converting the number of affected people to the number of IDPs. As no transparent methodology is provided on how displacement is defined and IDPs are tracked, in contrast to the GIDD, caution should be taken on their usage for displacement analysis. With this introduction to the terminology and uncertainties surrounding displacement, the vulnerability to displacement is discussed next.

1.2.2 Vulnerability of displacement

Following the IPCC, risk is determined not only by the physical properties of flooding (hazard) or the people living in floodplains (exposure), but also by the susceptibility of being displaced (vulnerability) (Cardona et al., 2012; Oppenheimer et al., 2014). Vulnerability, also described as predisposition, fragility, or lack of capacities that foster adverse impacts on exposed elements (Cardona et al., 2012), is a dynamic component of risk that varies across temporal and spatial scales (Cissé et al., 2022). Vulnerability results from a complex set of drivers and interacting conditions that describe the social, cultural, environmental, political and economic context in which the flood hazard occurs (Cissé et al., 2022). Only when a certain level of vulnerability is exceeded, a hazardous flood event can become a disaster for the population exposed (Few et al., 2021). Therefore, effective adaptation and disaster risk management strategies also depend on a profound understanding of the manifold dimensions of vulnerability, as well as a thorough assessment of potential changes of future vulnerability levels (Cardona et al., 2012). Yet, due to its complexity, vulnerability remains poorly understood and is justifiably considered to be the “missing link” in the risk equation (Jongman et al., 2015; Mechler and Bouwer, 2015).

Only few studies cover flood-induced displacement risk and its drivers at the global scale, limiting our understanding of the underlying socio-economic processes and methods to represent vulnerability in the modeling frameworks. Drivers of vulnerability can be broadly categorized into environmental, social and economic dimensions (Cardona et al., 2012), which can be extended with political and demographic dimensions in the context of human migration (Black et al., 2011). These and similar categorization attempts are related to social vulnerability of the population exposed, differing from the concept of vulnerability of physical infrastructure (Flanagan et al., 2011). Focusing only on the latter one, the few existing displacement risk studies mostly apply intensity-damage functions to estimate an expected level of damage to homes and other structures and thus the associated displacement risk (Anzellini et al., 2017; Kam et al., 2021). For example, displacement risk is estimated using a simplified 1 m step function related to flooding depth (Kam et al., 2021). One study on global-scale flood-induced displacement suggests that limited economic resources and adaptive capacity influence vulnerability in some world regions (Kakinuma et al., 2020), however, no distinctive functional relationship exists yet.

Insights on vulnerability to non-flood extremes or non-displacement impacts, e.g., mortality or economic losses, are to be treated with caution within the context of flood-induced displacement. The rate of onset, intensity, duration, spatial extent and damage type varies between climate hazards (Seneviratne et al., 2021); the vulnerability to the inherent adverse effects and its drivers may hence differ between the hazard types. Nonetheless, insights about the causal relationships between different vulnerability and its drivers across different societal impact categories and hazard types serves as a starting point for understanding the highly complex contexts in which disaster-displacement occurs. For example, TC-related

displacements heavily depend on the damage to housing and livelihood assets, however, also other factors, such as responsive capacity of the government or level of poverty play a role (Cissé et al., 2022).

More knowledge exists about the vulnerability associated with flood induced mortality and economic losses, demonstrating regional differences and for most parts a declining trend over time (Formetta and Feyen, 2019; Jongman et al., 2015; Tanoue et al., 2016). Global-scale studies focus mostly on economic variables to explain vulnerability, e.g., GDP per capita or income levels, neglecting the multitude of other drivers that can also substantially influence vulnerability (Oppenheimer et al., 2014). A reduction of vulnerability, however, is often also associated with development indicators fostering adaptive capacity, such as strong institutions or educational quality (Bowen et al., 2012). As for example, TC mortality risk is not only depending on poverty, but also on the level of governance (Peduzzi et al., 2012). Widely agreed drivers of vulnerability to flooding, such as age cohorts, strongly depend on the context and vary not only in magnitude but also in the direction (Rufat et al., 2015). Mortality of various hazards is linked with the national development level and environmental quality, for example, GDP per capita, urban growth, modified percentage of arable land or forest coverage (Peduzzi et al., 2009). These broad measures of development, most of which are available only at the national level, do not, however, explain vulnerability comprehensively enough (Noy, 2016). For instance, Bangladesh exhibits a high degree of poverty, nonetheless, its vulnerability to TC impacts is relatively low due to a set of disaster risk reduction measures (Paul, 2009; Peduzzi et al., 2012). Yet, globally consistent, not to mention spatially explicit, information on early-warning systems, shelters, reforestation and other measures is not available, making it difficult to account for these indicators in global-scale analysis of vulnerability. Global-scale models, methods, and datasets are limited, nonetheless, their usage may provide internationally consistent insights for decision makers, especially for data-scarce regions (Ward et al., 2015). Despite all these difficulties, our understanding of the factors that determine vulnerability to flood-induced displacement needs to be enhanced to target populations that are most at risk of being displaced and to ensure that adequate preventative and disaster risk reduction measures are implemented. Climate change is undermining such actions, its role in various types of flooding and ways to attribute events to global warming are discussed in the next section.

1.2.3 Climate change and the attribution question

It is of primary societal concern to understand if recent flood events can be attributed to climate change (van Oldenborgh et al., 2021). Understanding how the probability or intensity of extreme flooding has already changed is tremendously important for disaster risk reduction, e.g., in the field of adaptation planning (Trenberth et al., 2015). Answering such an attribution question, however, depends on the hazard category and the framing (Shepherd, 2016). For example, it is relevant what type of flood is being studied or whether the goal is to understand

the underlying mechanisms of how global warming affects floods. The following section presents the various impacts of climate change on flooding and explains how these impacts can be attributed to climate change.

Flooding can be categorized into pluvial (flash/urban) flooding, fluvial (freshwater/river) flooding, and coastal flooding (Seneviratne et al., 2012). Each type is affected by climate change differently in terms of frequency, magnitude, duration, and timing (Seneviratne et al., 2012). Fluvial and pluvial flooding are mostly the result of extremes of processes in the hydrological cycle, in particular precipitation, runoff, and streamflow (Kundzewicz et al., 2014; Seneviratne et al., 2021). Increased greenhouse gasses in the atmosphere lead to an intensification of the global hydrological cycle, resulting in changes in annual-mean precipitation and runoff trends (Dai, 2021). This can be partially explained by the Clausius-Clapeyron (CC) relationship stating that the water-holding capacity of the atmosphere increases by 7% per °C of global warming (Seneviratne et al., 2021). This temperature sensitivity is similar for the magnitude of extreme precipitation at a global-scale (Fischer and Knutti, 2016; Guerreiro et al., 2018; Sun et al., 2021), with short-duration rainfall extremes increasing even at twice the rate or more in some regions (Fowler et al., 2021; Ye et al., 2017).

Despite the intensification of extreme precipitation following the CC relationship, high stream discharge is decreasing in many places, e.g., in the United States (Do et al., 2020); possible due to decreases in antecedent soil moisture and snowmelt (Sharma et al., 2018).The issue is more complex, however, as the rarest floods are more likely to increase, while less extreme floods, especially occurring in larger, less-urbanized catchments, tend to decrease (Do et al., 2017; Fowler et al., 2021; Sharma et al., 2018). Signals of climate change regarding changes in timing (Blöschl et al., 2017), frequency, magnitude (Berghuijs et al., 2017), and regional discharges (Blöschl et al., 2019) of flooding can be detected. Still, some studies find a dominance of multidecadal variability, e.g., Atlantic Multidecadal Oscillation, over long-term trends (Hodgkins et al., 2017).

The intensification of coastal flooding due to global warming, on the other hand, is driven by SLR and an increase in (extra-)tropical cyclone and storm wind speeds (Walsh et al., 2019). Global mean SLR is approximately 0.2 m and will further increase (Gulev et al., 2021), with regional SLR varying substantially (Fox-Kemper et al., 2021). Average TC wind speeds and precipitation rates are expected to increase with higher SSTs, again with regional differences among TC basins (Knutson et al., 2020, 2015). Both SLR and intensified wind speeds amplify storm surges and associated coastal flooding, higher rainfall rates pose a more severe risk for both coastal and inland flooding (Knutson et al., 2020).

The rapidly advancing field of event attribution aims to disentangle climate change from natural variability sources, such as the El Niño–Southern Oscillation, and assess its contribution to individual extreme events (Titley et al., 2016). Generally, two event attribution approaches exist: 1) observational data is used to investigate probabilities of occurrence of an event, or 2) the manifestation of an event in a world with climate change is compared to a

counterfactual world without climate change using model simulations, also called the “storyline approach” (Philip et al., 2020; Shepherd, 2016; Titley et al., 2016).

Depending on the hazard category type, our understanding of climate change effects on the extreme event, the choice of attribution approach and consequently the confidence in attributing single events varies. The comprehension on how climate change affects temperature-related extreme events, such as heats and cold spells, is high, as observation series are long and model simulations work well, allowing to draw conclusions from changes in long-term mean conditions on extreme events (Titley et al., 2016). Hydrological event attribution poses a more challenging task as not only thermodynamic aspects of the climate system but also dynamic aspects are involved (Shepherd, 2016). Nonetheless, the CC relationship between temperature and atmospheric moisture content demonstrates a relatively direct connection between human-induced warming and changes in precipitation (Titley et al., 2016).

In contrast, large-scale parameters define the frequency and intensity of TCs; their relationship to climate is more complex and less direct than changes in either temperature or water vapor alone (Titley et al., 2016). TCs are comparatively rare events with no continuous time series (Knutson et al., 2019), making the usage of probabilistic attribution of a single TC event, e.g., via extreme value theory, still very challenging (Titley et al., 2016; Trenberth et al., 2015). Examples of probability-based approaches cover Hurricane Sandy (Lin et al., 2016), Hurricane Harvey (Oldenborgh et al., 2017), or Storm Xaver (Dangendorf et al., 2016). The storyline approach for TCs, on the other hand, provides a direct physical basis for impact attribution (Shepherd, 2016) as coastal flooding starts from a higher baseline water elevation due to anthropogenic-induced SLR. The storyline approach allows one to investigate how different drivers of extreme events are affected by climate change to answer the attribution question deterministically rather than from a probabilistic point of view (Shepherd, 2016). One example is the attribution study on economic damages from Hurricane Sandy exacerbated by SLR due to climate change (Strauss et al., 2021).

1.3 Objectives and structure

Our understanding of global flood-induced displacement risk is limited by several factors, such as the correct reproduction of flood hazard and the representation of vulnerability within the modeling chain. It is unknown what socio-economic factors cause a population that is resilient against the adverse impacts of flooding to become a displacement-prone society. Additionally, the role of climate change on forced mobility is unclear, which poses potentially high risk in the light of rising atmospheric greenhouse gas emissions. This thesis consists of four main chapters (Figure 1.2) that elaborate on these topics by addressing the following three **Research Questions (RQs)**:

RQ 1: How can the modeling of flood events that lead to displacement be improved?

Chapter 2 investigates how well a global-flood modeling chain can reproduce flood hazards of historic events that lead to displacement. Global flood models are a relatively new tool and little is known on to what extent the choice of input data has an effect on the model output. As a consequence, a particular focus is set on determining whether different combinations of climate reanalysis data and global hydrological model are interchangeable or some setups are to be favored.

RQ 2: What are the underlying processes that shape the vulnerability to displacement?

Chapter 3 describes the development of a new dataset that links flood footprints derived from remote sensing with displacement and other societal impacts for hundreds of events. First, a displacement database is geocoded, meaning the allocation of affected sub-national administrative units to every event based on text information. In the next step, the geocoded events are matched in time and space with satellite imagery of 913 floods. For every successful match, the corresponding number of IDPs, affected people and a variety of socio-economic indicators encompassing the events are determined. Based on this new dataset, a displacement vulnerability assessment is presented in Chapter 4. Linear and non-linear regression models are applied to identify vulnerability drivers of high explanatory power. It is investigated to what degree vulnerability is dependent on specific predictors and whether trends are positive or negative.

RQ 3: How can displacement events be attributed to climate change?

Chapter 5 explores a new way of attributing the effects of climate change on TCs and associated displacement risk. A storyline approach is employed to assess how SLR and an increase of extreme wind speed lead to an intensification of coastal flood hazard and the corresponding humanitarian crisis. This method allows investigating how the drivers of coastal flooding are affected differently by global warming and how these changes are translated into changes in the number of estimated displacements.

Chapter 6 comprises a discussion of the main chapters in the light of the **Overarching Research Question** and the three **RQs**. Recommendations for further advancements and an outlook into future challenges are presented in this part as well. Finally, a conclusion that distills the main findings of this thesis is given in Chapter 7.

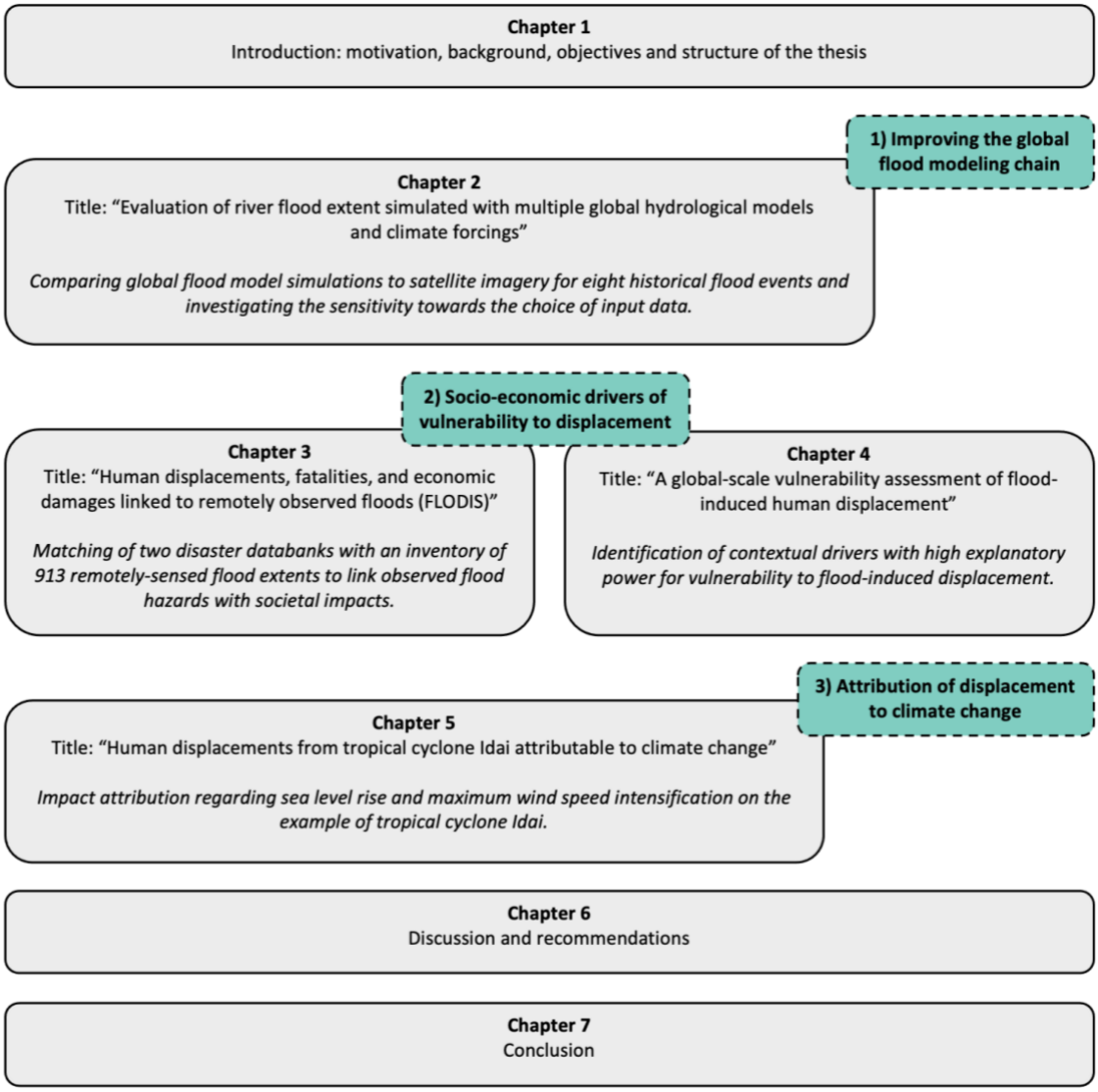

Figure 1.2: Overview of the thesis structure

1.4 Author contributions

The following four chapters contain manuscripts which are intended for publication in international and peer-reviewed journals. The manuscript of Chapter 2 is published; the manuscripts of Chapter 3 and Chapter 5 are currently under review by the time of the submission of this thesis; the manuscript of Chapter 4 is finalized and intended for submission to a peer-reviewed journal. The main text and figures of the original manuscripts have been retained, while layouts have been adjusted to the formatting of this dissertation. The majority of the underlying work was carried out by the author of this dissertation (Benedikt Mester), which is reflected by four first-authorships. Nonetheless, the contribution of all other co-authors

to various parts of the manuscript preparation, including the study design, numerical modeling, results analysis, and writing process, is greatly acknowledged. I wish to express my gratitude especially to my co-authors Dr. Jacob Schewe and Dr. Katja Frieler for their thorough support, intensive guidance and motivating approach to teamwork.

Chapter 2: Mester, B., Willner, S.N., Frieler, K., and Schewe, J., 2021. Evaluation of river flood extent simulated with multiple global hydrological models and climate forcings. *Environmental Research Letters*. https://doi.org/10.1088/1748-9326/ac188d

B.M. and J.S. designed the study, with contributions from K.F. S.N.W. designed and performed global flood model simulations. B.M. and J.S. analyzed the results, and K.F. contributed to the interpretation. B.M., S.N.W., K.F., and J.S. jointly wrote the paper.

Supplementary material: https://iopscience.iop.org/article/10.1088/1748-9326/ac188d

Chapter 3: Mester, B., Frieler, K., and Schewe, J. (submitted). Human displacements, fatalities, and economic damages linked to remotely observed floods (FLODIS). *Under consideration for Scientific Data*.

B.M. and J.S. designed the study, with contributions from K.F. B.M. developed the methodology and code to extract the subnational information and merge the datasets. B.M. and J.S. conducted the technical validation, and K.F. contributed to the interpretation. B.M. and J.S. jointly wrote the paper.

Supplementary material: /

Chapter 4: Mester, B., Desai, B., Frieler, K., Korup, O., and Schewe, J. (in progress). A global-scale vulnerability assessment of flood-induced human displacement.

B.M., K.F., and J.S. designed the study. B.M. performed the regression analysis, computed the feature importance and partial dependence plots. B.M. and J.S. analyzed the results, and O.K., B.D. and K.F. contributed to the interpretation. B.M. and J.S. wrote the paper with contributions from B.D., K.F. and O.K.

Supplementary material: see Appendix

Chapter 5: Mester, B., Vogt, T., Bryant, S., Otto, C., Frieler, K., and Schewe, J. (submitted). Human displacements from tropical cyclone Idai attributable to climate change. *Under consideration for Natural Hazards and Earth System Science*s. EGUsphere [preprint], https://doi.org/10.5194/egusphere-2022-1308, 2023.

B.M. and J.S. designed the study, with contributions from T.V., C.O., and K.F. T.V. designed and performed coastal flood model calculations. S.B. estimated flood depths from satellite imagery. B.M. computed the number of affected people and displacements. B.M. and J.S. analyzed the results, and C.O., and K.F. contributed to the interpretation. B.M., T.V., S.B., C.O. and J.S. jointly wrote the paper.

Supplementary material: https://doi.org/10.5194/egusphere-2022-1308

In addition to these four manuscripts, the author of this thesis also contributed to the following publications, which are not part of this dissertation, during the time of the PhD:

van den Hurk, Bart and Baldissera Pacchetti, Marina and Ciullo, Alessio and Coulter, Liese and Dessai, Suraje and Ercin, Ertug and Goulart, Henrique and Hamed, Raed and Hochrainer, Stefan and Koks, Elco and Kubiczek, Patryk and Levermann, Anders and Mechler, Reinhard and van Meersbergen, Maarten and **Mester, Benedikt** and Middelanis, Robin and Minderhoud, Katie and Mysiak, Jaroslav and Nirandjan, Sadhana and Otto, Christian and Sayers, Paul and Sillman, Jana and Schewe, Jacob and Shepherd, Theodore G. and Stuparu, Dana and Vogt, Thomas and Witpas, Katrien, Climate Impact Storylines for Assessing Socio-Economic Responses to Remote Events. *Climate Risk Management*. Available at SSRN: https://ssrn.com/abstract=4090562 or http://dx.doi.org/10.2139/ssrn.4090562. ***Under review***

Imagiire L.O.K.M., **Mester B.**, Haun S., Seidel J. (2022) Open-Access Precipitation Networks and Machine Learning Algorithms as Tools for Flood Severity Prediction. In: Kolathayar S., Mondal A., Chian S.C. (eds) *Climate Change and Water Security*. Lecture Notes in Civil Engineering, vol 178. Springer, Singapore. 10.1007/978-981-16-5501-2_11.

Mester, B., Noack, M. & Wieprecht, S. (2020). Der Weg zur perfekten Surfwelle - helfen experimentelle Untersuchungen der Praxis? *WASSERWIRTSCHAFT*, 110(7–8), 27–31. https://doi.org/10.1007/s35147-020-0412-0.

Chapter 2 Evaluation of river flood extent simulated with multiple global hydrological models and climate forcings

Authors:
Benedikt Mester
Sven Norman Willner
Katja Frieler
Jacob Schewe

Published as:
Mester, B., Willner, S.N., Frieler, K., and Schewe, J., 2021. Evaluation of river flood extent simulated with multiple global hydrological models and climate forcings. *Environmental Research Letters 16 094010*. https://doi.org/10.1088/1748-9326/ac188d

Abstract

Global flood models (GFMs) are increasingly being used to estimate global-scale societal and economic risks of river flooding. Recent validation studies have highlighted substantial differences in performance between GFMs and between validation sites. However, it has not been systematically quantified to what extent the choice of the underlying climate forcing and global hydrological model (GHM) influence flood model performance. Here, we investigate this sensitivity by comparing simulated flood extent to satellite imagery of past flood events, for an ensemble of three climate reanalyses and 11 GHMs. We study eight historical flood events spread over four continents and various climate zones. For most regions, the simulated inundation extent is relatively insensitive to the choice of GHM. For some events, however, individual GHMs lead to much lower agreement with observations than the others, mostly resulting from an overestimation of inundated areas. Two of the climate forcings show very similar results, while with the third, differences between GHMs become more pronounced. We further show that when flood protection standards are accounted for, many models underestimate flood extent, pointing to deficiencies in their flood frequency distribution. Our study guides future applications of these models, and highlights regions and models where targeted improvements might yield the largest performance gains.

2.1 Introduction

Of all natural disasters worldwide, fluvial (river) flooding is among the most frequent and devastating hazards (Jha et al., 2012). In the recent years of 2010–2018, it caused 115 million human displacements (IDMC, 2019), 49 595 fatalities, and US$ 360 billion in economic losses (Munich Re, 2020). For example, 11 million displacements (IDMC, 2019), 1985 deaths, and US$ 9.5 billion in economic losses (EM-DAT, 2020) were recorded in the aftermath of the Pakistan floods in 2010. Flooding killed 6054 people in India in 2013 (EM-DAT, 2020) and caused an estimated US$ 33 billion losses in China in 2016, with only 2% of losses insured (Floodlist, 2016). Beyond these records, one can expect further losses such as of cultural heritage and ecosystem services, which are, however, difficult to assess (Hurlbert, 2018).

Continental-scale changes in flood discharge have been observed recently, in line with theoretical expectations about the effects of global warming on the hydrological cycle (Blöschl et al., 2019; IPCC, 2014). This poses the question to what extent the societal impacts of floods have already been shaped by anthropogenic climate change. However, displacements, damages and losses associated with floods are a function not only of the physical flood hazard, but also of socioeconomic factors. The latter, in particular, determine exposure - the number of people or the value of assets potentially affected by flooding -, and vulnerability - the susceptibility of exposed elements to the hazard (IPCC, 2012; Jongman et al., 2015). Together, these controlling risk factors form a dynamic, spatially and temporally variable balance used for risk assessment. Since not all three factors are generally known, it is challenging to quantify their relative contributions to the ultimate impacts of historical floods.

Global flood models (GFMs) can be used to estimate historical flood extents based on observed weather, and could thereby provide the physical flood hazard component for such assessments when direct observations of flood extent are lacking. This approach is increasingly being used, for instance, to estimate past changes in vulnerability (Tanoue et al., 2016) or attribute trends in reported flood-induced damages (Sauer et al., 2021). However, the degree to which such studies can explain the observed variations in damages and affected population varies substantially, and can be fairly low for many parts of the world. It is unclear to what extent this is due to short-comings in the simulated flood hazard, exposure, or assumptions about vulnerability.

This highlights that a thorough understanding of the reliability of global flood hazard estimates is important. However, validation and benchmarking studies are rare (Hoch and Trigg, 2019), which is mainly due to the scarce availability of reference flood maps outside of some high-income countries and regions such as the European Union, North America, or Australia (Dottori et al., 2016). A comparison of several GFMs to satellite imagery in three African river sections showed considerable differences between models in terms of how

accurately they reproduced observed flood extent; most models both missed flooding in some areas and falsely simulated flooding in others (Bernhofen et al., 2018). The agreement between these models in simulated flood extent was shown to be only 30%–40%, with considerable differences in hazard magnitude and spatial patterns (Trigg et al., 2016).

It is hardly known to what extent such differences between GFM simulations and their predictive capacities are related to the GFMs themselves, for instance, due to differences in model structure or the underlying digital elevation models; and to what extent they are related to the boundary conditions used to force the GFMs. Depending on the modelling framework, these boundary conditions consist either of gauged river flow datasets, or - for the majority of GFMs - of gridded runoff estimates from global hydrological model (GHM) or land-surface models (Trigg et al., 2016). Those runoff simulations in turn need meteorological variables as input, which come from global climate reanalyses or climate models. Most global flood hazard simulations thus are the result of a cascade of different models and data products, with multiple options available at each step in the cascade. The influence of choices in the upstream steps of this cascade on the resulting flood extent estimate has hardly been systematically investigated (Zhou et al., 2021).

In this study we address this research gap. We run a state-of-the-art GFM with runoff forcing from 11 different GHMs, each in turn forced by three different climate reanalyses. We evaluate the resulting simulation ensemble against satellite-derived flood extent observations for eight recent large flood events on four continents, covering different climatic and hydraulic environments, and assess the influence of the choice of both climate forcing and GHM on the performance of the GFM simulations. We do this under different assumptions about flood protection, to also assess the realism of simulated return intervals.

2.2 Data and methodology

2.2.1 Models

We use the GFM CaMa-Flood (Yamazaki et al., 2011), driven by an ensemble of 11 GHMs and three gridded climate forcing datasets, leading to 33 combinations in total. The climate forcing datasets used to drive the GHMs are the Princeton Global Forcing data set version 2 (PGFv2) (Sheffield et al., 2006), the Global Soil Wetness Project phase 3 forcing data set (GSWP3) (Hyungjun, 2014) and the WATCH forcing data methodology applied to ERA-Interim reanalysis data (WFDEI) (Weedon et al., 2014, 2011). All three datasets are based on reanalysis products (ERA-Interim for WFDEI; 20CR for GSWP3; NCEP/NCAR for PGFv2) that assimilate information from local weather stations, and subsequently apply corrections to the

precipitation data and other variables using station-based observational data; two datasets (WFDEI and GSWP3) also correct for precipitation undercatch by rain gauges. Given these methodologies, and the gridded nature of the forcing products, direct comparison with local station data is not straightforward, but existing validation exercises show reasonable agreement with station data as well as with gridded observational datasets (Essou et al., 2017; Weedon et al., 2014).

The set of GHMs comprises CLM4.0 (Leng et al., 2015), DBH (Tang et al., 2007), H08 (Hanasaki et al., 2008), JULES-W1 (Best et al., 2011), LPJmL (Sitch et al., 2003), MATSIRO (Pokhrel et al., 2014), MPI-HM (Stacke and Hagemann, 2012), ORCHIDEE (Traore et al., 2014), PCR-GLOBWB (Wada et al., 2014), VIC (Liang et al., 1994) and WaterGAP2 (Müller Schmied et al., 2016). An overview of the GHMs' main characteristics, e.g. evaporation and runoff schemes, is available in the supplementary material - table S1. All GHM simulations follow a common protocol (ISIMIP2a, www.isimip.org) to ensure a standardized input scheme for CaMa-Flood. Simulations are performed under naturalized conditions, i.e. storage in man-made reservoirs or agricultural water with-drawl are not included.

The runoff of the respective GHM then constitutes the input for CaMa-Flood v3.6.2 which yields discharge as well as flood depth on a 0.25◦ resolution grid. The underlying river network in CaMa-Flood has been derived by the model author based on the flow direction maps HydroSHEDS (Lehner et al., 2008) and GDBD (Masutomi et al., 2009) as well as the digital elevation model SRTM3 (Farr et al., 2007) using their FLOW method (Yamazaki et al., 2009). Using these same data, we downscale flood depth to 18 arc sec. i.e. the daily flood volume in a low-resolution (0.25°) grid cell is distributed onto the underlying high-resolution (18 arc sec) grid cells according to their elevation. We then assign to each high-resolution grid cell the annual maximum daily value, resulting in an annual flood depth timeseries. The event duration according to the satellite imagery matches with the rising limb or the peak of the flood simulations for most regions of interest; and coincides with no second flood event in the year of investigation, which legitimizes this approach (Figures S22–S33 in the supplementary material (available online at stacks.iop.org/ERL/16/094010/mmedia)). This dataset is used to produce Figure 2.2. Finally, we calculate the flooded fraction on an intermediate-resolution (2.5 arc min) grid, i.e. the fraction of flooded high-resolution grid cells within each intermediate-resolution grid cell. This flood fraction dataset is used to calculate the performance scores (see below).

Whereas this constitutes our default simulation setup ('default'), we also assess setups assuming protection against floods with an average recurrence interval (ARI) of 2 years ('protect 2y' setup), and assuming flood protection standards according to the FLOPROS database (Scussolini et al., 2016) ('protect FLOPROS' setup). FLOPROS incorporates

modelled protection, infrastructure, and policy measures in a best estimate ('merged' layer) on a sub-national level. Fitting, for each climate forcing and GHM, a generalized extreme value (GEV) distribution to the annual maximum discharge for each cell and in the simulation period available for all models (1971–2010), we obtain the return period in dependence of discharge. We then compare the return period for each studied event to the protection level for the respective cell; i.e. either 2 years, or the protection level given by FLOPROS. In the 'protect' settings, we thereby only account for flood events in cells in which this protection level is exceeded and assume no flooding for events with lower return period.

It should be noted that there are well-established practices used in floodplain planning processes internationally (World Meteorological Organization, 2009) that do not rely on GFMs but instead use more complex, locally calibrated hydrodynamic models (Raadgever and Hegger, 2018). However, these techniques require elaborate calibration for each individual catchment (Canning and Walton, 2014), and rely on local observational data that is not commonly available in all parts of the world. For instance, in a new, comprehensive global streamflow database (Do et al., 2018; Gudmundsson et al., 2018), local gauge records are available for only one of the events studied in this paper (the 2010 flood in Dalby, Australia; see below), and are entirely unavailable for some of the study regions. Thus, while the global models evaluated here are likely inferior to more complex, locally-informed flood prediction models where those exist, the global models nonetheless are important tools widely used in continental- or global-scale applications (Bates et al., 2021).

2.2.2 Observational data

For the comparison of our simulated flood extent we use satellite imagery from the archive of the Dartmouth Flood Observatory (DFO), which is based on NASA MODIS satellite sensors (https://floodobservatory.colorado.edu/) (Brakenridge, 2006), and from the UNOSAT Flood Portal (UFP) providing flood extent maps derived from a variety of satellite sensors (http://floods.unosat.org/geoportal/catalog/main/home.page). The number of eligible events is limited, because consistent geospatial imagery starts in 2010 for DFO and 2006 for UFP, respectively, and most the climate reanalysis products used here extend only until 2010 or (for PGFv2) 2012. Only large-scale disasters with a large river size are taken into account to ensure that the inundated areas can be adequately captured given the spatial resolution of the GFM. It is essential that observational validation data is available, consistent and comprehensive for the entire area of interest. Additionally, a spread across different climate zones and continents is desirable for a comprehensive global comparison study (Dottori et al., 2016). We exclude flash flood events, storm surge flooding, as well as floods caused by

mismanagement or failure of man-made structures, since these types of floods cannot be modelled by the GFM.

We identify ten regions of particular interest in the context of eight major flood events, as shown in Figure 2.1. The following regions, named after the central city or town affected, are used for validation: Huainan in China (year of flood event: 2007), Sayaxché in Guatemala (2008; the westernmost part is located in Mexico), Trinidad in Bolivia (2008), Alipur and Ghotki in Pakistan (2010), Phimai in Thailand (2010), Dalby in Australia (2010), Chemba in Mozambique (2007), as well as Lokoja and Idah in Nigeria (2012). Chemba (MOZ; we will indicate each location's ISO3 country code throughout the paper for ease of reference), Lokoja (NGA), and Idah (NGA) are studied in a recent GFM intercomparison study, thus facilitating comparison of our results with that study (Bernhofen et al 2018). The selected areas are located in monsoon climates, tropical savannas and rainforests, subtropical climates, and deserts, on four continents (Peel et al., 2007). The selection covers a variety of hydraulic characteristics, ranging from confined watercourses of the Niger River and the anabranching Condamine River in Queensland to highly braided and slow sections of the Indus River. A more detailed description of the chosen events and the river hydraulics can be found in the supplementary material - table S2.

The satellite imagery of flood extents for the regions Alipur (PAK), Ghotki (PAK), Phimai (THA), and Dalby (AUS) are taken from the DFO. Satellite imagery for Huainan (CHN), Sayaxché (GTM) and Trinidad (BOL) are downloaded from the UFP. For some events, the data consists of several days of imagery and is hence merged into one maximum flood extent per event.

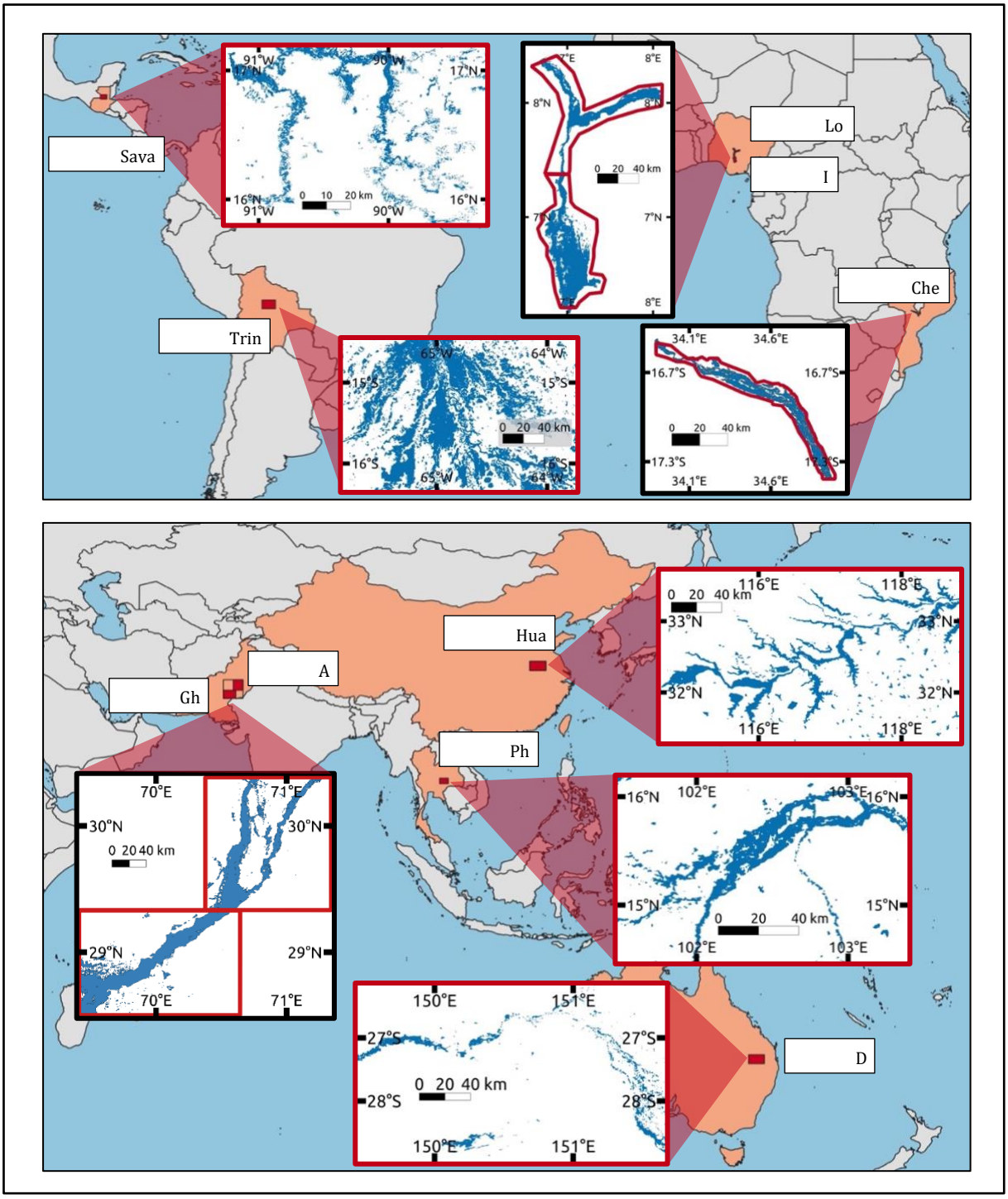

Figure 2.1: Satellite imagery of flood extent (blue) in the study areas (red). Note: the outlines of Chemba (MOZ), Lokoja (NGA) and Idah (NGA) follow the flood shape and are not rectangular. Country shapes by www.gadm.org.

Rectangular analysis regions are defined for the events above (red rectangles in Figure 2.1). Flood footprints and outline data for the regions Chemba (MOZ), Lokoja (NGA) and Idah (NGA) are derived from Research Data Leeds (http://archive.researchdata.leeds.acuk/411/), which is intended for GFM validation (Bernhofen et al., 2018) and also based on the DFO archive. In contrast to the other regions, data for these regions is only available inside an irregularly shaped polygon roughly outlining the main inundation area, which limits the analysis of both observations and simulations to these polygons (we will discuss the implications of this below). The satellite imagery for all regions is at a 209 m resolution. Only the simulations of eight GHMs forced with PGFv2 extend to the year 2012, which limits the analysis of Lokoja (NGA) and Idah (NGA).

2.2.3 Analysis

The analysis procedure starts with a visual comparison of the simulated and the observed flood extent. For the former, we use the gridded CaMa-Flood flood depth output downscaled to 18 arc sec resolution (approx. 550 m at the equator). This yields a binary grid with two grid cell states (flooded or not flooded) for each climate forcing and GHM. For each climate forcing and grid cell we then count the number of GHMs showing flooding in the respective cell, to create a model agreement map. We use the flood outlines for each region (red outlines in Figure 2.1) to mask both the model agreement map and the satellite imagery. The masked images are then superimposed onto each other (Figure 2.2). Next, in order to quantify model performance, we use two different performance metrics (Aronica et al., 2002; Bates and De Roo, 2000; Bernhofen et al., 2018; Werner et al., 2005). First, the critical success index (CSI) is defined as:

$$CSI = \frac{F_m \cap F_o}{F_m \cup F_o}$$

where F_m is the modelled flooded area by CaMa-Flood and F_o is the observed flooded area by the satellite imagery. $F_m \cap F_o$ is the intersection area between modelled and observed flood extent, i.e. the area correctly simulated as flooded by the model; and $F_m \cup F_o$ is the union area between modelled and observed flooded area. The CSI is perceived as the one of the most comprehensive scores (Bernhofen et al 2018). It ranges from 0 to 1, where 1 represents a perfect model ‘fit’ (Sampson et al., 2015), and penalizes overprediction. The Bias score is defined as:

$$Bias = \frac{(F_m \cap F_o) + F_m}{(F_m \cap F_o) + F_o} - 1$$

An unbiased model has a Bias score of 0, positive and negative values indicate a tendency towards over- or under prediction of flood extents, respectively. The Bias score rewards a large intersection area between modelled and observed flood extent.

At high spatial resolution, mismatches in river geometry between the satellite imagery and the digital elevation models used in the GFM could deteriorate the performance scores in confined floodplains; e.g. if a river channel in the DEM is offset relative to its real location (Yamazaki et al., 2011). Since we want to evaluate simulated flood extent per event, rather than DEM accuracy, we therefore calculate performance scores at the coarser resolution of 2.5 arc min. For that, we downsample both the binary satellite imagery and the CaMa-Flood binary flood data to 2.5 arc min using simple linear sampling, yielding the share of flooded area per cell. Incorporating absolute cell area we thus compute absolute flooded area per cell for both CaMa-Flood output and satellite imagery. Summing over all cells within an analysis region yields F_m and F_o respectively. The intersection area $F_m \cap F_o$ is calculated analogously but multiplying, in each cell, the smaller flooded fraction of either CaMa-Flood or satellite data with the cell area; for the union area $F_m \cup F_o$ the larger value of either model or data is used. This approach is based on the assumption that the location of flooding at the sub-grid scale is, for a given grid-scale flood extent, constrained by topography. For comparison, we also show CSI and Bias scores computed directly on 18 arc sec resolution in supplementary material Figures S36 and S37.

In the section 3, along with the performance metrics for individual simulations and regions, we also show the median over all regions as well as median, minimum, maximum and spread over all hydrological models. Lokoja (NGA) and Idah (NGA) were excluded from the computation of the regional median, in order to allow a fair comparison of the median values between the three climate forcing datasets.

2.3 Results

We first analyse results for the default simulations not accounting for flood protection; and subsequently, in section 3.3, discuss the simulations with flood protection.

2.3.1 Model agreement map

Figure 2.2 displays the model agreement overview for all three climate forcings and ten regions, for the default simulations. Results differ substantially between the regions. The

agreement between models is high, and the simulated flood outline in relatively good agreement with observations, for Sayaxché (GTM), Trinidad (BOL), Lokoja (NGA), Idah (NGA), and Phimai (THA), although the models miss some extended parts of the flood in Trinidad (BOL) and Phimai (THA), and somewhat overestimate the flood extent in Idah (NGA). Agreement between models is also high (indicated by reddish colours) in Huainan (CHN); however, the models overestimate the extent of flooding there, including a large area in the north- western part of the region where most models falsely simulate flooding. In Chemba (MOZ), as well as in Alipur (PAK) and Ghotki (PAK), most models agree on flooding along the main river branches, but partly underestimate the extent of this flooding; while many models falsely simulate flooding in an extensive area to the east of the Indus River in Ghotki (PAK), and along the Sutlej river estuary in Alipur (PAK). Finally, in Dalby (AUS), only some models capture the more extensive parts of the flood; at the same time, several models simulate flooding alongside long stretches of the river channel where no flooding is observed.

The simulation of flooding in large areas where no flooding was observed—found for the floods in China, Pakistan, and Australia—could theoretically be induced by contamination of our flood extent estimate by a different flood event: i.e. an event occurring in the same year which had an even higher flood magnitude in that part of the region, and would thus be picked up when taking the annual maximum discharge in every grid cell. However, analysis of daily flood data confirms that this is not the case; while there can be a considerable delay of the flood peak in CaMa-Flood compared to observations (Zhao et al., 2017), the estimated flood extent is largely related to one coherent flood event, except for outliers in marginal grid cells (supplementary material, Figures S1–S33).

Regarding the climate forcing, the GSWP3 and WFDEI reanalysis datasets lead to very similar results. The PGFv2 dataset leads to markedly smaller simulated flood extents in Alipur (PAK), Ghotki (PAK), and Huainan (CHN), with most or all GHMs. This partly remedies the overestimation of flooding outside the main river floodplains, but also leads to a more substantial underestimation of flood extent along the main rivers in Alipur (PAK) and Ghotki (PAK), compared to the other two forcing datasets.

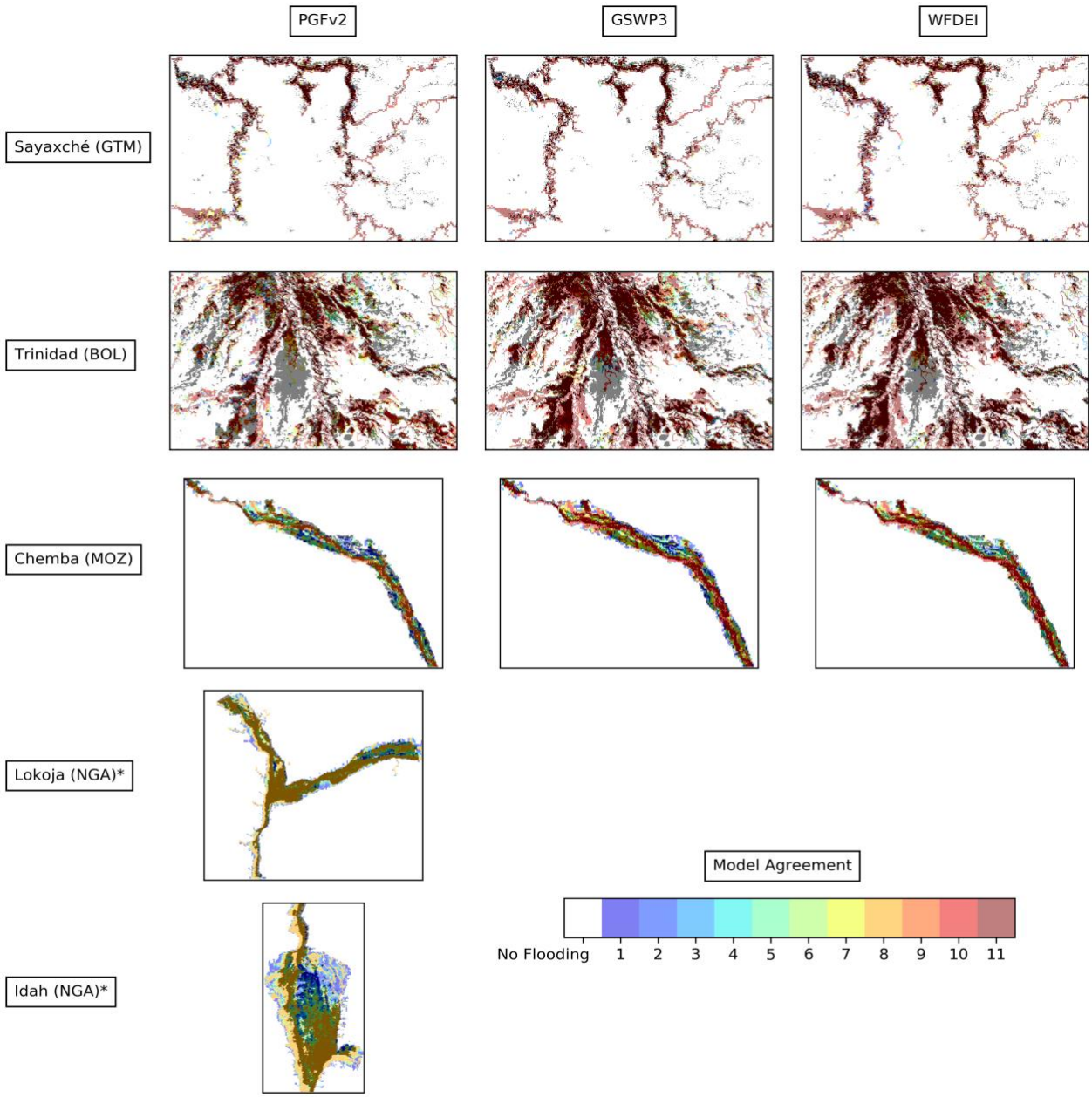

Figure 2.2: Model agreement map indicating the flood extent overlap between the 11 GHMs and the satellite data for each study region (row) and climate forcing (column). The cell color represents the number of GHMs that computed the corresponding cell to be flooded. The underlying flood extent of the satellite imagery (light grey) is assigned a dark color tone if it matches with at least one GHM. For the 2012 flood in Lokoja (NGA) and Idah (NGA) (marked with an asterisk *), only eight GHMs, driven with PGFv2, were available.

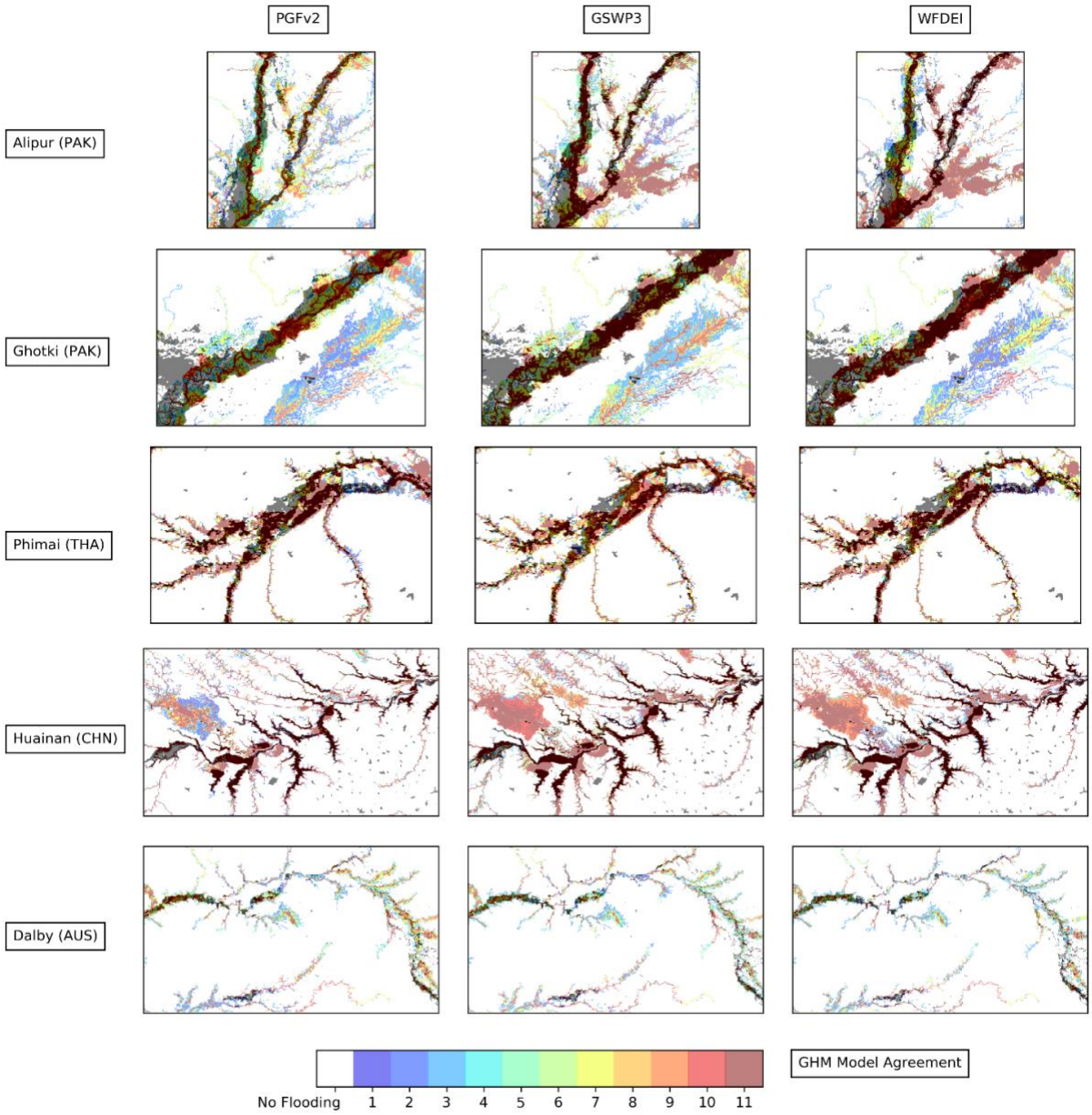

Figure 2.2: Continued

2.3.2 Model performance scores

In line with the observations from the model agreement maps, the CSI scores vary substantially between the different regions (Figure 2.3). A comparatively low CSI is found for Alipur (PAK), Ghotki (PAK), Huainan (CHN), with scores between 0.3 and 0.4, and especially Dalby (AUS) with scores below 0.3. High CSI scores of around 0.5 and higher are found for Sayaxché (GTM), Trinidad (BOL), Chemba (MOZ), Lokoja (NGA), and Idah (NGA). Intermediate scores of around 0.45 are found for Phimai (THA). Since the CSI score also

depends on the flood magnitude (Stephens et al., 2014), this numerical comparison between regions and events should be interpreted with caution, and in conjunction with the model agreement maps. In particular, for a given region with a concave topography (e.g. extensive floodplain), the larger the flood magnitude, the more the flood extent will be constrained by topography, and the less variation in flood extent will be induced by a given variation in flood discharge; potentially leading to more favourable CSI scores than for smaller floods. These caveats however do not affect comparison between models and datasets within one region and event, which we turn to next.

We find differences in performance between climate forcings and between GHMs to be mutually dependent, and we discuss them together in the following. The spread across GHMs (rightmost column in Figure 2.3) is by far largest for Chemba (MOZ). This is primarily because there the CSI with the VIC model is zero for all three forcings, and the CSI with the MATSIRO model is zero for the PGFv2 forcing; indicating that there is no intersection between simulated and observed flood extent. The MATSIRO model with PGFv2 forcing also has very low CSI scores in Alipur (PAK) and Ghotki (PAK). However, even if the MATSIRO and VIC models were excluded, Chemba (MOZ), Alipur (PAK) and Ghotki (PAK) would still remain the regions with the largest differences in CSI scores across GHMs, under the PGFv2 forcing; for instance, compare CLM and PCR-GLOBWB for Alipur (PAK) and Ghotki (PAK), or MPI-HM and ORCHIDEE for Chemba (MOZ). Using the other two climate forcings, these inter-GHM differences are much smaller, mostly with a difference of about 0.1 or less between the scores of the best and worst performing model. The median CSI scores over all regions (bottom row in each subplot in Figure 2.3) indicate that none of the GHMs performs consistently better or worse than the others. Even the VIC model, which fails to capture the flood in Chemba (MOZ), achieves reasonable scores in the other regions, and has a region-median CSI only slightly below the other GHMs (between 0.36 and 0.39 depending on the climate forcing). The MATSIRO model, which shows very low CSI scores in three of the regions under PGFv2 forcing, is among the best performing GHMs in some of the other regions; in particular, it achieves the highest CSI score of all GHMs in Huainan (CHN) for all three forcings, and has the highest region-median CSI score under the WFDEI forcing.

Similarly, the statistics over all GHMs (rightmost four columns in Figure 2.3), and the combined statistics across regions and GHMs (bottom right in each sub-plot in Figure 2.3, as well as Figure 2.5), show that neither of the three climate forcing datasets is generally superior to the others: the GHM-region median CSI is 0.42, 0.43, and 0.44, respectively, for PGFv2, GSWP3, and WFDEI. PGFv2 exhibits slightly lower GHM-median CSI scores, and lower minimum scores, than the other two forcings in many of the regions; on the other hand, in

Huainan (CHN), all GHMs achieve substantially higher scores with PGFv2 than with GSWP3 or WFDEI.

There is thus no climate forcing dataset that performs best in all regions; nor is there one GHM which consistently performs best in all regions and with all forcings (see black boxes in Figure 2.3).

We now turn to the Bias scores. While a low CSI score generally already implies a high bias, the Bias score additionally indicates whether the observed total flood extent is over- or under predicted by the model. We find that with WFDEI and GSWP3 forcing, Bias scores are generally either small or positive (with the exception of VIC in Chemba (MOZ)) (Figure 2.4). This confirms the observation made in the model agreement maps that flood extent is generally either matched relatively well, or overestimated, by the model simulations. With the PGFv2 climate forcing, the overall result is similar, but substantial negative Bias scores—indicating an under prediction of flood extent—occur in several cases: for Alipur (PAK), Ghotki (PAK), and Chemba (MOZ), with CLM, MATSIRO, and MPI-HM; corresponding to the anomalous CSI values for these combinations described above. On the other hand, the PGFv2 forcing leads to much smaller (positive) biases than the other two forcings in Huainan (CHN).

Calculating the performance scores on the higher-resolution (18 arc sec) binary flood outputs confirms these overall results, though the scores are somewhat lower (supplementary material, Figures S36 and S37).

PGFv2	CLM	DBH	H08	JULES-W1	LPJmL	MATSIRO	MPI-HM	ORCHIDEE	PCR-GLOBWB	VIC	WaterGAP2	Median GHMs	Min. GHMs	Max. GHMs	Spread GHMs
Sayaxché (GTM)	0.52	0.55	0.52	0.53	0.53	0.56	0.52	0.52	0.54	0.53	0.56	0.53	0.52	0.56	0.04
Trinidad (BOL)	0.47	0.51	0.52	0.50	0.51	0.34	0.52	0.51	0.48	0.43	0.51	0.51	0.34	0.52	0.18
Chemba (MOZ)	0.43	0.71	0.68	0.67	0.67	0.00	0.40	0.71	0.53	0.00	0.56	0.56	0.00	0.71	0.71
Alipur (PAK)	0.23	0.37	0.39	0.35	0.40	0.11	0.34	0.36	0.44	0.39	0.38	0.37	0.11	0.44	0.33
Ghotki (PAK)	0.20	0.34	0.42	0.34	0.35	0.11	0.34	0.32	0.43	0.38	0.41	0.34	0.11	0.43	0.32
Phimai (THA)	0.44	0.46	0.41	0.50	0.47	0.49	0.45	0.45	0.44	0.43	0.50	0.45	0.41	0.50	0.09
Huainan (CHN)	0.38	0.34	0.39	0.38	0.39	0.46	0.43	0.42	0.32	0.39	0.40	0.39	0.32	0.46	0.14
Dalby (AUS)	0.24	0.17	0.22	0.16	0.19	0.24	0.24	0.20	0.21	0.26	0.26	0.22	0.16	0.26	0.10
Lokoja (NGA)*	-	-	0.73	0.74	0.74	0.74	0.76	0.68	0.72	-	0.75	0.74	0.68	0.76	0.08
Idah (NGA)*	-	-	0.66	0.69	0.69	0.60	0.70	0.60	0.60	-	0.69	0.68	0.60	0.70	0.10
Median Region	0.40	0.42	0.42	0.44	0.44	0.29	0.42	0.44	0.44	0.39	0.45	0.42	0.24	0.48	0.16

GSWP3	CLM	DBH	H08	JULES-W1	LPJmL	MATSIRO	MPI-HM	ORCHIDEE	PCR-GLOBWB	VIC	WaterGAP2	Median GHMs	Min. GHMs	Max. GHMs	Spread GHMs
Sayaxché (GTM)	0.53	0.56	0.54	0.56	0.55	0.58	0.54	0.54	0.56	0.55	0.56	0.55	0.53	0.58	0.05
Trinidad (BOL)	0.53	0.54	0.54	0.53	0.54	0.49	0.53	0.54	0.53	0.46	0.53	0.53	0.46	0.54	0.08
Chemba (MOZ)	0.69	0.71	0.70	0.60	0.71	0.53	0.70	0.62	0.71	0.00	0.53	0.69	0.00	0.71	0.71
Alipur (PAK)	0.32	0.33	0.36	0.33	0.35	0.33	0.35	0.35	0.36	0.35	0.37	0.35	0.32	0.37	0.05
Ghotki (PAK)	0.34	0.40	0.44	0.35	0.35	0.42	0.43	0.34	0.42	0.40	0.34	0.40	0.34	0.44	0.10
Phimai (THA)	0.46	0.45	0.42	0.50	0.47	0.41	0.47	0.46	0.45	0.43	0.46	0.46	0.41	0.50	0.09
Huainan (CHN)	0.28	0.28	0.29	0.33	0.30	0.38	0.31	0.31	0.28	0.31	0.32	0.31	0.28	0.38	0.10
Dalby (AUS)	0.23	0.18	0.24	0.18	0.20	0.23	0.25	0.22	0.22	0.26	0.25	0.23	0.18	0.26	0.08
Median Region	0.40	0.43	0.43	0.42	0.41	0.42	0.45	0.40	0.44	0.38	0.42	0.43	0.33	0.47	0.09

WFDEI	CLM	DBH	H08	JULES-W1	LPJmL	MATSIRO	MPI-HM	ORCHIDEE	PCR-GLOBWB	VIC	WaterGAP2	Median GHMs	Min. GHMs	Max. GHMs	Spread GHMs
Sayaxché (GTM)	0.52	0.53	0.50	0.51	0.51	0.53	0.50	0.51	0.53	0.51	0.52	0.51	0.50	0.53	0.03
Trinidad (BOL)	0.53	0.53	0.54	0.54	0.54	0.53	0.54	0.54	0.54	0.51	0.53	0.54	0.51	0.54	0.03
Chemba (MOZ)	0.65	0.71	0.70	0.61	0.71	0.55	0.66	0.71	0.71	0.00	0.49	0.66	0.00	0.71	0.71
Alipur (PAK)	0.27	0.36	0.37	0.38	0.36	0.30	0.36	0.34	0.37	0.31	0.38	0.36	0.27	0.38	0.11
Ghotki (PAK)	0.37	0.34	0.48	0.40	0.35	0.47	0.47	0.37	0.44	0.42	0.41	0.41	0.34	0.48	0.14
Phimai (THA)	0.47	0.46	0.41	0.50	0.47	0.49	0.47	0.47	0.46	0.45	0.49	0.47	0.41	0.50	0.09
Huainan (CHN)	0.29	0.28	0.30	0.32	0.31	0.37	0.33	0.32	0.27	0.31	0.31	0.31	0.27	0.37	0.10
Dalby (AUS)	0.25	0.18	0.24	0.20	0.20	0.27	0.25	0.25	0.22	0.26	0.27	0.25	0.18	0.27	0.09
Median Region	0.42	0.41	0.44	0.45	0.42	0.48	0.47	0.42	0.45	0.36	0.45	0.44	0.31	0.49	0.10

*Figure 2.3: CSI scores for all combinations of GHMs and PGFv2 (top), GSWP3 (middle), and WFDEI (bottom) forcing. The "Median Region" across the even number of regions is calculated as the mean of the two middle values. Lokoja (NGA) and Idah (NGA) (marked with *) were excluded from the computation of the "Median Region". "-" means no input data was available and a black box indicates the best-performing GHM(s) for a given region.*

WFDEI protect 2y	CLM	DBH	H08	JULES-W1	LPJmL	MATSIRO	MPI-HM	ORCHIDEE	PCR-GLOBWB	VIC	WaterGAP2	Median GHMs	Min. GHMs	Max. GHMs	Spread GHMs
Sayaxché (GTM)	0.52	0.53	0.50	0.51	0.51	0.53	0.50	0.51	0.53	0.51	0.52	0.51	0.50	0.53	0.03
Trinidad (BOL)	0.53	0.53	0.50	0.54	0.52	0.53	0.52	0.53	0.53	0.51	0.51	0.53	0.50	0.54	0.04
Chemba (MOZ)	0.65	0.71	0.70	0.61	0.71	0.55	0.66	0.71	0.71	0.00	0.00	0.66	0.00	0.71	0.71
Alipur (PAK)	0.16	0.35	0.37	0.38	0.36	0.30	0.36	0.34	0.38	0.31	0.38	0.36	0.16	0.38	0.22
Ghotki (PAK)	0.40	0.34	0.58	0.48	0.35	0.49	0.49	0.40	0.48	0.45	0.46	0.46	0.34	0.58	0.24
Phimai (THA)	0.47	0.46	0.41	0.50	0.47	0.49	0.47	0.47	0.46	0.45	0.49	0.47	0.41	0.50	0.09
Huainan (CHN)	0.29	0.28	0.29	0.32	0.31	0.36	0.33	0.31	0.27	0.31	0.31	0.31	0.27	0.36	0.09
Dalby (AUS)	0.09	0.14	0.24	0.20	0.20	0.27	0.25	0.25	0.22	0.26	0.27	0.24	0.09	0.27	0.18
Median Region	0.44	0.40	0.45	0.49	0.42	0.49	0.48	0.44	0.47	0.38	0.42	0.46	0.31	0.52	0.14

WFDEI protect FLOPROS	CLM	DBH	H08	JULES-W1	LPJmL	MATSIRO	MPI-HM	ORCHIDEE	PCR-GLOBWB	VIC	WaterGAP2	Median GHMs	Min. GHMs	Max. GHMs	Spread GHMs
Sayaxché (GTM)	0.48	0.31	0.48	0.54	0.53	0.53	0.48	0.48	0.55	0.53	0.54	0.53	0.31	0.55	0.24
Trinidad (BOL)	0.44	0.43	0.47	0.48	0.47	0.45	0.47	0.48	0.48	0.44	0.44	0.47	0.43	0.48	0.05
Chemba (MOZ)	0.00	0.00	0.00	0.00	0.00	0.00	0.00	0.00	0.71	0.00	0.00	0.00	0.00	0.71	0.71
Alipur (PAK)	0.03	0.34	0.13	0.39	0.33	0.05	0.05	0.25	0.34	0.14	0.34	0.25	0.03	0.39	0.36
Ghotki (PAK)	0.00	0.57	0.58	0.54	0.12	0.00	0.00	0.00	0.54	0.51	0.57	0.51	0.00	0.58	0.58
Phimai (THA)	0.26	0.05	0.25	0.00	0.33	0.26	0.06	0.26	0.26	0.25	0.00	0.25	0.00	0.33	0.33
Huainan (CHN)	0.12	0.14	0.12	0.14	0.03	0.05	0.12	0.06	0.18	0.04	0.03	0.12	0.03	0.18	0.15
Dalby (AUS)	0.00	0.00	0.00	0.00	0.00	0.00	0.02	0.00	0.00	0.00	0.00	0.00	0.00	0.02	0.02
Median Region	0.08	0.22	0.19	0.26	0.22	0.05	0.06	0.16	0.41	0.2	0.18	0.25	0.02	0.44	0.29

Figure 2.4: CSI scores for all combinations of GHMs and WFDEI for "protect 2y" (top) and "protect FLOPROS" (bottom). The "Median Region" across the even number of regions is calculated as the mean of the two middle values. Lokoja (NGA) and Idah (NGA) were excluded from the computation of the "Median Region". A black box indicates the best-performing GHM(s) for a given region.

2.3.3 Flood protection

We now analyse the simulations accounting for flood protection infrastructure, by counting only those flooded pixels whose ARI (estimated through fitting a GEV function) is longer than either 2 years ('protect 2y') or the protection standard indicated in the global database FLOPROS (Scussolini et al 2016) ('protect FLOPROS').

Under the WFDEI forcing, CSI scores in the 'protect 2y' simulations change only little compared to the default simulations. Most notably, there are now two GHMs simulating no

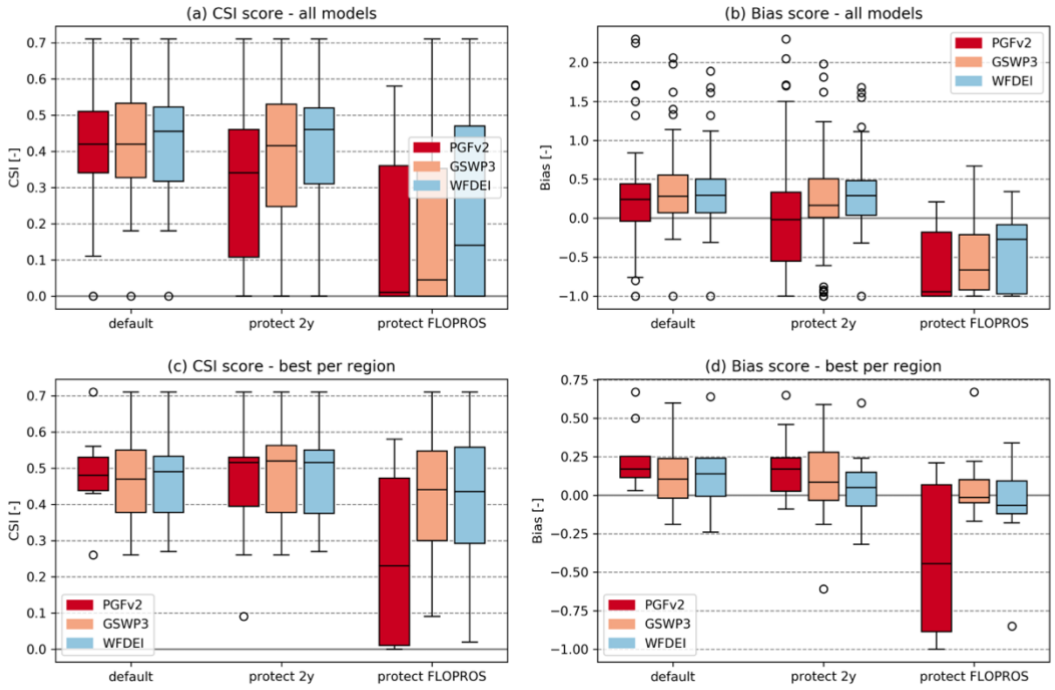

Figure 2.5: Comparison of CSI and Bias scores between the default setting ("default"), protection against floods with an average return interval of 2 years ("protect 2y") and protection standards according to FLOPROS ("protect FLOPROS") for the climate forcings PGFv2, GSWP3 and WFDEI. (a) and (b) include all GHMs and regions, (c) and (d) only account for the best GHM per region. The regions Lokoja (NGA) Idah (NGA) were excluded from the computation.

flooding in Chemba (MOZ): WaterGAP2, in addition to VIC; and the CLM model shows lower CSI scores in Alipur (PAK) and Dalby (AUS) (Figure 2.4). More widespread deterioration of CSI scores appears under the other two forcings. With GSWP3, there are multiple GHMs each in Chemba (MOZ), Alipur and Ghotki (PAK) that show no or almost no flooding (supplementary Figure S39). With PGFv2, the CSI drops to zero in Chemba (MOZ) for almost all models, with the exception of DBH which still shows a high CSI score there; and CSI scores in Huainan (CHN) are seriously degraded for all GHMs. In summary, while for most regions the maximum CSI scores achieved are preserved when assuming protection against ARI of 2 years, the spread among models and among forcings increases notably compared to the default simulations (Figure 2.5 (a) and (c)).

This pattern becomes even more pronounced when assuming flood protection according to FLOPROS. CSI scores degrade in the majority of regions and forcing-GHM combinations (Figure 2.4, Figure 2.5 and supplementary Figure S41). While all of the 'protect FLOPROS' simulations still exhibit significant CSI scores in Trinidad (BOL), they all show zero or almost zero CSI in Dalby (AUS). In most other regions, we find both: multiple GHM-forcing combinations that still achieve relatively high CSI scores, often preserving the maximum CSI

for the region found in the ‘default’ setup; as well as many combinations showing zero or very low CSI scores. Chemba (MOZ) is an interesting case as here the CSI score drops to zero for most of the ‘protect FLOPROS’ simulations, while, with WFDEI forcing, one single GHM (PCR-GLOBWB) still achieves the same CSI as in the default setup; and the same is true for three GHMs (CLM, ORCHIDEE, and PCR-GLOBWB) with GSWP3 forcing.

While the Bias scores were mostly positive in the ‘default’ simulations, the ‘protect FLOPROS’ setup mostly results in negative biases, which are in many parts of substantial magnitude (Figure 2.5(b) and supplementary Figure S42). This corresponds to the decreased and, often, zero CSI scores found in this setup. Bias scores in the ‘protect 2y’ setup are, as expected, closer to those in the ‘default’ setup; with more pronounced overestimation of flood extent under WFDEI forcing, and more pronounced underestimation in some regions under PGFv2 forcing (supplementary Figure S40).

Considering the entire simulation ensemble, the lowest median bias in flood extent is achieved in the ‘protect 2y’ setup, in particular the simulations forced with PGFv2 and GSWP3 yielding a lower median bias than in the ‘default’ setup (Figure 2.5(b)). On other hand, the spread among simulations is largest for ‘protect 2y’. In the ‘protect FLOPROS’ setup, the majority of simulations show a large negative bias, as discussed above. However, when considering for each region only the best-performing model, the least biased results are achieved with WFDEI forcing in the ‘protect FLOPROS’ setup; the corresponding GSWP3 simulations being only slightly more biased (Figure 2.5(d)).

2.4 Discussion and conclusions

A number of key results emerge from our analysis:

1) The performance of a global river flood modelling chain in reproducing observed flood extent for major recent floods differs considerably between events. While CSI scores of 0.7 and higher are obtained for Chemba (MOZ), Idah (NGA), Lokoja (NGA) (similar as in Bernhofen et al. (2018)), scores are much lower for many other events, dropping below 0.3 for Dalby (AUS).

2) The choice of GHM and climate forcing have mutually dependent effects on flood model performance.

3) PGFv2 performs somewhat poorer than the other two climate forcing datasets for many regions and GHMs, but better for some. The performance spread between GHMs is largest with PGFv2.

4) No climate forcing or GHM performs best for all regions. Considering the median over all regions, the PCR-GLOBWB model stands out as achieving the best, or among the best, results for all forcings and in particular for the ‘protect’ setups.

5) Accounting for flood protection according to the FLOPROS database dramatically degrades the average agreement between simulations and observations, by reducing or eliminating simulated flood extent in many cases. However, individual forcing-GHM combinations remain in almost every region that achieve high CSI and low Bias scores.

Regarding key result no. 1, we reiterate that CSI scores should not be compared between regions at face value, because of the varying flood extents. However, it is also evident from the maps in Figure 2.2 that both the overall match between models and observations, and the level of agreement among models, differ depending on the region and event that is analysed. This may be explained by varying topographies among the regions, leading to different errors in simulated flood extent due to cross-floodplain slopes. Another important caveat is that the shape of the study area is not consistent across regions. While the study areas for most regions are rectangular and include large parts where no flooding was observed, the study areas for Chemba (MOZ), Lokoja (NGA), and Idah (NGA) are irregularly shaped polygons narrowly outlining the observed flood extent along the main river channels. This means that potential flooding along tributaries is excluded from the analysis (supplementary Figures S45–S48). Considering an example of a model overestimating observed flood extent, the overestimation may appear less severe if parts of the flood that are further away from the main channel are cut off. With the rectangular study areas, such excess simulated flood extent would be more visible and would degrade the CSI score to a larger degree. This might go some way in explaining why Chemba (MOZ), and especially Lokoja (NGA) and Idah (NGA), exhibit systematically higher CSI scores than other regions. These scores are similar to those found for the same three regions by Bernhofen et al (2018), who used the same study area outlines. This may indicate that the general level of model performance found in our study is comparable to that in Bernhofen et al. (2018), and that the lower CSI scores in the additional regions in our study may also be related to the layout of the study area, rather than only to a poorer model performance in those regions.

Regarding key result no. 2, the importance of the choice of GHM is confirmed by a recent study that compared different sources of uncertainty in CaMa-Flood estimates: the GHM runoff inputs, variables for flood frequency analysis and fitting distributions (Zhou et al., 2021). Of these three, the GHMs were found to be by far the largest source of variation in the estimate

of flood depth and inundation. That study used a single reanalysis forcing dataset (WFDEI) as input to the GHMs and did not evaluate different GHMs' performance in relation to observed flooding; rendering our study a useful complement. It should be pointed out that the hydrological modelling approach underlying many of these GHMs is traditionally aimed at evaluating water and energy balances at longer timescales (also termed catchment yield-type models, in contrast to rainfall-runoff-type models), without specific focus on flood generation; which may partly explain their deficiencies in estimating flood magnitudes and timing. Disparities between GHM-simulated and actual runoff may thus be a fundamental reason for the relatively poor performance of the flood modelling methodology applied here, compared to conventional basin-scale flood analysis; also affecting the results summarized in key results no. 3 and 4.

Regarding key result no. 3, Müller Schmied et al. (2016) evaluated hydrological simulations with a single GHM (WaterGAP2) driven by the same climate forcing datasets as in our study, and found substantial differences in long-term average runoff and other hydrological indicators. In particular, relatively low precipitation and runoff estimates were found with PGFv2, compared to GSWP3 and WFDEI; likely related to the lack of a precipitation undercatch correction in this dataset, but potentially also to a different observational product that precipitation was corrected against (CRU TS3.21 for PGFv2; GPCC version 6 for GSWP3 and WFDEI). While runoff extremes were not directly assessed in that study, systematically lower precipitation forcing could nonetheless explain the larger negative biases in flood extent that we find in our default simulations with PGFv2 for some regions and GHMs; and might likewise explain the smaller positive biases and higher CSI scores in Huainan (CHN), where flood extent is strongly overestimated with GSWP3 and WFDEI forcing.

Nevertheless, the differences even between GSWP3- and WFDEI-driven flood simulations highlight some remaining uncertainty in the forcing data. To test whether using observational datasets directly as input to the GHMs might be beneficial, we performed a set of simulations where, for each event and grid cell, the return period simulated by a given GHM-forcing combination was mapped to the corresponding flood volume given by a benchmark simulation of MATSIRO which was driven with station-based (GPCC) rather than reanalysis precipitation data (Kim et al., 2009). This adjustment procedure was originally devised to correct biases in climate model-derived runoff (Hirabayashi et al., 2013), and has been applied in other global flood modelling studies (Dottori et al., 2018; Sauer et al., 2021; Willner et al., 2018a). However, in our study, the adjustment using the MATSIRO benchmark simulation does not systematically improve the agreement between simulated and observed flood extent (supplementary material Figures S43 and S44); suggesting that neither a particular GHM nor

the observations-based precipitation forcing are generally superior to the GHM ensemble and the reanalysis-based forcings studied here, respectively.

Regarding key result no. 5, one striking finding is that the incorporation of flood protection standards according to FLOPROS leads to zero simulated flood extent in some regions with many or all GHMs and climate forcings. This can either mean that the protection standard indicated in the FLOPROS database is higher than in reality for these regions; or that the return period simulated by the models is too short—in other words, that the models simulate too frequent flooding; or both. It must be remembered that the FLOPROS protection levels are purely model-based estimates for most of the events; except for those in Mozambique, China and Australia, where information about the actual design standards or about corresponding policy regulations entered the estimates provided in the database. Thus, FLOPROS values may not exactly reflect the flood protection standards actually implemented in the study regions.

Reported estimates of the average recurrence interval (ARI) are only available for some of the flood events studied here, and available estimates often differ between sources and/or come with considerable uncertainties. Nevertheless, the actual ARI appears to be higher than the FLOPROS protection standard for most events (supplementary table S3). This suggests that the deterioration of model results when applying FLOPROS may not be predominantly related to errors in FLOPROS. Instead, it suggests that the ARI in the affected model simulations may be too short; i.e. the model too frequently simulates a flood of the given magnitude.

The ‘protect FLOPROS’ simulations thus serve to highlight those GHM-climate forcing combinations that correctly simulate an ARI larger than the protection standard, according to FLOPROS. For instance, applying FLOPROS, the CSI for Chemba (MOZ) drops to zero for almost all simulations except for PCR-GLOBWB with GSWP3 and WFDEI forcing, and for CLM and ORCHIDEE with GSWP3 forcing (supplementary Figure S41). Similarly, imposing FLOPROS flood protection levels in Sayaxché (GTM), the majority of models still achieve a reasonable CSI with GSWP3 and WFDEI forcing but simulate no flooding with PGFv2 forcing. In Alipur (PAK) and Ghotki (PAK), only JULES-W1 and PCR-GLOBWB realistically simulate a large ARI with all three climate forcings. Interestingly, not a single simulation shows substantial flooding in Dalby (AUS) in the ‘protect FLOPROS’ setup; suggesting that here, the protection standard of a 100 year ARI assumed in FLOPROS may indeed be too high; which is also in line with reports of a 90 year ARI for the 2010/2011 flood event (supplementary table S3).

Generally though, many of the runoff simulations used here may still be in need of improvement with respect to the high-end of the runoff distribution. Indeed, a recent evaluation

of monthly runoff simulated by six GHMs, including H08, LPJmL, MATSIRO, PCR-GLOBWB, and WaterGAP2, found that most models—except MATSIRO and WaterGAP2—tended to overestimate high-flow runoff (more precisely, Q5, the magnitude of runoff that is exceeded 5% of the time) (Zaherpour et al., 2018). GHMs particularly struggle to capture the levels and variability of runoff and, consequently, river discharge in more arid environments such as parts of the Murray–Darling basin (Haddeland et al., 2011; Hattermann et al., 2017; Zaherpour et al., 2018). While the CaMa-Flood river routing model has been shown to improve the discharge hydrograph compared to GHMs' native routing schemes in many basins (Zhao et al., 2017), it may not always be able to compensate a systematic overestimation of high-flow runoff by the GHMs, which may then result in an overestimation of flood extent. Moreover, CaMa-Flood does not account for human water management such as water withdrawals or dams, which may in some cases have significant effects on flood volume and timing (Mateo et al., 2014; Zhao et al., 2017). Other limitations of the GFM include the accuracy of the baseline topography, and the use of a global empirical equation to calculate channel depth as function of annual river discharge, without separate calibration for each river (Yamazaki et al., 2014).

We can thus derive from our study some recommendations for future applications of GFMs to simulate flood extent. One is that the choice of GHM (or more generally, the runoff model) and climate forcing should be carefully considered, because it can strongly impact performance. The good news is that serious losses in flood extent performance occurred only with a limited number of individual climate forcing-GHM combinations. Two of our three climate forcings, and the majority of GHMs used, showed very similar levels of performance. The more difficult news is that there is no general recommendation on which forcings or runoff models not to use; because even those that perform particularly poorly in some regions may actually be the best choice in a different region, or in a different GHM-climate forcing combination. A multi-model, multi-forcing ensemble approach may be advisable when there is no prior knowledge about a certain combination's performance for the specific type of event and region under investigation. That being said, validating the underlying runoff model(s) separately from the flood model is a crucial component of robust flood risk analysis; and the performance of each part in the modelling chain should be taken into account to determine whether the modelling chain is fit for a given purpose.

Global flood modelling capacities could profit from further development of GHMs, for instance, addressing the difficulty to accurately capture runoff extremes in arid and semi-arid regions. Weighted ensembles of models may provide a useful method when systematic differences in model performance can be identified (Zaherpour et al., 2018). A closer coupling of runoff and flood modelling, accounting for human alterations of river flow, could improve

flood estimates in highly managed river basins (Boulange et al., 2021; Mateo et al., 2014). Not least, improving the availability and fidelity of observational data, e.g. by extending direct observations of precipitation, runoff, or flood levels, and by making existing data more accessible—including on human-made alterations of the natural river flow—would help with both the calibration and validation of the different parts in the flood modelling chain (Müller Schmied et al., 2016).

2.5 Data availability statement

The data that support the findings of this study are available upon reasonable request from the authors.

2.6 Acknowledgments

The research was supported within the European Union Horizon 2020 projects RECEIPT, CASCADES, and HABITABLE, as well as BMBF project ISIpedia. The ISIMIP modelling teams are gratefully acknowledged. We would like to thank two anonymous reviewers for providing insightful and valuable comments that greatly improved the manuscript.

Chapter 3 Human displacements, fatalities, and economic damages linked to remotely observed floods (FLODIS)

Authors:
Benedikt Mester
Katja Frieler
Jacob Schewe

Under consideration for Scientific Data:
Mester, B., Frieler, K., and Schewe, J. (submitted). Human displacements, fatalities, and economic damages linked to remotely observed floods (FLODIS).

Abstract

We present a new open source dataset FLODIS that links estimates of flood-induced human displacements, fatalities, and economic damages to flooded areas observed through remote sensing. The dataset connects displacement data from the Internal Displacement Monitoring Centre (IDMC), as well as data on fatalities and damages from the Emergency Events Database (EM-DAT), with the Global Flood Database (GFD), a satellite-based inventory of historic flood footprints. It thereby provides a spatially explicit estimate of the flood hazard underlying each individual disaster event. FLODIS contains event-specific information for 335 human displacement events and 695 mortality/damage events that occurred around the world between 2000 and 2018. Additionally, we provide estimates of affected population, assets, and critical infrastructure, as well as socio-economic indicators such as the human development index (HDI), corresponding to the flooded area; and we provide geocoding for displacement events ascribed to other types of disasters, such as tropical cyclones or droughts, so that they may be linked to corresponding hazard estimates in future work. FLODIS facilitates integrated flood risk analysis, allowing, for example, for detailed assessments of local flood-damage and displacement vulnerability.

3.1 Background & summary

Disaster databases record hundreds of flood events every year and gather information on their societal impacts, such as displacements (recorded by the Internal Displacement Monitoring Centre, IDMC), fatalities and damages (recorded in the Emergency Events Database, EM-DAT). However, they do not include any estimates of the corresponding physical hazard, e.g. inundated area or flood depth. That also means that the exposure to flooding, in terms of affected people and assets, associated with each disaster is generally unknown.

The delineation of flood hazard, and exposure, in space and time, is however a critical issue for risk analysis (Formetta and Feyen, 2019). Risk is commonly understood as the product of hazard, exposure, and vulnerability (Cardona et al., 2012; Oppenheimer et al., 2014). Flood impacts reported in disaster databases can serve as empirical realizations of risk, and high-resolution estimates of the distribution of population (and partly also assets) are available for the calculation of exposure. But to understand flood vulnerability, or changes in risk over time, the corresponding hazard must be known. Past studies often used simulated hazard information, e.g., based on modeled annual maximum daily flood water depth (Jongman et al., 2015; Tanoue et al., 2016) or modeled 100 year return period inundation maps (Formetta and Feyen, 2019). This has many advantages such as extensive geographical and temporal coverage, but the fidelity of the models also puts limitations on the accuracy of flood simulations. Using a single maximum flood value per year can also lead to an underestimation in exposure if more than one flood actually occurred in a given year. Additionally, yearly numbers of affected people and fatalities/damages were used, all neglecting that vulnerability is event-specific (Jonkman, 2005).

It is therefore desirable to make use of satellite-based observations of flooded areas, to overcome the limitations of flood model simulations. Satellite-based remote sensors can capture actual flooded areas, implicitly accounting for flood protection (Alfieri et al., 2018) and other non-climate related determinants of flood extent such as land use and infrastructure (Tellman et al., 2021). Until recently, only a limited number of satellite observations of past floods were publicly available, mainly provided by the archive of the Dartmouth Flood Observatory (DFO; https://floodobservatory.colorado.edu/), and the United Nations Operational Satellite Applications Programme (UNOSAT; http://floods.unosat.org). With the release of the Global Flood Database (GFD; http://global-flood-database.cloudtostreet.info/), a product based on the DFO, an unprecedented inventory of satellite imagery is now available, including 913 large flood events from 2000 to 2018 (Tellman et al., 2021). Here, we connect this new data set of observed flood extents to reported flood impacts, enabling large-N global studies of flood vulnerability, its socio-economic drivers, and related questions. We link impact records from IDMC and EM-DAT with the GFD satellite imagery of historic floods event by

event, to develop the new open source dataset FLODIS which provides observed, spatially explicit flood hazard data for hundreds of human displacement and emergency events.

We first assign an affected area to each entry in the IDMC database, using geographic information contained in the database and a tailored geocoding algorithm. Affected areas for EM-DAT are provided by the Geocoded Disasters (GDIS) dataset (Rosvold and Buhaug, 2021). We then match affected areas of IDMC and EM-DAT with the GFD satellite imagery in space and time. The final product FLODIS contains 335 human displacement (IDMC) entries and 695 mortality/damage (EM-DAT) entries linked with GFD flood information (Figure 3.1). FLODIS allows investigations on cross-country but also within-country variations in flood risk. In addition, we overlay the flood extent with sub-national, rasterized socio-economic data, to estimate the number of affected people, affected assets, and critical infrastructure as well as event-specific societal and environmental conditions. This extensive set of socio-economic variables associated with each flood-impact event further facilitates various types of studies, for example multivariate analyses of the drivers of flood vulnerability.

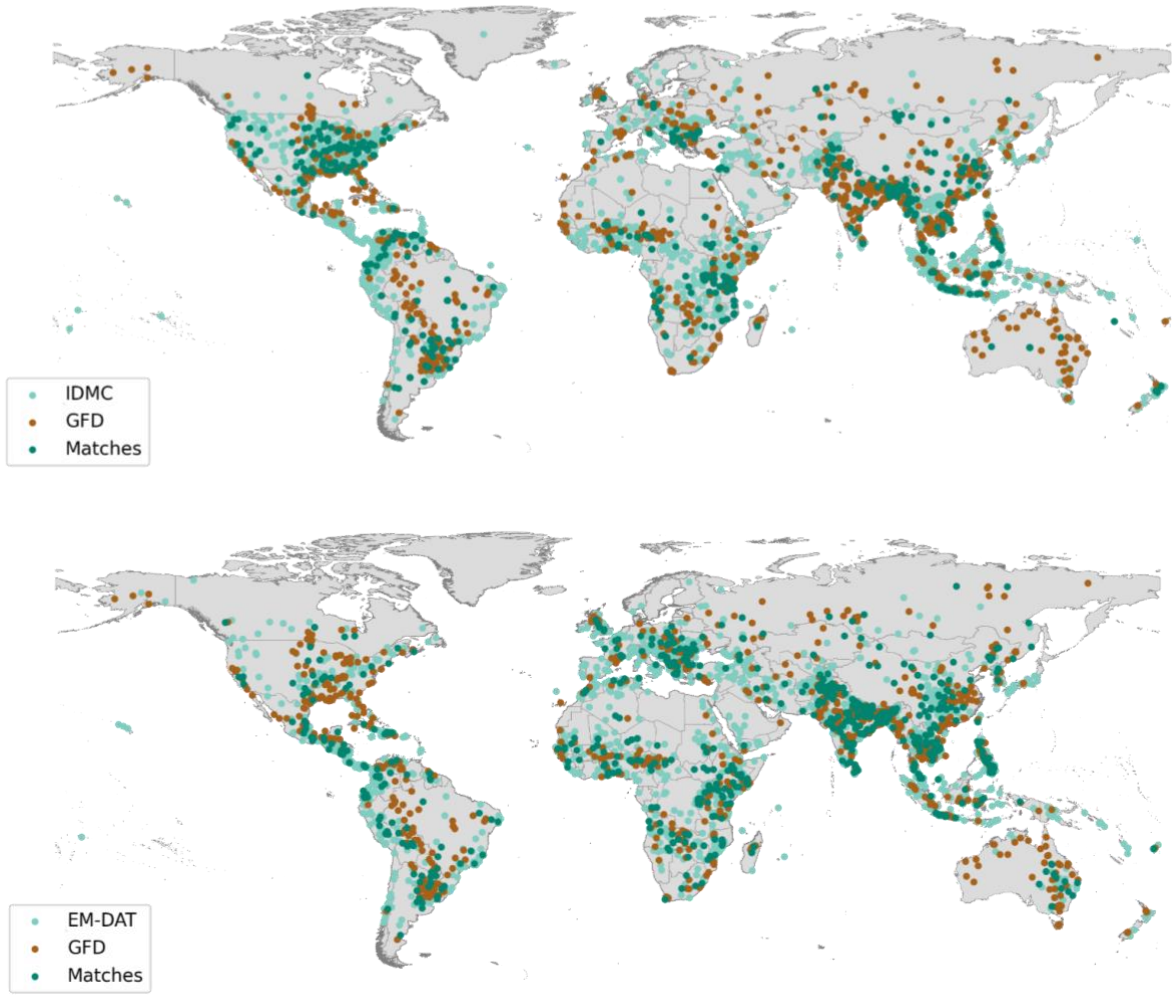

1

Figure 3.1: Location overview of all GFD floods (brown), as well as IDMC events (top), and GDIS events (bottom) associated with flooding between 2000 and 2018. Affected disaster areas are displayed (light green), as well as the ones successfully matched with the GFD (dark green). Note: Only the centroids of the polygons are shown, some polygons are merged to a single FLODIS disaster entry in the final processing steps.

3.2 Methods

The IDMC database contains 3083 unique displacement events with the cause being indicated as “Flood” between 2008 and 2018, each including the number of displaced persons and a starting date. For some events, more detailed information is given in the “Event Name” variable. This string can vary from being empty to containing additional information describing the event, such as flood type, duration and affected locations. In a first step we exploit the “Event Name” variable to identify one or several sub-national regions (provinces or districts)

where the event occurred (Figure 3.2, step a), using the Global Administrative Areas (GADM) database v.3.4 (GADM, 2018). Note that for provinces and districts in Great Britain we used the 2nd and 3rd sub-national level GADM data, as England, Wales, Scotland and Northern Ireland are listed on the 1st level.

We perform a transliteration process, which converts diacritics to letters of the alphabet for Modern English, e.g., the French accents la cédille “ç” and l'accent aigu “é” become “c” and “e”, respectively. An automated script then calculates for every word within the “Event Name” string its spelling similarity with the 3610 provinces and 45.962 districts in the GADM database, using a similarity score defined as:

$$Similarity\ Score = \frac{2*M}{T} \qquad (1)$$

where M is the sum of sizes of all matched sequences and T is the total number of characters in both sequences. It ranges from 0 to 1, where 1 represents a perfect similarity. A successful match between a IDMC word and a GADM province or district name requires the same ISO3 country code as well as a Similarity Score greater than 0.8. This threshold was found to assure a high degree of similarity while allowing for smaller deviations. For example, the Algerian province “Tamanghasset” (GADM) is written as “Tamanrasset” in an IDMC entry, resulting in a similarity value of 0.87 with M=10 and T=23. We additionally computed similarity scores for the “VARNAME_1” and “VARNAME_2” variables in the GADM database, which cover spelling variants of the provinces and districts, respectively, and assigned the province or district to the event if at least one of the scores exceeded 0.8. Referring to the previous example, “Tamanrasset” is also found as a spelling variant in the “VARNAME_1” variable. The geometries of all matched GADM provinces or districts are then merged for every event into a single area, which represents the smallest identifiable area associated with the displacement event (“displacement region”). If no provinces or districts are found, the national area of the country within the event occurred is used. For entries between 2008 and 2012 in the IDMC database, the “Event Name” column is empty, thus the corresponding national areas are used for all those events. Matching displacement events to observed floods, as described below, yields accurate location information for many of these early events too.

For a total of 3083 IDMC entries labeled as “Flood” we geocoded 1702 entries (1157 entries with at least one province, 1074 entries with at least one district, and 529 entries with both at least one province and one district). It should be noted that 688 entries do not contain any event information and others only non-location related information, e.g., “March Floods”.

For information on fatalities and damages, we use the GDIS (Rosvold and Buhaug, 2021), which provides GIS polygons for each disaster location in the EM-DAT database. We

extract 2390 entries with the disaster type “flood” between 2000 and 2018, for which we also obtain the corresponding disaster information, e.g., number of fatalities or total damage, from the EM-DAT database.

In the next step, we perform a spatial and temporal event matching procedure between the IDMC displacement events and EM-DAT/GDIS disaster events on the one hand, and the GFD floods on the other hand (Figure 3.2, step b). The GFD provides surface water extent for 913 large flood events documented by DFO (Tellman et al., 2021). The data covers the years from 2000 to 2018 and is based on MODIS satellite imagery at 250 m resolution. The matching procedure needs to consider the fact that some flood events affected multiple countries, and could therefore be related to multiple displacement or disaster entries, but are only assigned to one country in the GFD inventory. Simply matching the ISO3 country codes between GFD and the IDMC or EM-DAT databases is therefore not sufficient, and we instead consider the actual spatial overlap between flooded area and the region associated with the disaster, as identified above. A second consideration is that distinct floods may have occurred simultaneously in the same country but in different locations, and we use both temporal and spatial information to avoid false matches in such cases.

Two conditions must be hence fulfilled for a successful match: (i) the affected disaster area must intersect with the GFD event polygon and (ii) the starting date difference must be equal or less than 30 days. We thereby ensure a merging of the databases with high accuracy while allowing for minor deviations in time and space due to, e.g., inaccurate or ambiguous starting date information (e.g. the displacement database might indicate the first day of the month when the exact day is unknown; or the date of satellite observation might not match the date of the disaster record during longer events). If two or more GFD entries are matched to a single disaster entry, we keep entries with a starting date difference equal or less than 14 days. In the case no entries meet this criteria, the smallest date difference for this event is determined and GFD entries with a higher date difference are discarded (Figure 3.2, step c). The resulting GFD flooded areas are merged and cropped to the extent of the IDMC/EM-DAT affected disaster area.

We then compute the number of affected people using the Global Human Settlement Layer (GHSL) (Schiavina et al., 2019), and gridded population of the world version 4 (GPW) (CIESIN, 2018a), the number of affected assets using gridded Gross Domestic Product counts (GDP) (Kummu et al., 2018) and the number of affected critical infrastructure entities/units. As the population and asset count data is only available for certain years (GHSL: 2000 and 2015; GPW 2000, 2005, 2010, 2015, and 2020; GDP: 2000-2015), we linearly interpolate/extrapolate the missing years to create a continuous annual time series for every dataset between 2000 and 2018. The critical infrastructure entities are extracted from the

Critical Infrastructure (CI) dataset (Nirandjan et al., 2022), which is based on Openstreetmap and lists the number of entities per grid cell, e.g., 20 communication masts are located in one cell. The information on critical infrastructure is based on the year 2022 and values within FLODIS are assumed to be the same for the period of 2000 to 2018. By overlaying the (merged) GFD flood extent with each gridded dataset, we compute the sum and mean of affected entities, accounting for every grid cell touched by the flood extent (Table 3.1). Additionally, we also append FLODIS with a set of gridded socio-economic indicators (Table 3.2) by computing the mean of all grid cells touched by the flood extent. If several disaster entries are assigned to the same GFD flood(s) and the same country, all entries are merged to link the GFD flood extent to one combined disaster (Figure 3.2, step d). This procedure reduces the number of displacement entries from 524 to 335, and the number of mortality/damage entries from 816 to 695. In the last step, the entries are cleaned and merged to the final FLODIS disaster dataset (Figure 3.2, step e).

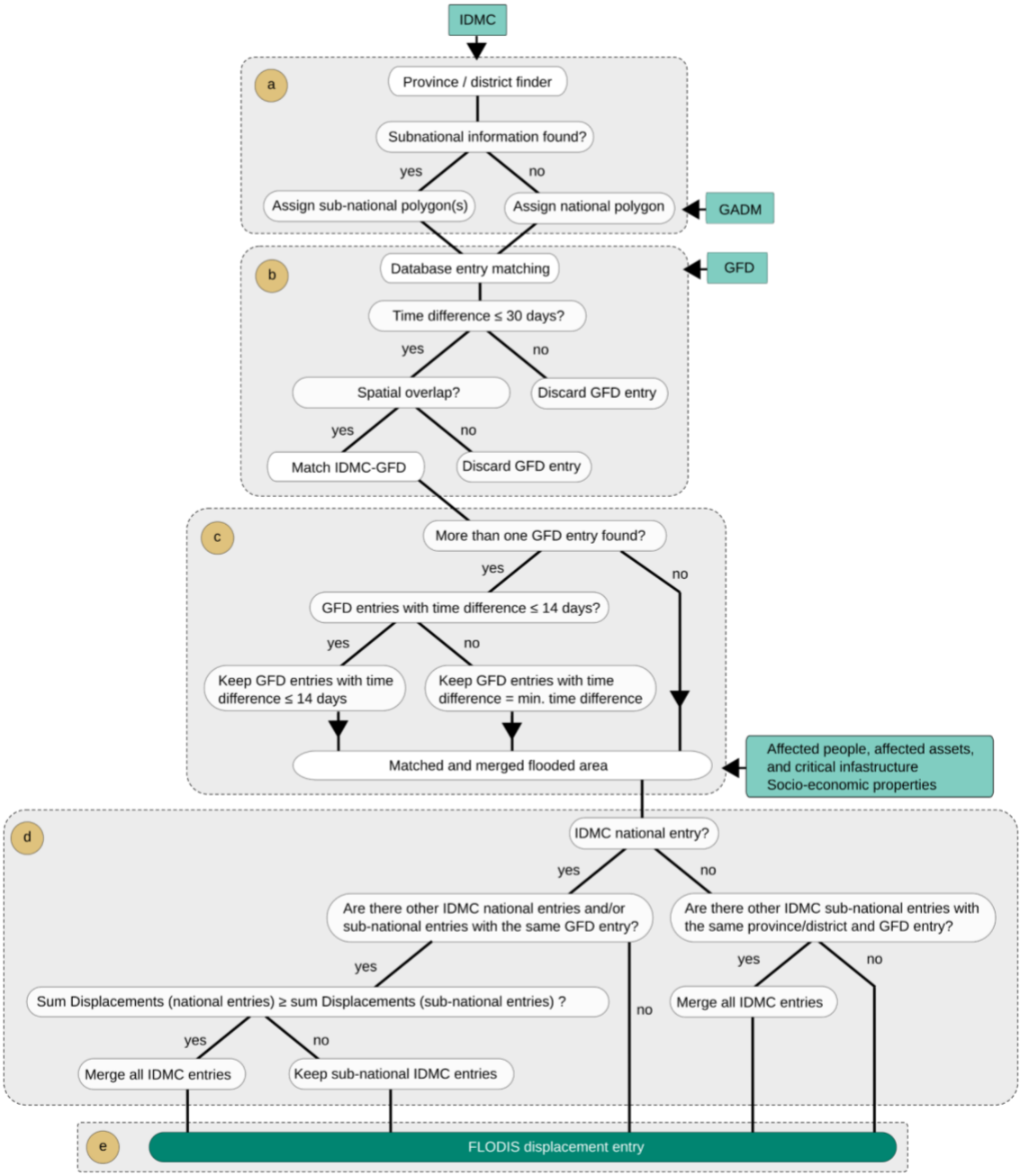

Figure 3.2: Flowchart of the database merging process between IDMC and GFD database, including the used datasets (light green) and processing steps (brown, a-e). Sub-national information (provinces and districts) is extracted for 3083 entries of the IDMC displacement data bank ***(a)****. 913 flood events of the Global Flood Database serve as a hazard approximation, and are matched with every IDMC entry using location information and time stamps* ***(b)****. If several GFD entries are matched, a multi-criteria scheme is applied to identify and merge flood extents belonging to the same displacement event* ***(c)****. The matched and merged flooded area is used to estimate the affected people, assets, critical infrastructure as well as sub-national, socio-economic characteristics of the disaster. Next, it is checked whether (sub-)national IDMC entries belong to the same disaster (****d)*** *to generate a final FLODIS displacement entry* ***(e)****. Note: for EM-DAT no (sub-)national information is available as no matching process as in* ***(a)*** *is performed, hence the duplicate check is simplified in* ***(d)****.*

Table 3.1: Overview of affected entity datasets, including their spatial and temporal resolution. Population counts and assets datasets are linearly interpolated and extrapolated between 2000 and 2018. "Critical Infrastructure Total" is a dimensionless value ranging between 0 and 1.

Affected entity dataset	Category	Spatial resolution	Temporal resolution	Source
Population count (GHSL)	Development	0.5 arcmin	2000, 2015	(CIESIN, 2018a; Schiavina et al., 2019)
Population count (GPW)	Development	0.5 arcmin	2000, 2005, 2010, 2015, 2020	(CIESIN, 2018b)
Assets (GDP PPP const. 2011 int. USD)	Economic	5 arcmin	2000-2015	(Kummu et al., 2018)
Reservoir (water storage)	Water	6 arcmin	2022	(Nirandjan et al., 2022)
Electric cable	Energy	6 arcmin	2022	"
Power line	Energy	6 arcmin	2022	"
Power plant	Energy	6 arcmin	2022	"
Power pole	Energy	6 arcmin	2022	"
Power tower	Energy	6 arcmin	2022	"
Communication tower	Telecommunication	6 arcmin	2022	"
Communication mast	Telecommunication	6 arcmin	2022	"
Doctor	Health	6 arcmin	2022	"
Hospital	Health	6 arcmin	2022	"
Pharmacy	Health	6 arcmin	2022	"
Primary road	Transportation	6 arcmin	2022	"
Tertiary road	Transportation	6 arcmin	2022	"
School	Education	6 arcmin	2022	"
University	Education	6 arcmin	2022	"
Critical Infrastructure Total	Development	6 arcmin	2022	"

Table 3.2: Overview of gridded socio-economic indicator datasets used to characterize the area affected by the flooding, including their spatial and temporal resolution. Population density datasets are linearly interpolated and extrapolated between 2000 and 2018. Human development index and GDP per capita datasets are linearly extrapolated between 2015 and 2018.

Socio-economic dataset	Category	Spatial resolution	Temporal resolution	Source
Population density (GHSL)	Development	0.5 arcmin	2000, 2015	(CIESIN, 2018a; Schiavina et al., 2019)
Population density (GPW)	Development	0.5 arcmin	2000, 2005, 2010, 2015, 2020	(CIESIN, 2018b)
Female population (% of total population)	Demographic	0.5 arcmin	2010	(CIESIN, 2018a)
Population ages 0-14 years (% of total population)	Demographic	0.5 arcmin	2010	(CIESIN, 2018a)
Population ages 65+ years (% of total population)	Demographic	0.5 arcmin	2010	(CIESIN, 2018a)
Human development index	Economic / Development	5 arcmin	2000-2015	(Kummu et al., 2018)
GDP per capita PPP const. 2011 int. USD	Economic	5 arcmin	2000-2015	(Kummu et al., 2018)
Forest cover	Environment	30 m (resampled to 300 m)	2010	(Hansen et al., 2013)
Land use	Environment	30 arcmin	1901-2019	https://www.isimip.org; (Goldewijk, 2016; Hurtt et al., 2020; Monfreda et al., 2008)
Urbanization	Development	30 arcmin	1901-2019	https://www.isimip.org; (Goldewijk, 2016; Hurtt et al., 2020; Monfreda et al., 2008)
Modeled flood protection	Development / Adaptation	1st subnational layer (province)	approx. 2015	(Scussolini et al., 2016)
Merged flood protection	Development / Adaptation	1st subnational layer (province)	approx. 2015	(Scussolini et al., 2016)

3.3 Data records

FLODIS is publicly available from a Zenodo repository (Mester et al., 2022a), and the following GitHub repository: https://github.com/BenediktMester/FLODIS (Mester et al., 2022b). Three datasets exist: (i) the IDMC displacement dataset appended with the detected provinces and districts and the corresponding GADM sub-national codes; this also includes displacement events which were not matched with any flood data as well as other hazard types. For a total of 11731 IDMC entries we geocoded 7915 entries (5893 entries with at least one province, 5740 entries with at least one district, and 3718 entries with both at least one province and one district. 1202 entries do not contain any event information. The data is available as a CSV file. (ii) IDMC displacement events linked with GFD entries, and (iii) EM-DAT fatality and asset damage events linked with GFD entries. (ii) and (iii) are available as CSV files, including the GFD IDs, GDIS disaster numbers, and GADM codes. The GitHub repository and Zenodo repository contain more detailed information on the datasets used.

3.4 Technical validation

As FLODIS is the first data product of its kind, a direct comparison with existing datasets is not possible. Nonetheless, to assess the quality of FLODIS, we analyze the detection rates of the geocoding algorithm, and check for temporal and spatial biases within the FLODIS datasets.

First, we assess the geocoding algorithm used to extract subnational information out of IDMC entries. The number of entries within the IDMC database continuously increases between 2013 and 2021 (Figure 3.3). The share of entries without any detectable subnational information is decreasing, which indicates an improved reporting on affected locations over time. For almost 20% of all IDMC entries no geocoding is possible, even though event information is available (Figure 3.4). This can be mostly explained by missing location information, or the geocoding algorithm failing to extract the information, e.g., if it is embedded in more complex sentence structures. The number of detected provinces is higher than the number of detected districts, which likely reflects that detailed subnational disaster information is still often missing.

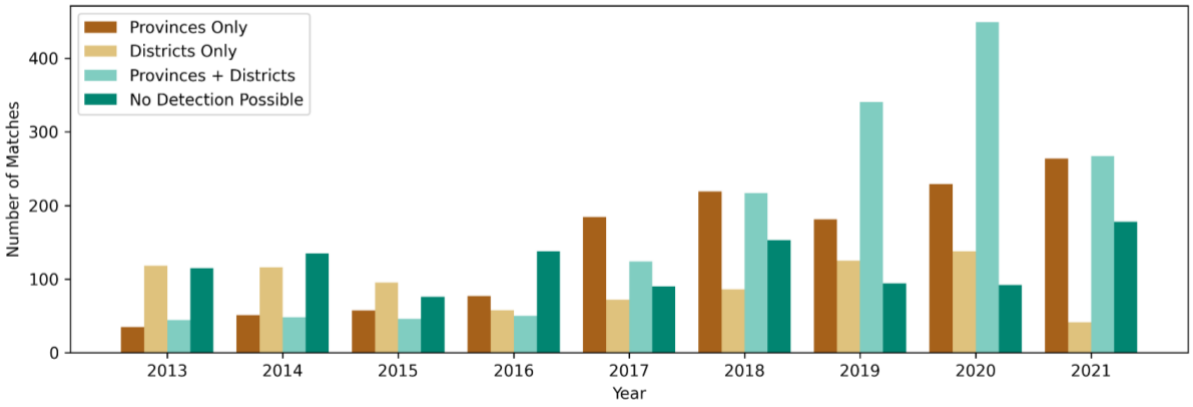

Figure 3.3: Number of detected provinces and districts by the IDMC database geocoding over time . No subnational event information is available before 2013.

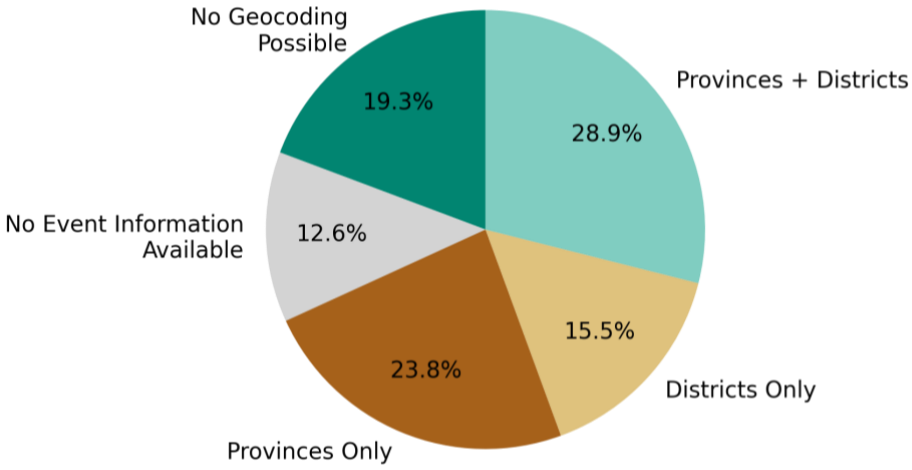

Figure 3.4: Share of detected provinces and districts by the IDMC database geocoding (2008-2021). Note: prior to 2013 no event information is available.

We then determine the number of matches between the GFD and IDMC/EM-DAT over time. Starting in 2014, the number of successful matches increases for the IDMC database, which can be mostly explained with an increase in event reporting (Figure 3.5). The rate for the EM-DAT quickly increases, peaks in 2007, and then continuously decreases. Global warming, population growth, and shifting settlement patterns lead to changes in event frequency, however, the number of yearly reported EM-DAT entries tends to have stabilized since the early 2000s (Rosvold and Buhaug, 2021). Most matches are located in India, China, and USA; for IDMC many matches can be also found in Indonesia and Argentina, whereas matches for EM-DAT accumulate in Pakistan and the Philippines (Figure 3.1). It is observable that a low ratio of matched IDMC events is present in some countries and world regions, e.g.,

Afghanistan or Central America. Additionally, more events are reported by the GFD than by the disaster databases in some regions, e.g., several provinces in Australia. For both databases, approximately 85% of all matches are associated with only one GFD entry, while matches with two (11-12%) or more GFD entries (3-4%) are relatively rare (Figure 3.6).

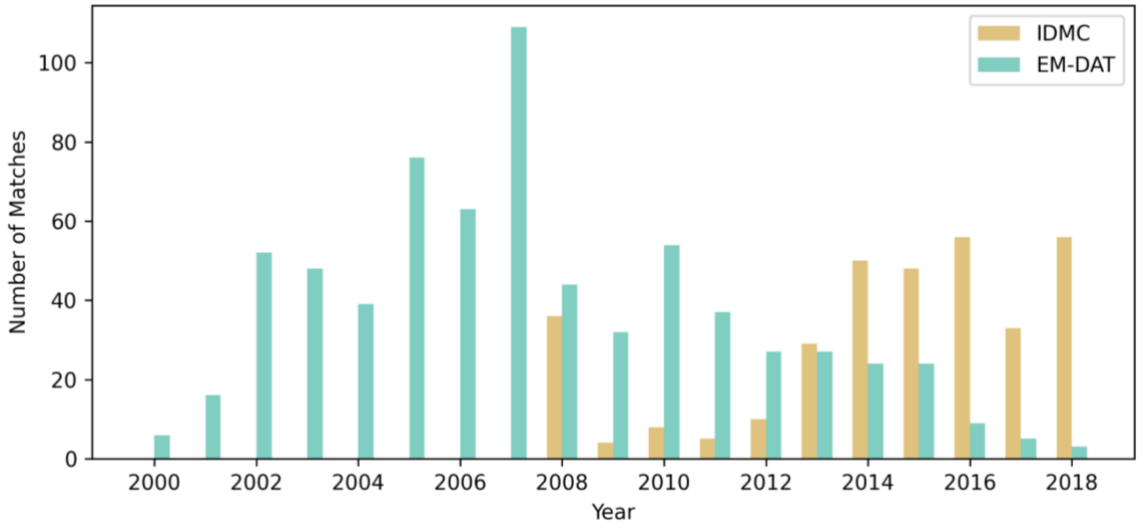

Figure 3.5: Number of GFD matches with IDMC/EM-DAT per year over time. Note: No subnational event information is available for the IDMC database before 2013.

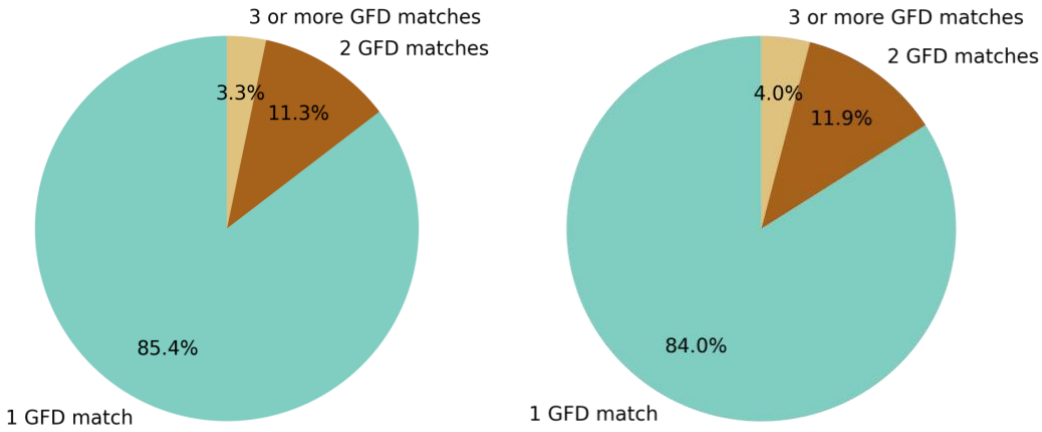

Figure 3.6: Number of GFD events matched per IDMC entry (left) and EM-DAT entry (right).

3.5 Usage notes

Eight matched IDMC entries and 114 matched EM-DAT entries provide no information on the number of displacements, and fatalities/damages, respectively. Nonetheless, it is now possible with FLODIS to determine the exposure and estimate the number of displacements, fatalities, and damages using, for example, vulnerability functions. In addition, FLODIS provides EM-DAT information on the “No Injured”, “No Affected”, ”No Homeless”, and “Total Affected”.

The analysis of FLODIS datasets can be extended by calculating derivatives, e.g., the vulnerability by dividing an observed impact with the number of affected entities. The FLODIS entries can also be appended with additional affected entities or socio-economic indicators using the temporal information, the provided disaster area IDs for gridded datasets, or ISO3 codes for national information.

The geocoded IDMC dataset may be linked with other hazard databases using the provided start date information, GADM codes, and the matching scripts. The geocoding script may also be used to identify locations within other disaster database entries. A manual/automatic inspection is recommended to ensure a sufficiently high geocoding rate. The Similarity Score threshold can be adjusted for this purpose.

3.6 Code availability

The source code for this study is publicly available through the following GitHub repository: https://github.com/BenediktMester/FLODIS (Mester et al., 2022b). It includes the geocoding algorithm to extract subnational information out of the IDMC database, as well as the main scripts to match the IDMC/EM-DAT database with the GFD. We also provide code for the preprocessing of input datasets, the validation procedure, and the development of the figures. The repository includes an extended list of input datasets with download links and additional information.

3.7 Acknowledgments

This research received funding from the European Union’s Horizon 2020 research and innovation programme under grant agreement No 820712 (RECEIPT).

Chapter 4 A global-scale vulnerability assessment of flood-induced human displacement

Authors:
Benedikt Mester
Bina Desai
Katja Frieler
Oliver Korup
Jacob Schewe

Manuscript in progress:
Mester, B., Desai, B., Frieler, K., Korup, O., and Schewe, J. (in progress). A global-scale vulnerability assessment of flood-induced human displacement.

Abstract

Floods displace an average of 12 million people every year, being responsible for 54% of all disaster-induced displacements. While flood hazard is expected to increase in many regions due to climate change, displacement also depends on the specific vulnerability of affected populations, which is poorly understood at the global scale. This study aims to identify factors that influence vulnerability to flood-induced displacement, and that might help explain observed differences in vulnerability between countries and regions, and potentially predict changes in vulnerability over time. We combine global databases of flood observations and displacement events to calculate vulnerability - the ratio of displacement to exposure - for 311 historical flood events. We find that between and within continental regions, national average displacement vulnerability varies by several orders of magnitude. We apply a machine learning framework to identify the most important determinants of displacement vulnerability. Random forest methods explain variance with R2s of up 0.3, however, singling out the best predictors remains difficult. We show that in most cases the level of human development, e.g., urbanization, is positively related to a reduction in vulnerability. Some predictors which exhibit a high correlation with GDP per capita, such as infant mortality rate or age cohorts, have a better explanatory power than economic wealth itself. We therefore recommend that, in addition to economic dimensions, a number of contextual indicators be considered in studies of vulnerability to displacement. Our study is a first step towards a better understanding of

displacement vulnerability which is strongly under-researched compared to vulnerabilities to direct economic damages.

4.1 Introduction

In the last decade alone, more than 100 million people worldwide have been displaced due to flooding (IDMC, 2022). Displacement is a product of the physical properties of flooding (hazard), the exposure of people living in floodplains, and the susceptibility and lack of resilience to being displaced (vulnerability) (Cardona et al., 2012; Oppenheimer et al., 2014). Flood hazard has been changing (Berghuijs et al., 2017; Blöschl et al., 2020; Fowler et al., 2021; Gudmundsson et al., 2021) and, in particular with respect to rare, large floods, is expected to increase in many regions under continued climate change (Hirabayashi et al., 2013; Lange et al., 2020; Milly et al., 2002). At the same time, more than 20% of the world's population are currently exposed to high flood risk (Rentschler et al., 2022), and population growth and urbanization are set to further increase exposure particularly in lower-income countries (Jongman et al., 2012; Winsemius et al., 2016). Against this backdrop, it is important to understand and quantify flood displacement vulnerability - the third component of the risk equation. Knowing what determines vulnerability is useful for deciphering the relative roles of different drivers of past displacement, for instance, the contribution of climate change to recent displacement events (Mester et al., 2023b); it is necessary for estimating future changes in displacement risk; and it could help identify ways to improve the resilience of affected communities, thereby reducing displacement risk.

However, there is no quantitative framework that explains the vulnerability to flood-induced displacement at the global scale. It has been shown that the ratio between displacement and exposure (the empirical vulnerability) at the national level is generally low in countries with gross national income above a certain level, while it can take both low and high values in poorer countries (Kakinuma et al., 2020). However, it is not clear how much of the variation in observed vulnerabilities can be explained by national income levels, nor through what functional relationship. Even less is known about the role of other, non-economic and/or more local factors, such as urban development, demographic composition of the population, or social disparities. Consequently, the single existing study of future changes in global flood-displacement risk only accounts for changes in hazard and exposure, whilst assuming constant levels of vulnerability (Kam et al., 2021). Specifically, it assumes that all people exposed to inundation larger than a certain threshold (e.g. 1 m) are at risk of being displaced. This is based on estimates of expected structural damage to residential buildings (Nadal et al., 2010; Custer & Nishijima, 2015). Similarly, an operational model of displacement

risk developed by the Internal Displacement Monitoring Center (IDMC) is based on housing destruction as a proxy for displacement (Anzellini et al., 2017). Thus, these methods incorporate an important aspect of physical vulnerability, namely, the susceptibility of residential buildings to be damaged or destroyed by flooding. However, they do not represent the potential role of other physical factors, such as local flood protection infrastructure or damages to critical infrastructure related to energy, water, or other public services; nor do they consider socio-economic factors that might make some populations more vulnerable than others to being displaced, even under similar physical circumstances. Related to this, it is unknown whether and how displacement vulnerability has changed over time, or how it differs between different countries and subnational regions, apart from differences in prevalent building types which are implicitly considered in the IDMC model (Anzellini et al., 2017).

This contrasts with the literature on other types of flood impacts, namely economic losses and fatalities. It has been shown that vulnerabilities to losses and mortality from flooding have been changing over the last half-century in non-trivial ways, and that these changes can at least partly be explained by changes in income levels and improvements in flood protection measures (Jongman et al., 2015; Tanoue et al., 2016; Formetta et al., 2019; Sauer et al., 2021). These global studies also find different trends between different world regions and country groups. There is no analogous research with respect to displacement vulnerability, which may be due in part to the shortness of displacement records compared to records of losses and fatalities: The IDMC provides systematic accounts of displacement events starting in 2008, and corresponding subnational location information is available mostly after 2012. Nevertheless, even if the record is too short to derive meaningful trends in displacement vulnerability, it is of high interest to understand how and why observed vulnerabilities differ between individual events and between countries and regions.

Here we address this research question. We combine reported displacement data with remote sensing-derived flood extent data and gridded population estimates in order to calculate vulnerability, as the ratio between displacement and flood exposure, for 311 recent large flood events around the world. We then employ two multivariate regression techniques - simple linear regression and non-linear random forest (Breiman, 2001) - within a machine learning framework to examine the ability of a set of potential predictors to explain the observed variation in event-specific vulnerabilities. Several aspects set this study apart from previous global studies of flood vulnerability (e.g. Jongman et al. (2015); Tanoue et al. (2016); Kakinuma et al. (2020)). First, using remotely sensed, rather than modeled, flood hazard data eliminates flood modeling uncertainty and allows us to estimate exposure associated with each event relatively accurately. Second, utilizing partially geocoded displacement information on level-1 or level-2 subnational administrative units (e.g. province or district, respectively),

allows the use of the corresponding subnational predictor values in the multivariate regression. Thus our analysis addresses not only across-country but also within-country variations in displacement vulnerability. Third, multivariate regression has not been applied in any of the above-mentioned vulnerability studies, which focused instead on individual predictors of flood impacts such as national income or population size. Drawing from a larger set of plausible predictors, and employing both linear and non-linear regression techniques, our analysis can also account for non-linear effects of individual explanatory factors, as well as for interactions between different explanatory factors.

4.2 Data and methodology

4.2.1 Flood-induced displacement vulnerability

Here we go beyond previous national-level studies by analyzing vulnerability for individual events, as measured by the ratio of reported displacement to estimated exposure. Estimating flood exposure requires spatially resolved flood extent data. Given that comprehensive in-situ observational data, such as from water level gauges, are rarely available, global flood models or remote sensing products are the only viable options to estimate flood extent for a large number of events on a global scale (Alfieri et al., 2018).

On the one hand, global flood simulations forced by observational weather data clearly have the advantage of complete spatial coverage and have already demonstrated to provide significant explanatory power when it comes to reported annual damages and mortalities. Recent studies of vulnerability related to damages and mortality (Jongman et al., 2015; Sauer et al., 2021; Tanoue et al., 2016) and displacement (Kakinuma et al., 2020) are all based on global hydrological simulations, and often use the information about flood depth provided by the models. However, despite remarkable improvements over the past years (Bates et al., 2021, 2018; Yamazaki et al., 2014) and extensive model intercomparison projects (Bernhofen et al., 2018; Trigg et al., 2016), the realism of global flood model simulations is still limited due to a number of factors, such as the flood frequency analysis (Zhou et al., 2021), the representation of flood defenses (Bates et al., 2021), or the river channel geometries (Ward et al., 2015). The ability of models to reproduce observed flood extents also depends on the river runoff data used to force them, and many of the global hydrological models providing this runoff data appear to overestimate the frequency of high-runoff events, resulting in a mismatch between simulated flood frequency and reported flood protection levels (Mester et al., 2021). Thus, estimates of event-level flood exposure using global flood models may carry large biases.

Remote sensing, on the other hand, can partly overcome these limitations. Satellite imagery captures actual observed flooded areas, implicitly accounting for flood protection (Alfieri et al., 2018) and other non-climate related determinants of flood extent such as land use and infrastructure (Tellman et al., 2021). However, until recently, only a limited number of spatially resolved satellite records of past floods was publicly available, mainly provided by the archive of the Dartmouth Flood Observatory (DFO) and the United Nations Operational Satellite Applications Programme (UNOSAT). With the release of the Global Flood Database (GFD; http://global-flood-database.cloudtostreet.info/), a product based on the DFO (http://floodobservatory.colorado.edu), an unprecedented inventory of satellite imagery is now accessible (Tellman et al., 2021). The GFD includes gridded observations of 913 large flood events from 2000 to 2018 on a fine spatial scale of 250 m.

Here, we utilize this database to estimate flood exposure for several hundred events for which we were able to identify associated displacement records. First, we geocode the Global Internal Displacement Database (GIDD) to allocate sub-national administrative units (provinces and districts) to each displacement event related to flooding. Next, the GFD and the geocoded GIDD are merged in space and time using the geographic information and timestamps, respectively. This yields the unique dataset FLODIS compromising both flood hazard and the associated number of displacement for 311 events that occurred in 72 countries between 2008 and 2018 (Mester et al., 2023a). Here, we make use of this dataset to develop a better understanding of flood-induced displacement vulnerability and its contextual indicators, which are provided for each FLODIS entry as well (Figure 4.1).

For each observed event, we compute the empirical displacement vulnerability by dividing the reported number of displaced people by the estimated number of exposed people. We also compute for each of the 72 countries the median vulnerability across all events observed in the country. This allows us to perform two separate regression analyses of the predictors of flood-induced displacement vulnerability: First, a country-level analysis with the 72 national median entries and predictor variables measured at the national level; second, an event-level analysis using all 311 events and predictor variables measured at the sub-national level. In this second analysis, we account for country-specific random effects on the error distribution of the regression model.

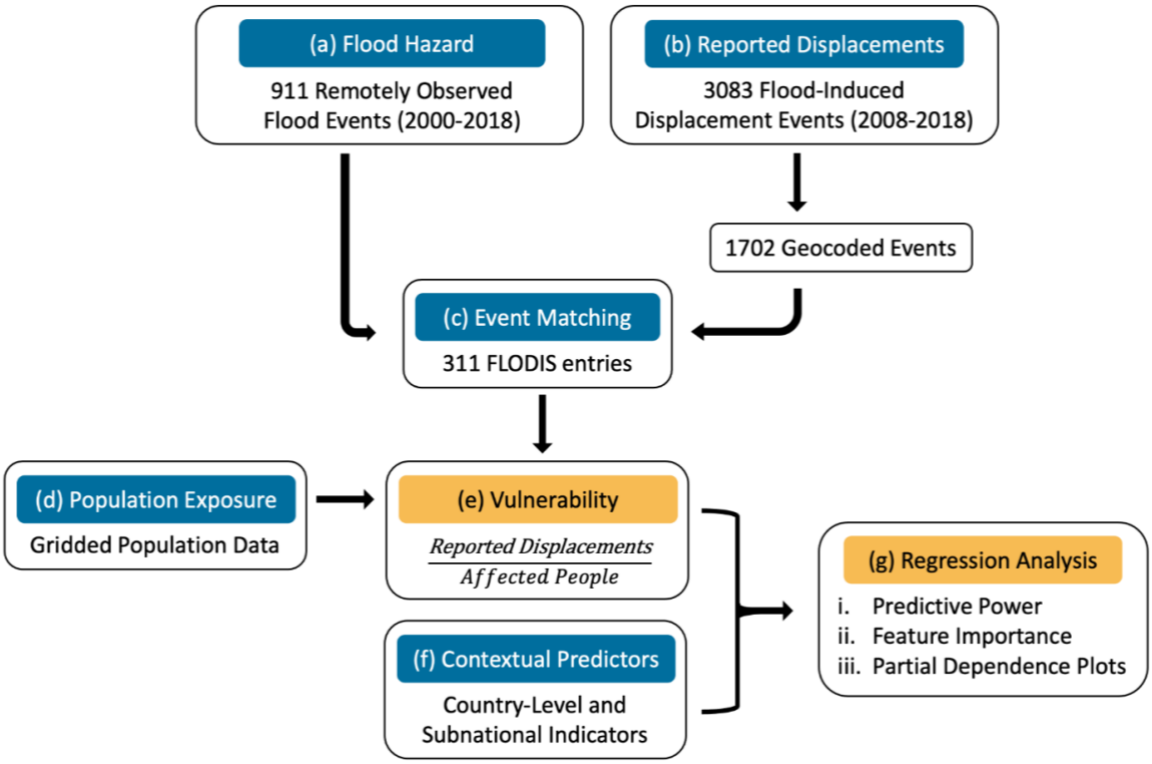

Figure 4.1: Schematic workflow of the data and methods used to derive event-specific vulnerabilities and the predictor assessment. 913 flood events of the GFD ***(a)*** *serve as a hazard approximation; 3083 flood-induced displacement events of the GIDD exhibit information on the number of displacements* ***(b)****. After geocoding the GIDD, events of both databases are matched in space and time* ***(c)****. Dividing the number of reported displacements by the number of simulated affected people* ***(d)*** *yields 311 event-specific vulnerabilities* ***(e)****. Next, country-level and subnational predictors are assigned to each event* ***(f)****. In the final regression analysis, the most important predictors and their influence on vulnerability is assessed* ***(g)****.*

4.2.2 Vulnerability predictors

In the next step, the conditioning factors which drive the vulnerability to flood-induced displacement are selected. Displacement vulnerability refers to the tendency of exposed human beings to be evacuated or lose their homes. Generally, a low or uneven level of development is associated with multi-dimensional inequalities which increases vulnerability towards disaster-induced displacement (Oppenheimer et al., 2014; The Nansen Initiative, 2015). Factors that influence vulnerability can be categorized into families of drivers, such as socio-economic status, household characteristics, demography, education, or infrastructure (Black et al., 2011). Economic drivers, for example, household income or GDP per capita, are of primary focus for displacement risk, as poor populations reside disproportionately in proximity to exposed riverbanks (Winsemius et al., 2018), have less capacity to adapt and prepare in situ (Cissé et al., 2022; Morrow, 1999), and often live in poorly constructed houses or mobile homes with less resistance against extreme flooding (Daley et al., 2005; Flanagan

et al., 2011). Other non-economic drivers, such as age, gender, recent migrants, or health status, can also influence the vulnerability substantially (Oppenheimer et al., 2014).

However, drawing conclusions from other studies about the role of conditioning drivers of climate mobility should be treated with caution (Cattaneo et al., 2019), as it is unclear how these findings translate to vulnerability to flood-induced displacement, given the strong dependencies on the characteristics of the flood events and their societal context (Rufat et al., 2015). We therefore choose a set of the most common vulnerability predictors and assess the plausibility in the context of vulnerability to flood-induced displacement. Our selection aims to identify the most representative predictor per driver family while incorporating as many societal dimensions as possible. In total, the selection comprises 13 subnational predictors for the event-level analysis, 11 national predictors for the country-level analysis, and six predictors available in both analysis types. The event-level analysis comprises predictors of the FLODIS dataset covering the event duration, flood protection, elevation, slope and the density of health, education, and overall critical infrastructure. For the national-level analysis we apply World Bank's World Development Indicators (WDI) on infant mortality rate, population growth, urbanization growth, stock of international migrants (WDI, 2022). Additionally, we create a proxy for national flood experience by computing for every country the number of flood events during the last ten years according to DFO, normalized by the World Bank national population size. For both analysis types we use information on the population density, share of female population, GDP per capita, urbanization, population ages 0-14 and population ages 65+ years. An overview of all predictors, the associated driver families and potential causal mechanism is presented in Table 4.1. We also introduce a "dummy" variable to control for model variability.

Table 4.1: Overview of subnational and national predictors, including a description of (plausible) causal mechanisms. "/" indicates that the predictor is not available.

Predictor	Category	Spatial resolution sub-national	Source sub-national	Source national	(Plausible) Causal mechanism
Population density	Demographic	0.5 arcmin	(Schiavina et al., 2019)	(WDI, 2022)	Event-level: infrastructure/building types; national-level: development/wealth
Female population	Demographic	0.5 arcmin	(CIESIN, 2018a)	"	Gender inequality
Population ≤ 14 years	Demographic	0.5 arcmin	"	"	Lack of coping mechanisms and resources; development
Population ≥ 65 years	Demographic	0.5 arcmin	"	"	Physical limitations; development
GDP per capita PPP	Economic	5 arcmin	(Kummu et al., 2018)	"	Development/wealth
Urbanization	Demographic	30 arcmin	https://www.isimip.org; (Goldewijk, 2016; Hurtt et al., 2020; Monfreda et al., 2008)	"	Development/wealth
Urbanization growth	Demographic	/	/	"	Development/informal settlements
Population growth	Demographic	/	/	"	Development/growth in flood plains at high risk
Infant mortality rate	Social / Health	/	/	"	Social inequality/health
International migrant stock	Demographic	/	/	"	Closer social ties/lack of acculturation
Flood protection	Adaptation / Economic	1st subnational layer (province)	(Scussolini et al., 2016)	/	Flood risk awareness
Event duration	Flood characteristic	per event	(Tellman et al., 2021)	/	Intensified flooding
Flood experience	Adaptation	per country	/	http://floodobservatory.colorado.edu	Flood risk awareness
Education infrastructure	Infrastructure/ Education	6 arcmin	(Nirandjan et al., 2022)	/	Development/flood risk awareness
Health infrastructure	Infrastructure/ Health	6 arcmin	"	/	Development/social inequality
Total critical infrastructure	Infrastructure	6 arcmin	"	/	Development/wealth
Elevation	Flood characteristic	0.54 arcmin	(Amatulli et al., 2018)	/	Intensified flooding
Slope	Flood characteristic	0.54 arcmin	"	/	Intensified flooding

4.2.3 Predictor assessment

In this section we introduce the regression models, methods to assess the predictor importance, and visualization techniques for predictor dependence. First, we establish multivariate linear regression and random forest models that predict the level of vulnerability based on the diverse set of socio-economic predictors. Next, we rank the predictors by their relative contribution in predicting vulnerability. Lastly, we visualize and analyze the interaction between vulnerability and individual predictor variables.

4.2.3.1 Regression models

We use two types of regression models to estimate the relationship between the vulnerability to flood-induced displacement and its predictors: linear regression and random forests. The ordinary least squares linear regression predicts the target variables by a linear approximation and minimizes the residual sum of squares between the observed and predicted target variable (Pedregosa et al., 2011). Random forests are commonly used in flood risk analysis, such as flood-susceptibility mapping (Lee et al., 2017; Li et al., 2019), loss and damage modeling (Carisi et al., 2018; Schoppa et al., 2020; Wagenaar et al., 2017) or the identification of important damage-influencing variables (Sieg et al., 2017).

Random forests are a tree-based type of supervised machine learning method for classification and regression tasks (Breiman, 2001). Random forests consist of a number of decision trees that, used individually, have a tendency of overfitting and high variance (Pedregosa et al., 2011). Each tree consists of several decision rules that split the data (branching) into subsets (nodes) by establishing thresholds for the predictor variables which minimize the heterogeneity within subsets and maximize differences between subsets (Sieg et al., 2017; Vogel et al., 2019). For new data the decision rules are repeated to find the matching subset of the tree (leaf node) and a corresponding mean response value. The average prediction of all decision trees forms the final predicted response value by the random forest, which exhibits less variance, sometimes accompanied by a slight increase in bias (Pedregosa et al., 2011).

Random forest offers several advantages over linear models, such as the inclusion of nonlinearities and predictor interactions (Merz et al., 2013) or a robustness against collinearity (Cutler et al., 2007), which are important factors in the light of the complexity of vulnerability to displacement. In addition, the capabilities of random forests are not strongly hampered by small dataset sizes (Biau and Scornet, 2016), as present in this study. Here, we use the random forest regressor of the Python module “Scikit-learn” (Pedregosa et al., 2011) with the default settings of 100 trees and without sample bootstrapping due to the limited number of observations; no hyperparameter tuning was performed.

The global analysis datasets contain clustered data in terms of regional/country biases (Figure S 1) which should be controlled for in climate -related mobility studies (Hoffmann et al., 2021). To overcome these random effects, we employ a mixed-effects random forest (MERF) (Hajjem et al., 2014) and assign the ISO3 country code as random effect covariate using the “MERF” Python package (https://github.com/manifoldai/merf).

4.2.3.2 Predictor ranking

We employ multiple multivariate linear regression and random forest models using up to three predictors. We test all possible predictor combinations, except for a small number of predictors which are closely related and depict a high correlation (Figure S 2 and Figure S 3). A maximum of one of these three predictors may be present in the regression models. As we are interested in which predictors explain vulnerability best, we assess their performance across all models per regression type. Random forests are generally referred to as black-box methods (Biau and Scornet, 2016), i.e. it is difficult to extract the underlying decision rules and determine which predictors are of relevance, in contrast to linear regression.

For the interpretation of the model regarding its predictive capabilities, we first split the data into training sets and test sets that are used to fit the model and predict the vulnerability, respectively. As the number of observations is limited, a leave-one-out cross-validation (LOOCV) procedure is applied (Davis, 1987). This involves splitting the data *n* times into a single-item test set and using the rest for training the model, whereas *n* is the total number of observations. Thus, *n* models are constructed to predict the vulnerability of every entry. To test the capability in explaining vulnerability variance using the predictor variables, we compute R2 (coefficient of determination) values *n* times and compute the median to gain the ultimate model score.

As the true predictor importance may be obscured by the other predictors present in the model, it is disadvantageous to rank the importance of variables simply based on R2 values. Random forests exhibit a built-in feature importance ranking, however, this method is not model-agnostic and hence cannot be directly compared with linear regression models. Therefore, we use a measure of Breiman (2001) which postulates that randomly permuting the values of unimportant predictors does not decrease the accuracy. As our test set in LOOCV consists of only one item, shuffling is not feasible and we instead assign a randomly chosen value between 0 and 1. We repeat the computation of all R2s, this time with a “useless” version of the predictor of interest. The difference between the two R2 sets indicates changes in model performance and thus the level of importance. A positive decrease in R2 indicates that the predictor adds valuable information to the model; the higher the decrease the more

important is the predictor. We only consider models with R2 greater or equal than 0.01 to avoid that changes of negative values skew this procedure.

4.2.3.3 Partial dependence plots

We employ partial dependence plots (PDPs) to visualize and analyze the marginal effect of each predictor on the predicted vulnerability (Friedman, 2001). The PDPs are limited to a maximum of two variables due to the dimensional representation, however, a collection of PDPs can serve as an alternative by showing the partial dependence of each predictor (Hastie et al., 2009). We train a linear regression and random forest model with all data entries available and the predictors of the model with the highest drop in R2 after randomizing the predictor of interest. Next, we duplicate the training set 100 times and assign for all values of the predictor of interest one of 100 increments between its minimum and maximum value, as similarly done by Vogel et al. (2019). The trained models predict 100 times for every entry an estimated vulnerability value, which visualizes the functional relationship between the third predictor and the response. The PDPs consist of a median vulnerability value for every predictor increment as well as two uncertainty bands (5th/95th percentile and 33th/66th percentile).

4.3 Results

4.3.1 Global displacement vulnerability

Vulnerability to displacement varies between countries by several orders of magnitude, also within continental regions (Figure 4.2). Modest to high levels of vulnerability are found in sub-Saharan Africa and Central Asia (Afghanistan and Tajikistan) and Nepal. A low vulnerability is present in Europe but also within some African countries, such as Zambia, Egypt, or Namibia. A slight decrease in global median vulnerability over time is observable (Figure S 4), however, this trend is statistically not significant (Mann-Kendall trend test, see supplementary material section 3) and limited by the short observational period of 11 years. Given that observed event-specific vulnerabilities vary by orders of magnitude, in the following we will be analyzing their logarithm; that is, our analysis attempts to understand the determinants of the *magnitude* of vulnerability, rather than its precise value.

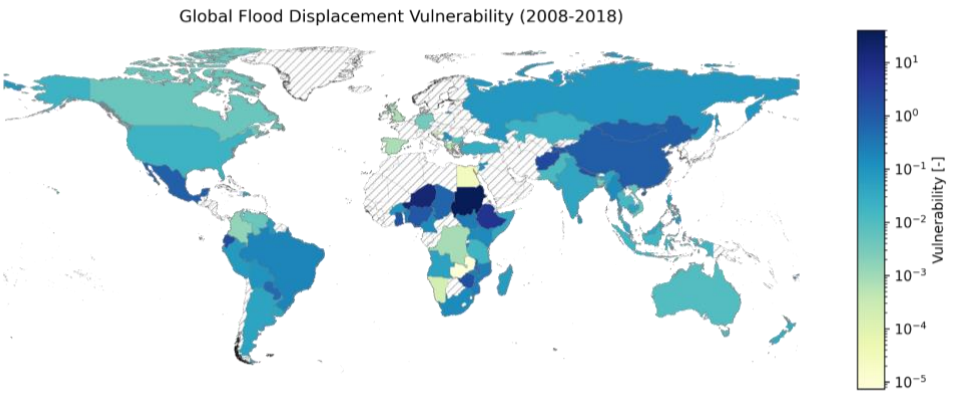

Figure 4.2: Global flood-induced displacement vulnerability (national median)

4.3.2 Predictive power

The best random forest models of the country-level analysis achieve R2s of 0.19 to 0.3, the linear regression yields R2 between 0.16 and 0.2 (Table 4.2). All best models consist of only two predictors, except for the second best linear regression model which exhibits only one predictor. This indicates an overfitting problem if more than two predictors are used, which is in turn penalized with lower R2s on the test data. By using less complex models (less predictors) overfitting and thus higher variance is avoided at the cost of higher bias on the training data, i.e. the model's ability to generalize and predictive capacity on unseen data increases. Urbanization and population ≥ 65 years are the most commonly used predictors in this ranking for random forest and linear regression, respectively. Other high ranked models involve international migrant stock, infant mortality rate, population ≤ 14 years, population density, flood experience, and urbanization growth. Only population ≥ 65 years and international migrant stock are present in both model types.

The MERF of the event-level analysis yields R2 of 0.19 - 0.26, with three out of five models using three predictors. As the dataset size is more than four fold in comparison with the country-level dataset, more complex models are able to find patterns in the data without the risk of overfitting. The most commonly used predictors are population density and event duration, followed by elevation. These predictors are combined with indicators on infrastructure, elevation, or slope. R2s of other predictor combinations show a high dependance on the choice of predictor, with some leading to poor results, similarly to the country-level analysis (Figure S 5).

Table 4.2: Explanatory power of the five best predictor combinations for random forest (top) and linear regression (bottom), ranked by R2.

RANDOM FOREST			
feature 1	feature 2	feature 3	R2
International migrant stock	Urbanization	/	0.30267
Infant mortality rate	Urbanization	/	0.25876
Population ≥ 65 years	Urbanization	/	0.2334
Population ≤ 14 years	Urbanization	/	0.18649
International migrant stock	Population ≥ 65 years	/	0.18629
LINEAR REGRESSION			
feature 1	feature 2	feature 3	R2
Population density	Population ≥ 65 years	/	0.19817
Population ≥ 65 years	/	/	0.16702
Population ≥ 65 years	Flood Experience	/	0.16585
International migrant stock	Population ≥ 65 years	/	0.16176
Population ≥ 65 years	Urbanization growth	/	0.15798
MERF			
Elevation	Population density	/	0.26296
Event duration	Total critical infrastructure	Population density	0.25478
Event duration	Education infrastructure	Elevation	0.20344
Event duration	Health infrastructure	Population density	0.20408
Slope	Population density	/	0.19386

4.3.3 Feature importance

Randomizing the predictor of interest yields and comparing it with the benchmark scores yields a feature importance ranking, expressed by a decrease in R2 (Figure 4.3). The order differs from the predictive power plots, for example, event duration drops from the fourth place (Figure S 5) to the last place, demonstrating the necessity of this more elaborated ranking technique. The ranking between the regression models of the country-level analysis differs substantially. The most important predictors for random forest are the infant mortality rate, urbanization and urbanization growth, followed by age cohorts and female population. Only one model incorporating urbanization growth yields a R2 greater than 0.01. This predictor appears to be not predictive of vulnerability, but it is when intersecting with urbanization, leading to the highest median decrease in R2 after randomizing urbanization growth. However, the median perspective and thus its ranking is limited in this case as only one model exists. GDP per capita is located in the middle section of this ranking. The (median) dummy results can be conceived as some sort of threshold of model variability. The median of the population density and flood experience fall below this threshold, indicating a low degree of importance. In contrast, the linear regression ranks these two predictors in the middle section; age cohorts and GDP per capita are the most important predictors. Female population is at the same level as the dummy predictor. The MERF applied in the all-event analysis shows a high importance of infrastructure predictors and population density, which are also all among the best individual models in terms of predictive power. GDP per capita is again only of medium importance. Interestingly, some predictors which excelled for the random forest models in the national-level analysis are only in the middle section of the event-level ranking, with urbanization and population ≥ 65 years even in the lower third. Even though some predictors are ranked low by the median decrease in R2, a few combinations yield a higher predictive power and decrease in R2 if randomized, e.g., slope. Randomizing of some predictors in both analysis types also yields an increase in R2, which reflects model variability, potentially due the small sample size.

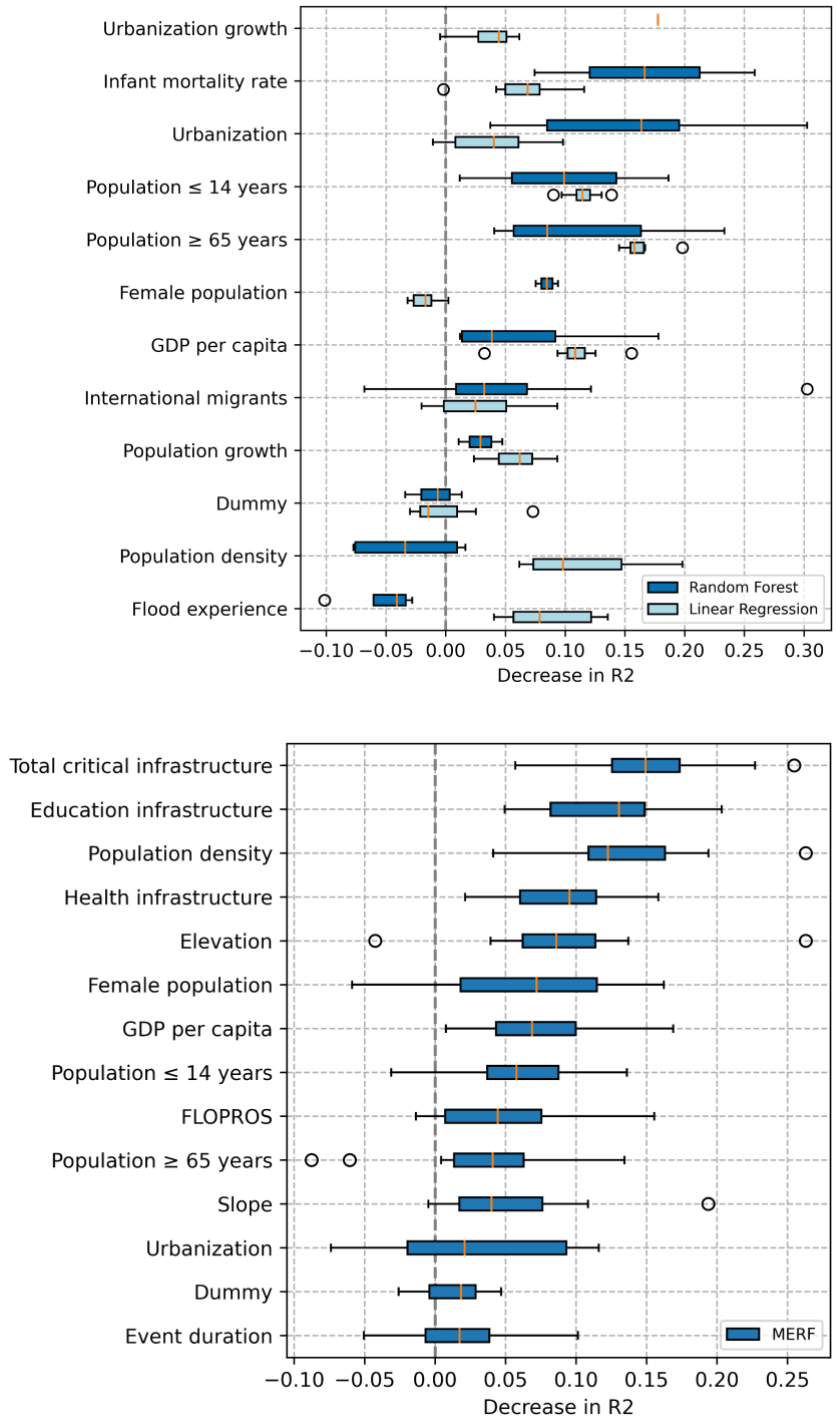

Figure 4.3: Predictive power of vulnerability predictors of the country-level analysis (top) and the event-level analysis (bottom), ranked by the drop in R2 after randomizing. Results relate to the test data using leave-one-out cross-validation. Each box plot represents all models using the predictor of interest; up to three predictors per model are chosen. Only models with R2s greater than 0.01 are displayed.

4.3.4 Partial dependence plots

The direction and magnitude on how predictors influence the displacement vulnerability in the linear regression PDPs can be observed for most parts also for the random forest results in the country-level analysis (Figure 4.4); the stronger the linear relationship, the more pronounced the trend of the random forest model. Generally, trends are more distinctive for the linear regression, while the random forest is sensitive to outliers. Despite the low importance ranking of some predictors, the PDPs are a helpful tool in visualizing their influence on vulnerability.

Regarding the country-level analysis, GDP per capita shows a negative relation with vulnerability, accompanied with a distinctive drop at approximately US$ 28,000 for the random forest model. The latter observation can be explained by a lack of data within this range GDP per capita values and thus represents model interactions, i.e., overfitting, with the data rather than an actual “cap” in vulnerability. Population ≤ 14 years (population ≥ 65 years) indicates a clear positive (negative) relationship with vulnerability. A low infant mortality rate suggests a low vulnerability, while at some level the displacement vulnerability is independent of this predictor for the random forest model. This continuous behavior can also be observed for other predictor sections, indicating again a lack of data points for a non-linear analysis. The partial dependence of individual predictors shows a moderate increase in vulnerability with higher urbanization growth and population growth; a decrease is present for female population, population density, and urbanization. A distinctive drop in vulnerability for the latter predictor demonstrates again the sensitivity of the model to outliers. A higher percentage of international migrants entails a steady decrease in vulnerability.

In the all-events analysis, a decline of vulnerability by two orders of magnitude is associated with total critical infrastructure, the highest ranked predictor in the feature importance (Figure 4.5). The other two infrastructure predictors on health and education indicate no distinctive trend. The PDP for the third-best predictor, subnational population density, as well as female population exhibit for greater parts no relationship with vulnerability. Other predictors suggest some connection with vulnerability, such as elevation, which is in fact part of the best MERF model. The age cohort indicators again show a relationship with vulnerability, however, to a lower degree than for the country-level analysis. Urbanization shows similar to the country-level analysis only a weak trend. Regarding GDP per capita, vulnerability is decreasing sharply between approximately US$ 6,000 to US$ 10,000, and then further levels out at a lower degree; suggesting more data prevents the distinctive drop present in the country-level analysis.

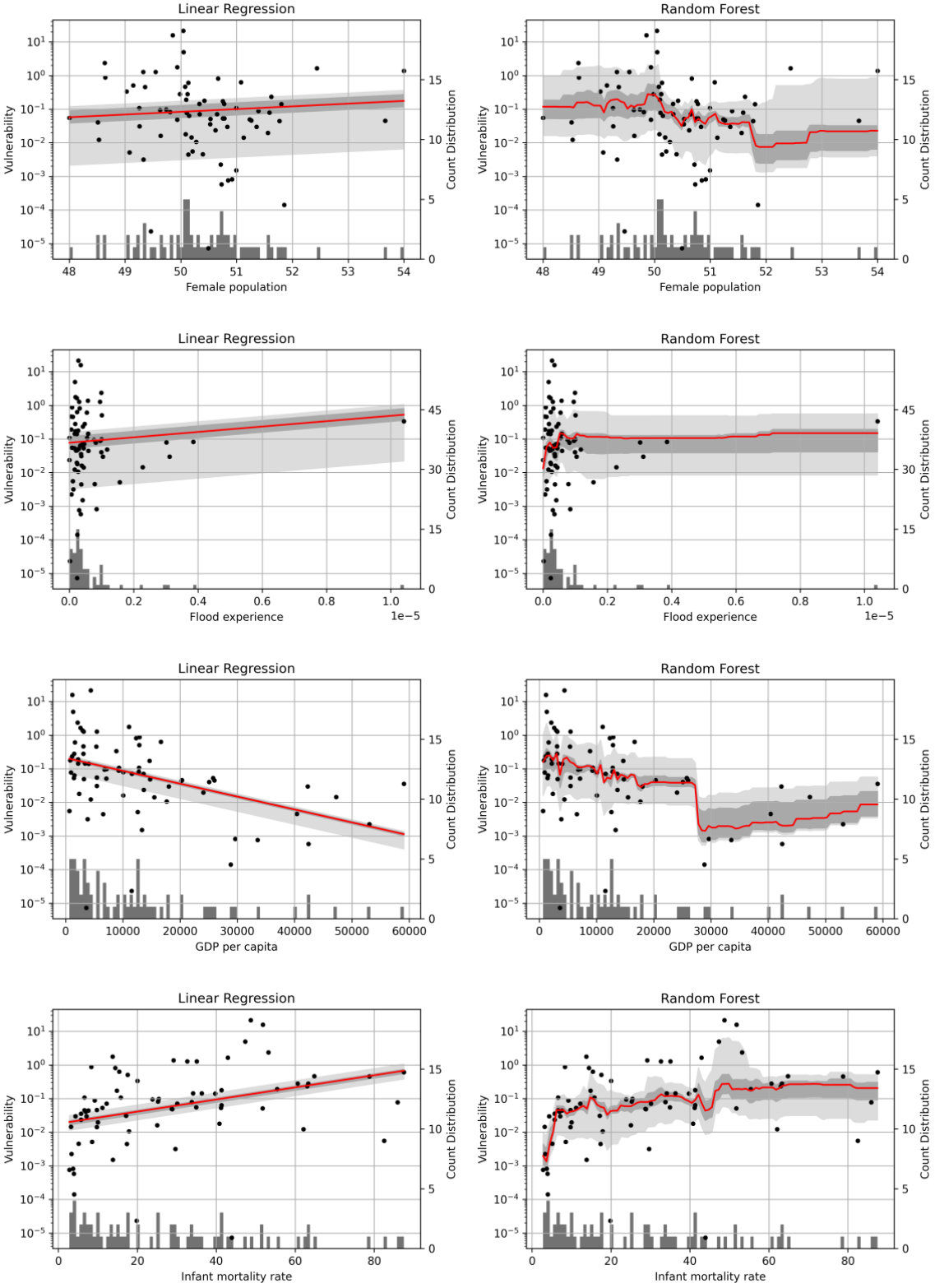
Linear Regression
Random Forest
Vulnerability
Count Distribution
Female population
Flood experience
1e−5
GDP per capita
Infant mortality rate

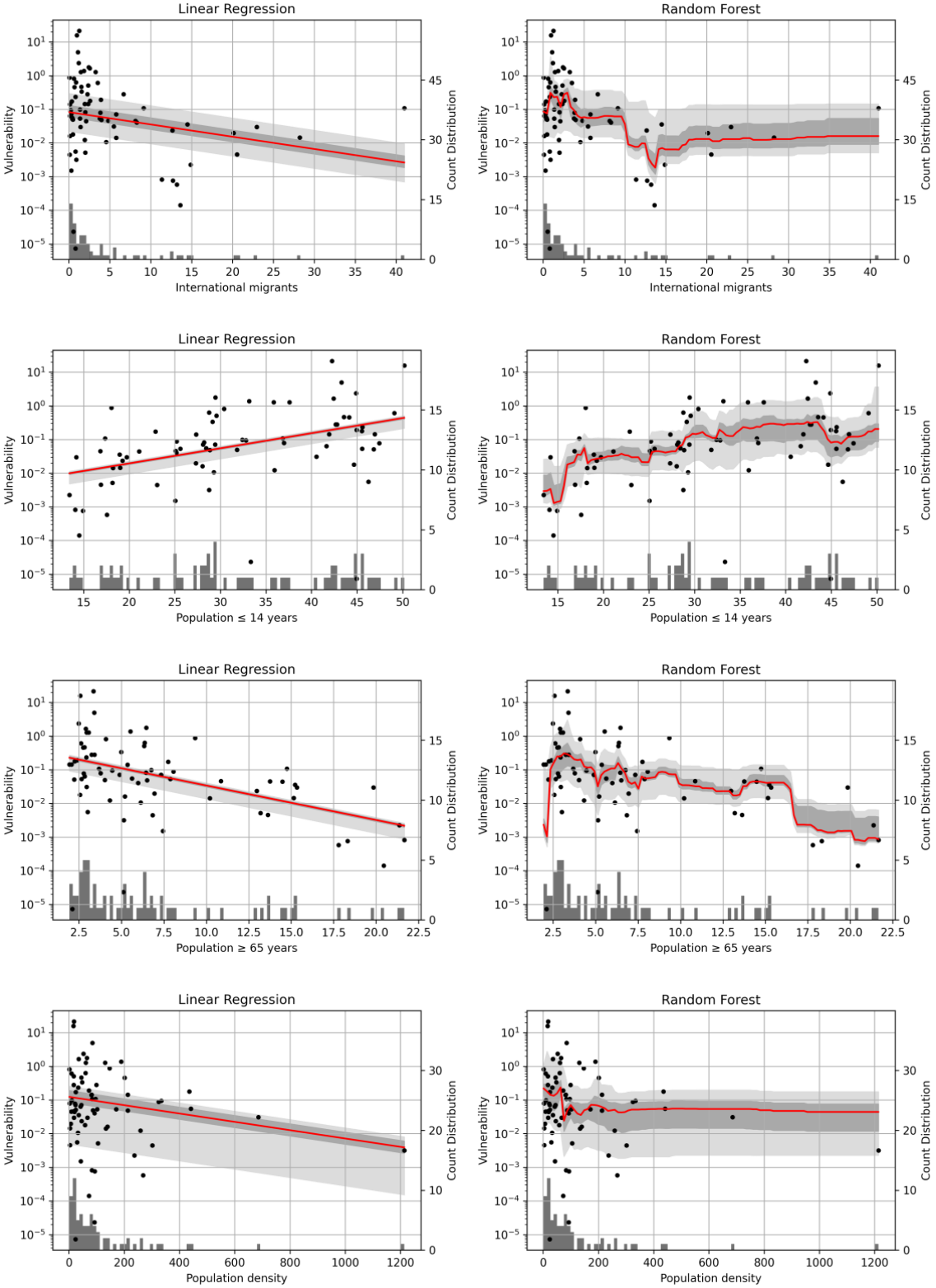
Linear Regression
Random Forest
Vulnerability
Count Distribution
International migrants
Population ≤ 14 years
Population ≥ 65 years
Population density

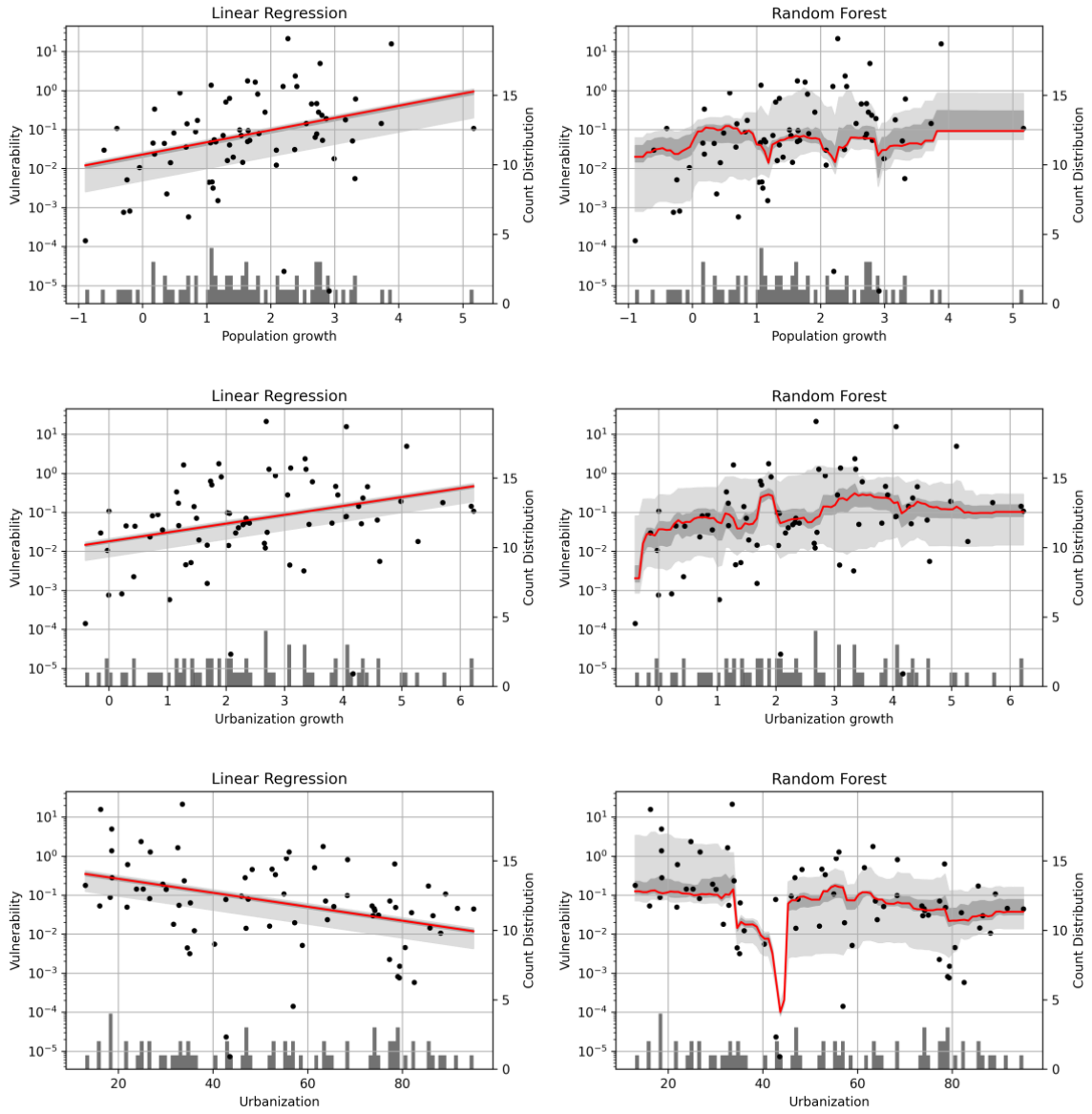

Figure 4.4: PDPs of the linear regression (left) and random forest models (right). Each PDP uses the model with the highest drop in R2 after randomizing the predictor of interest. The median vulnerability per predictor increment is indicated in red, uncertainty bands are displayed in light gray (5th/95th perc.) and dark gray (33th/66th perc.).

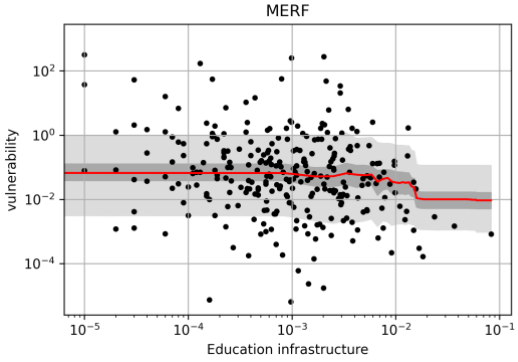
MERF
vulnerability
Education infrastructure

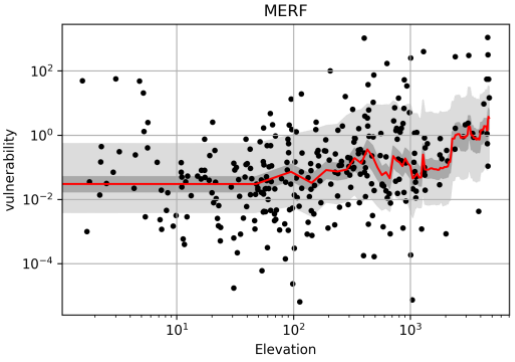
MERF
vulnerability
Elevation

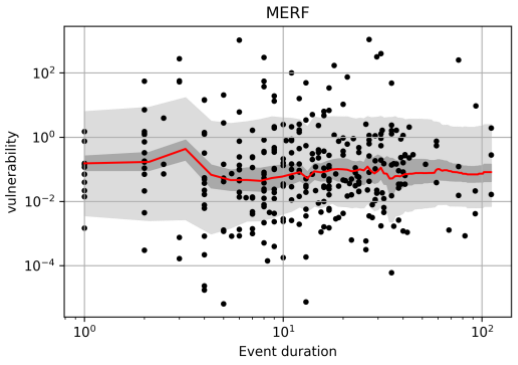
MERF
vulnerability
Event duration

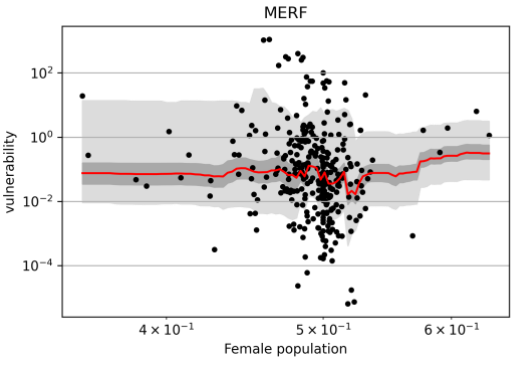
MERF
vulnerability
Female population

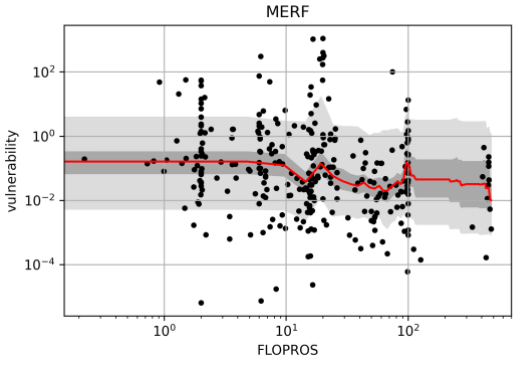
MERF
vulnerability
FLOPROS

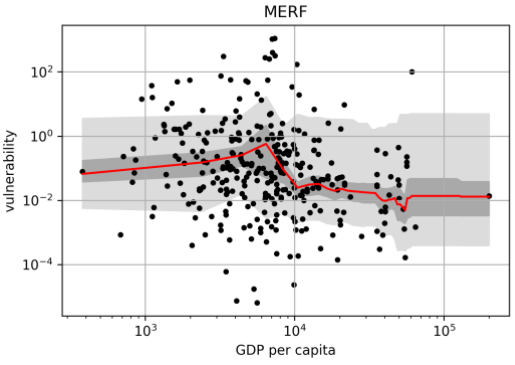
MERF
vulnerability
GDP per capita

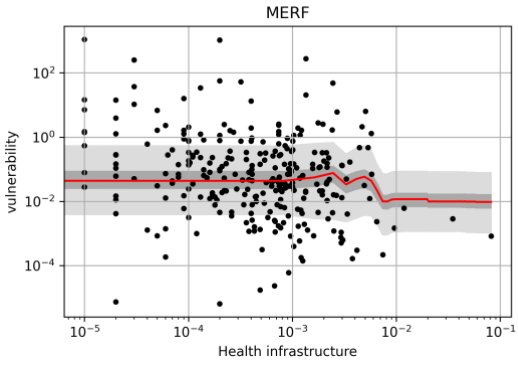
MERF
vulnerability
Health infrastructure

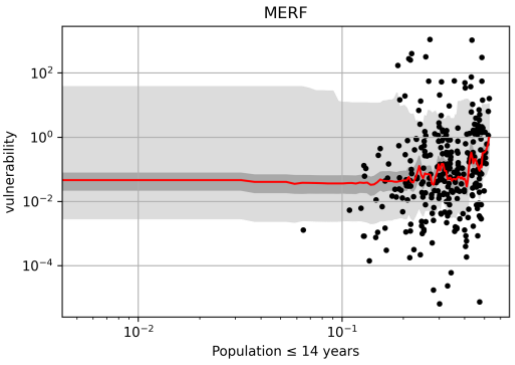
MERF
vulnerability
Population ≤ 14 years

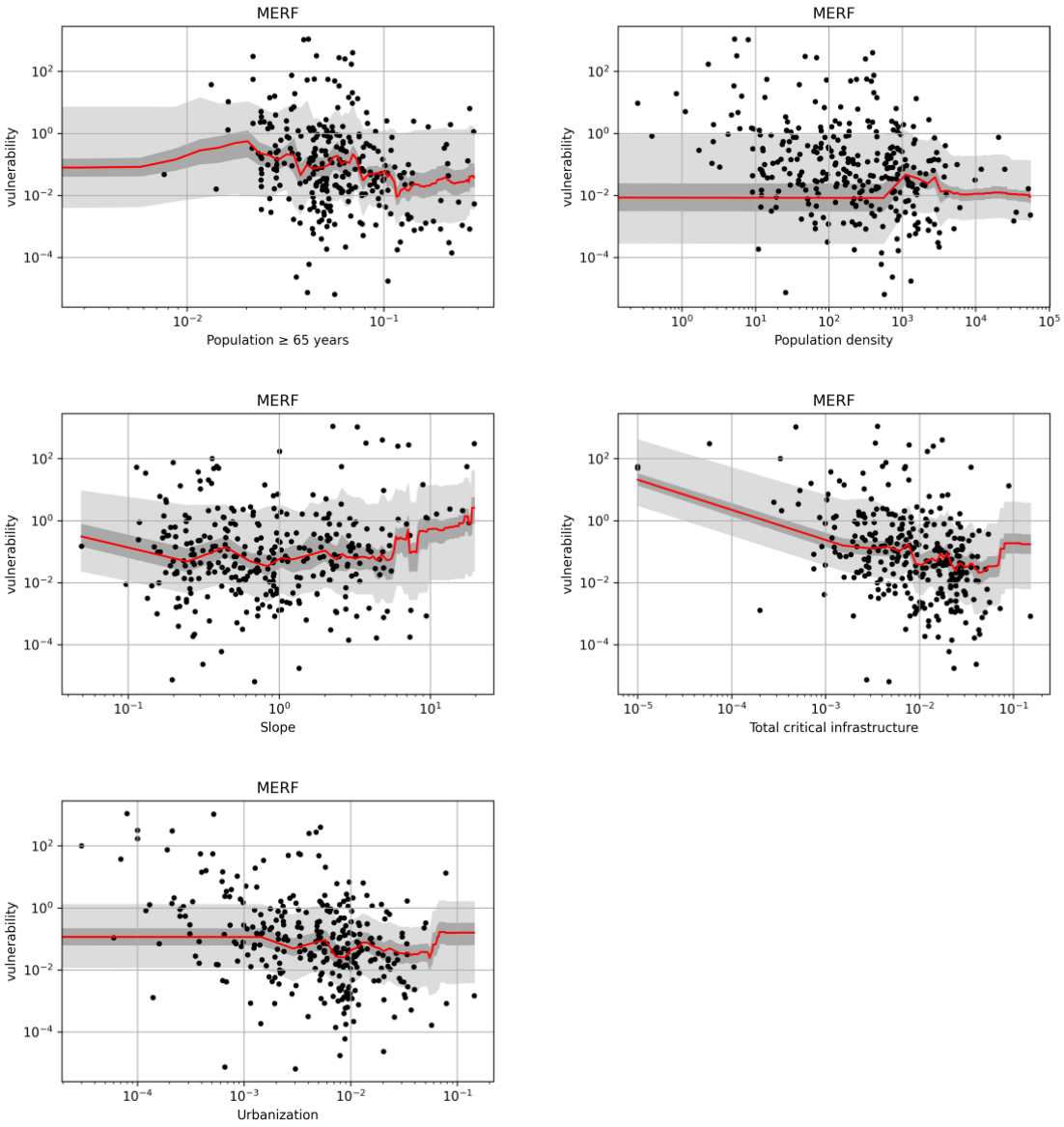

Figure 4.5: PDPs of the MERF in log-scale. Each PDP uses the model with the highest drop in R2 after randomizing the predictor of interest. The median vulnerability per predictor increment is indicated in red, uncertainty bands are displayed in light gray (5th/95th perc.) and dark gray (33th/66th perc.). Non-log-scale and count distribution of the event-level data are displayed in Figure S 6.

4.4 Discussion

This study takes a crucial step in deciphering the vulnerability to flood-induced displacement by providing new insights on the relevance of contextual indicators and their (non-)linear relationship with displacement vulnerability. The aim of this study is not only to identify but also to explain the predictors in terms of their causality, magnitude, and direction in relation to vulnerability. From the results, we synthesize the following four key findings:

1. Displacement vulnerability is varying between and within continental regions by several orders of magnitude
2. Important predictors include population density, population ≥ 65 years, urbanization, critical infrastructure, and infant mortality rate
3. Economic prosperity (GDP per capita) is of medium importance in explaining vulnerability
4. A higher level of development is generally linked with lower vulnerability, however, considerable uncertainties regarding the causality and direction of predictors remain

In the following, we discuss these key findings and further lay out how this study enhances our understanding of displacement vulnerability.

Regarding key finding 1): Few studies exist on displacement vulnerability; one compares simulated historical flood exposure to reported displacement numbers (Kakinuma et al., 2020). The analysis uses temporal average (2008–2013) national exposure and displacement to group countries into high, medium, low, exposure and high, medium, low displacement categories showing that vulnerability is particularly high in African countries that are often grouped into low exposure but medium to high numbers of displacement or medium exposure but high displacement categories. In contrast to this, our study based on satellite imagery-derived exposure depicts a more diverse level of vulnerability across the globe, in particular for the African continent. While some of the most vulnerable countries can be found in Africa, there are also several examples of medium to low vulnerability countries. Differences between the two studies can be partially explained by the hazard computation method, investigated time period and clustering of results. Aligned with the findings of Kakinuma and colleagues, we find similar vulnerability levels in Central Asia and China; also the USA exhibits a medium susceptibility to flood-induced flooding in both studies.

The identification of relevant predictors for vulnerability to flood-induced displacement is at the center of this study. An a priori selection only based on literature results is difficult as most findings are not specifically related to this type of vulnerability, e.g., slow-onset drought-

related displacement (Thalheimer et al., 2021a) or asylum migration (Schutte et al., 2021). As vulnerability might differ between extreme events (Cardona et al., 2012), and thus their predictors, another goal of this study is to confirm, or disapprove, findings of other studies also in the context of displacement vulnerability addressed in this work. The prediction capabilities in this study strongly depend on the choice of predictors and the analysis scope (country-level vs. event-level). R2s of up to 0.3 are comparable to a global flood risk assessment by (Carozza and Boudreault, 2021) who predicted the number of displacements of historic flood events listed in the DFO archive. The predictor ranking also varies greatly between the linear regression and random forest. This is somewhat anticipated as we deliberately choose a random forest model to capture non-linearities and predictor interactions. Synthesizing the results into key finding 2), we find that population density, population ≥ 65 years, urbanization, infant mortality rate, and critical infrastructure are relevant factors in determining vulnerability; followed by population ≤ 14 years, urbanization growth, international migrant stock, health, education, and elevation. Female population, GDP per capita, event duration, and flood experience show a medium to low contribution; the level of flood protection, population growth and the slope exhibit the lowest relevance.

The measurability, simplicity, and availability of the investigated features limit the representation of vulnerability in this work; additional drivers, such as coping capacity (Paul and Routray, 2011) or risk perception (Carroll et al., 2010; De Marchi and Scolobig, 2012), are difficult to assess globally and to express in national or even sub-national indices (Rufat et al., 2015). Empirical case studies suggest that the experience with past flood events is of great importance (Fielding, 2012; Siegrist and Gutscher, 2008), however, the corresponding indicator ranks low in this study, suggesting that our computation method is too simplified. Predictors covering governance, democracy levels, or political aspects are also listed in several indicator catalogs, e.g., in the WDI inventory or V-Dem Dataset (Coppedge et al., 2021). We deliberately did not include these predictors as either no clear indication of causality with regard to flood-induced displacement could be established, or the indicators are closely related to other predictors, such as GDP per capita. Nonetheless, future studies on vulnerability may also consider these predictors, along with ethnicity, class/caste, disability, and detailed health status (Oppenheimer et al., 2014; Rufat et al., 2015; The Nansen Initiative, 2015).

Regarding key finding 3), a negative relation between the economic status and vulnerability was found for a set of hazards in previous works, including flooding Formetta and Feyen (2019), Jongman et al. (2015), and Tanoue et al. (2016) find high mortality rates among countries with less than US$ 10k per capita, a vulnerability “threshold” for loss rates varies between US$ 10k and US$ 15k. Economic measures, such as poverty, income or

unemployment, are displayed also as important risk determinants of displacement and other forms of human mobility (Cissé et al., 2022; The Nansen Initiative, 2015). Kakinuma et al. (2020) showed that gross national income per capita is significantly negative associated with flood-induced displacements per 1,000 people and found a breakpoint at US$ 13k per capita. We also find a nonlinear negative relationship for GDP per capita, with the country-level analysis showing a drop at approximately US$ 28k and the event-level analysis a transit between US$ 6k to US$ 10k. Even though numbers are not directly comparable at face value, our findings are in line with those previous studies and suggest that vulnerability to displacement exhibits parallels mortality.

Several relevant predictors of this study exhibit a medium to high correlation with GDP per capita, which is surprisingly ranked only in the middle section for the random forest and MERF models; it is not clear whether these predictors act as complements or substitutes to GDP per capita. For instance, urbanization characterizes population shifts, and spatial planning and is closely related to the development process of a country; at the same time, it is also an indicator of economic prosperity (UN Habitat, 2010). Nonetheless, we come to the conclusion that economic drivers only partially explain vulnerability, however, may provide a crucial context for other predictors to unfold. This confirms the general expectation of vulnerability being dependent on multiple drivers and that non-economic variables also determine safety from extreme weather events (Toya and Skidmore, 2007). For example, evidence from surveys in several countries show that internal migration, although not specifically focused on disaster-induced displacement, is mostly motivated by social factors (UK Government Office for Science, 2011). In fact, non-economic factors, such as flood experience and related changes in land tenure, can even counterbalance economic deficiencies (UK Government Office for Science, 2011). The ranking of GDP per capita, however, is high for the linear regression in this study, suggesting this indicator is nevertheless useful for a coarse assessment on displacement vulnerability to flooding.

The PDPs partially display the connection between individual predictors and vulnerability, as already demonstrated for GDP per capita. The age cohort predictors show a clear trend that a young population is more prone to displacement than a society with a high share of elderly, potentially reflecting the (economic) development rather than social behavior. High infant mortality rate, population growth and urbanization growth are positively associated with displacement vulnerability, while urbanization and the infrastructure indicators exhibit a negative trend. These observations are in line with general theories postulating that a higher level of development leads to a decrease in vulnerability (Oppenheimer et al., 2014; The Nansen Initiative, 2015), leading to key finding 4). Age, health, infrastructure, and education indicators generally indicate the vulnerability to climate extremes for communities and

individuals (Cissé et al., 2022). For example, infant mortality rate and the health infrastructure indicator reflect the general level of population health (Reidpath and Allotey, 2003), and thus serve as proxies for public service delivery in the context of climate extremes (Rubin, 2014), e.g., emergency and recovery assistance. High infant mortality rates is also related to the marginalization of affected communities (Bishop-Royse et al., 2021), which is associated with higher flood risk (Sanders et al., 2023), caused by, for example, a lack of early warning systems, physical protection measures, or official emergency and recovery support. The hypothesis for the total critical infrastructure indicator is, next to the infrastructure predictors on health and education, its additional association with access to electricity, transportation, telecommunication, and other important infrastructure services that enable effective in-situ disaster response. Children are especially vulnerable during a disaster (Flanagan et al., 2011). Our indicator for the youngest age cohort also shows a clear connection with vulnerability to flood-induced displacement (see supplementary material section 2). However, it is unclear whether our predictor reflects the lack of coping mechanisms and disaster knowledge (Jonkman et al., 2009), or rather represents a broader indicator of under-development.

A major challenge in discussing the impact pathway of predictors lies within the nature of the GIDD displacement data, including not only (long-term) displacement but also pre-emptive evacuations. Regarding the former one, a high vulnerability may reflect inadequate housing protection, potentially due to restricted financial capabilities and poor structural measures. A high vulnerability associated with evacuations can mean both insufficient structural protection against extreme flooding and in fact a well-working early-alert system in place, which implies a higher level of preparedness. The latter one is financially costly, requiring a functioning infrastructure, and societal trust in a reliable state to follow instructions, all of which indicate a comparatively high level of development. In this case, displacement can also represent life-saving actions and be actually beneficial (IDMC and ADB, 2022). Nonetheless, displacement is generally viewed as a negative outcome of failed protection against the physical impacts of extreme flooding, as the (partial) destruction of homes is also not avoided in the case of evacuations.

Many global-scale studies use intensity-damage functions (IDFs) to represent vulnerability, for example, depth-damage functions are often used for flood risk assessments (Ward et al., 2020). Previous studies have shown that flood depth explains a substantial part but not all flood impact; simple models with only flood depth do not perform well (Wagenaar et al., 2017). This concept of vulnerability of physical infrastructure differs from social vulnerability (Flanagan et al., 2011), which we address in this study. The incorporation of IDFs is not possible as no flood depth estimates are available within FLODIS. We account for the exposure of critical infrastructure in this study, which represents a simplified infrastructure

vulnerability. Nonetheless, future studies on (displacement) vulnerability are encouraged to examine the interplay of physical infrastructure vulnerability, using intensity-damage functions for displacement risk (Anzellini et al., 2017; Kam et al., 2021), and social vulnerability, as outlined, for example, in this work.

4.5 Conclusion

Our study is a first step towards a better understanding of vulnerability to flood-induced displacement, which is poorly understood in comparison to mortality or vulnerabilities to economic losses. In the light of 12 million flood-induced displacements (IDMC, 2022), a better understanding of vulnerability is important to leverage risk reduction strategies and adaptation planning (Cardona et al., 2012; Jurgilevich et al., 2017). As vulnerability differs between regions, even down to the household-level (Cardona et al., 2012), a spatial explicit and event-specific representation (Jonkman, 2005) is necessary. To this end, we derive event-specific vulnerability values for 311 historic flood events, and investigate the importance of predictors for national-level and event-level vulnerability. We apply a machine learning framework consisting of linear regression and random forest models to investigate the predictive power of indicators, rank predictors by their importance and visualize the interactions with displacement vulnerability. Vulnerability proves to be a spatially highly variable element of risk, with high differences among events, countries, and continental regions. Population density, population ≥ 65 years, urbanization, infant mortality rate, and critical infrastructure are found to influence vulnerability the most; GDP per capita, a commonly used predictor for flood risk, is only of medium relevance. We use PDPs to illuminate the connection between individual predictors and vulnerability. Our results demonstrate that singling out the most important predictors depends on the context, and determining the magnitude and direction of individual predictors is difficult. Yet, our study confirms that generally the level of development is positively related with a reduction in vulnerability. We also draw hypotheses on the causality of individual predictors, however, large uncertainties remain, calling for more data on displacement events as well as a synthesis with findings from empirical case studies (Cardona et al., 2012; Rufat et al., 2015). In this study, we use flood hazard information derived from remote sensing for a large number of events around the world, which represents an alternative to the common approach of global flood modeling. Future work could also incorporate other social vulnerability predictors, such as governance, coping capacity, or risk perception, which are difficult to assess but have the potential to further close the gaps in understanding vulnerability. It is also recommended to pair social vulnerability with physical infrastructure vulnerability, represented by IDFs. Our analysis disentangles the vulnerability drivers to flood-induced displacement using novel approaches and datasets. The findings of this work allow

for a better understanding on the contextual drivers of vulnerability, and thus provide more insights for policymakers, planners, relief organizations, and other practitioners on how to effectively mitigate the risk of flood-induced displacement.

Chapter 5 Human displacements from tropical cyclone Idai attributable to climate change

Authors:
Benedikt Mester
Thomas Vogt
Seth Bryant
Christian Otto
Katja Frieler
Jacob Schewe

*Under consideration for Natural Hazards and Earth System Science*s:
Mester, B., Vogt, T., Bryant, S., Otto, C., Frieler, K., and Schewe, J. (submitted). Human displacements from tropical cyclone Idai attributable to climate change. EGUsphere [preprint], https://doi.org/10.5194/egusphere-2022-1308, 2023.

Abstract

Extreme weather events often trigger massive population displacement. A compounding factor is that the frequency and intensity of such events is affected by anthropogenic climate change. However, the effect of historical climate change on displacement risk has so far not been quantified. Here, we show how displacement can be partially attributed to climate change, using the example of the 2019 tropical cyclone Idai in Mozambique. We estimate the population exposed to flooding following Idai's landfall, using a combination of storm surge modeling and flood depth estimation from remote sensing images, for factual (climate change) and counterfactual (no climate change) mean sea level and maximum wind speed conditions. We find that climate change has increased displacement risk from this event by approximately 3.1 to 3.5%, corresponding to 16,000 - 17,000 additional displaced persons. Besides highlighting the significant effects on humanitarian conditions already imparted by climate change, our study provides a blueprint for event-based displacement attribution.

5.1 Introduction

Tropical cyclones (TCs) pose immense risks to coastal communities around the world. Between 1980 and 2021, an average of 45 TCs globally have been recorded per year, with the Philippines, China, Vietnam, USA and Mexico as the top-five most frequently exposed countries (Guha-Sapir et al., 2022). While related monetary losses are high due to the massive damages to housing and infrastructure, TCs also displace an average of 9.3 million people every year, with this hazard being responsible for 43% of all weather-related displacements (IDMC, 2022). Such forced displacements are associated with extensive human suffering, as well as substantial costs (e.g., for providing shelter or from loss of economic production) and often require international assistance for disaster relief funds and humanitarian response (Desai et al., 2021).

At the same time, global climate change is expected to alter TC characteristics, resulting in an increase in overall TC intensity (maximum wind speed and precipitation) and hence in the frequency of very intense TCs (category 4-5 on the Saffir-Simpson scale), fundamentally because of an increase in potential intensity due to warmer sea surface temperatures (SST) (Emanuel, 1987; Knutson et al., 2020). Rising sea levels, also driven by global warming, additionally compound coastal flood risk associated with TCs (e.g., Garner Andra J. et al. (2017); Lin et al. (2012); Resio and Irish (2016)). Given that global mean surface air temperature and sea level have already risen substantially above pre-industrial conditions (by about 1.1°C and 0.20 m, respectively (Gulev et al., 2021)), it is likely that recent TC landfalls have caused more severe impacts than would be expected without climate change. However, the portion of TC-induced human displacements attributable to climate change has so far not been quantified.

In this study, we address this research gap for the particular case of displacement triggered by TC Idai in 2019. We examine the floods in central Mozambique associated with TC Idai, considered to be “one of the Southern Hemisphere’s most devastating storms on record” (Warren, 2019). On the 14th of March, Idai made landfall near the densely populated port city of Beira, inhabited by more than 530,000 people (Figure 5.1). Alongside strong winds and extensive inland flooding caused by heavy rainfall, the cyclone also created an intense storm surge, leading to severe coastal flooding. In Mozambique alone, TC Idai claimed the lives of more than 600 people, and caused 478,000 internal displacements, as well as widespread structural damage totaling more than US$ 2.1 billion (Guha-Sapir et al., 2022; IDMC, 2022).

Here, we investigate how the coastal flooding would have manifested in a counterfactual world without climate change, and consequently, how many of the observed human displacements from TC Idai can be linked to climate change. For the attribution of the impacts

we follow the storyline approach introduced by Shepherd (Shepherd, 2016). To this end, we account for two known mechanisms through which global climate change could have affected coastal flood hazard: sea-level rise and amplification of storm intensity. We first estimate the influence of climate change on sea level and TC intensity in the South Indian Ocean. We employ a high-resolution hydrodynamic flood model to simulate TC Idai's peak coastal flood extent and depth, both under historical conditions and under counterfactual conditions with lower sea levels and lower maximum wind speed, corresponding to a world without climate change. We additionally use satellite imagery to account for inland (freshwater) flooding, and estimate the total number of people affected by flooding. We then model the number of displacements based on flood depth-specific vulnerability factors, and estimate the fraction of displacements that can be attributed to climate change by comparing results under factual vs. counterfactual conditions.

We use an estimate of sea level rise (SLR) that attempts to separate natural variability in ice sheet and glacier mass balance and retain only the long-term trend induced by global warming (Strauss et al., 2021). Beyond this, however, our analysis is indifferent to whether the trends in sea level and TC intensity are anthropogenic or not. This is in line with the definition of *impact attribution* put forward by the Intergovernmental Panel on Climate Change (IPCC), where "changes in natural, human, or managed systems are attributed to [a] change in [a] climate-related system" (O'Neill et al., 2022). Such a question can be separated from the *climate attribution* question of whether the change in the climate-related system - here, sea level and TCs - is due to anthropogenic forcing. This separation allows us to focus on the link between climate change and displacement despite remaining uncertainty about the exact anthropogenic contribution. We will return to this issue below.

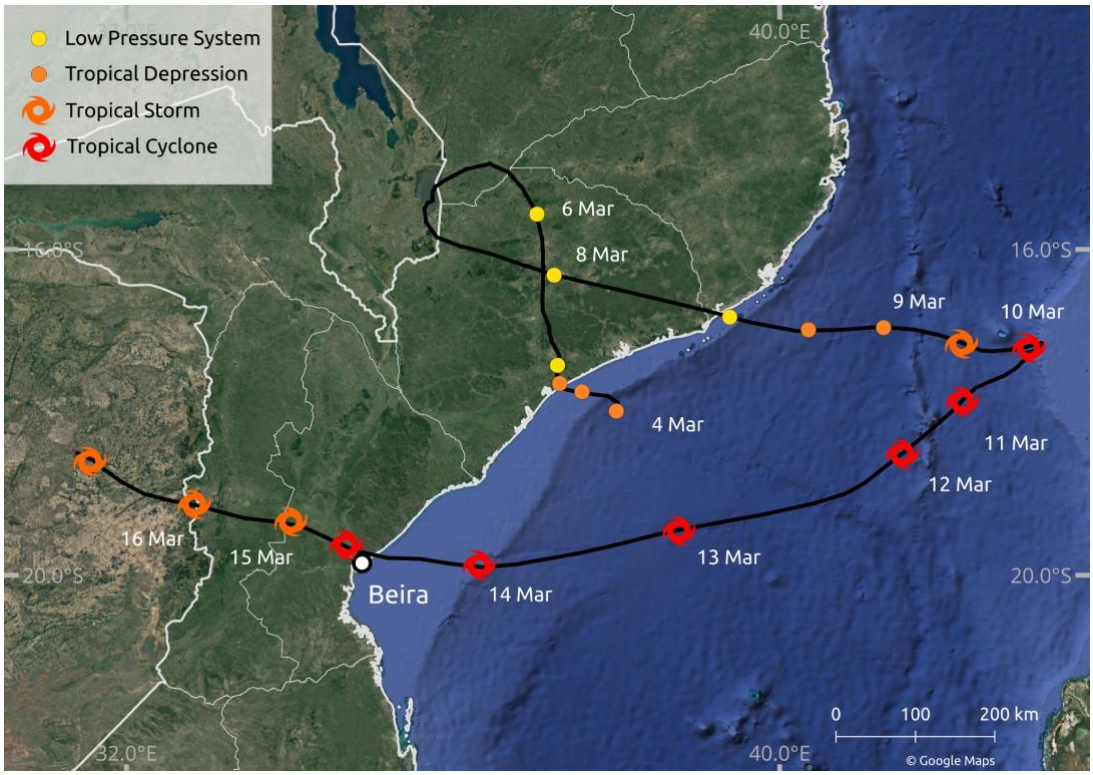

Figure 5.1: Trajectory of tropical cyclone Idai over the South Indian Ocean. Trajectory data is based on the IBTrACS database (Knapp et al., 2010). Mozambican administrative boundaries (GADM, 2018) in white; satellite image background by © Google Maps (Google Maps (a), 2022). Dates and tropical cyclone status adopted from Reliefweb (Reliefweb, 2019).

5.2 Methods

5.2.1 Coastal flood modeling

The storm surge flood simulations are generated using the open-source geophysical flow solver GeoClaw (Mandli and Dawson, 2014). GeoClaw uses an efficient adaptive mesh refinement to model wind- and pressure-induced wave dynamics in the 2-dimensional depth-averaged shallow water equations. The detailed model setup used here is described and evaluated by Vogt and colleagues (Vogt et al., 2022).

As the factual input for GeoClaw, the TC track data from IBTrACS (Knapp et al., 2010) provided by the WMO Regional Specialised Meteorological Center at La Reunion (operated by MeteoFrance) is used. For the counterfactual scenarios with modified TC intensity, we multiplied all wind speed values along the track by a scalar factor of 0.9 (for a decrease of 10% in intensity). The central pressure at each track position is increased by 0.1 times the difference between central pressure and environmental pressure.

From the wind speed, pressure, and radius information provided along the TC track, GeoClaw derives surface wind speeds and air pressure at arbitrary locations in space and time using a radially symmetric wind profile (Holland, 1980) combined with the influence from the storm's translational speed.

GeoClaw does not incorporate any tidal dynamics, nor meteorological forcings apart from the TC wind and pressure fields mentioned above. To account for the influence of astronomical tides, we configured GeoClaw to use an initial sea level according to gridded satellite altimetry for 2019 (CMEMS, 2021), optionally enhanced by the minimum, mean, or maximum simulated astronomical tides in the region of landfall according to the FES2014 global ocean tide atlas (Lyard et al., 2021). For the counterfactual sea level scenarios, the amount of sea level rise specified in the scenario description (between 6.5 and 17.0 cm) was subtracted from the initial sea level.

The topographical input for GeoClaw is taken from digital elevation models. We used a combination of CoastalDEM 2.1 (Kulp and Strauss, 2021, 2018) in coastal areas, SRTM 15+ V2.3 (Tozer et al., 2019) over the open ocean and Multi-Error-Removed Improved-Terrain (MERIT) digital elevation model (DEM) (Yamazaki et al., 2019) everywhere else. All datasets are converted to the same geoidal vertical datum (EGM96) at a spatial resolution of 9 arcseconds (approximately 300 m).

Due to a lack of tide gauges in Mozambique, it was not possible to validate the performance of GeoClaw for TC Idai in the factual model runs. However, we compared the water levels at a virtual tide gauge station off the coast of Beira, where the highest impacts from TC Idai have been reported, with simulated water levels from the Global Tide and Surge Model (GTSM) (Dullaart et al., 2021; Muis et al., 2020), and found the best agreement of maximum surge heights for the GeoClaw run with the maximum astronomical tide assumption, closely followed by the run with no tidal adjustment (Supplementary Figure S1).

5.2.2 Inland flood depth estimation

Gridded depth maximums for the flood event (Supplementary Figure S2) were calculated using the Rolling HAND Inundation Corrected Depth Estimator (RICorDE) algorithm (Bryant et al., 2022) supplied with terrain data from the MERIT DEM project, permanent surface water data from the Joint Research Centre (JRC) Global Surface Water project (Pekel et al., 2016), and flood extents from the FloodScan product (Atmospheric and Environmental Research & African Risk Capacity, 2022). MERIT DEM provides a roughly 90 m resolution global layer derived from multiple space-based sensors to minimize elevation errors. The maximum water extent layer from JRC's Global Surface Water project provides a roughly 30 m resolution global layer of locations detected as inundated on Landsat imagery (Wulder et al., 2016) from

1984-2019 (Pekel et al., 2016). Observed flood extents for TC Idai were obtained from Atmospheric and Environmental Research & African Risk Capacity's accumulated 2-tier standard flood extent depiction FloodScan product from 2019-03-01 to 2019-03-31, which has the same resolution as the MERIT DEM. Originally developed for applications in Africa, this FloodScan algorithm relies on satellite based low-resolution passive microwave data to estimate inundation areas. The algorithm was designed to minimize false-positives at the expense of small flood sensitivity (Galantowicz and Picton, 2021). All data layers were re-projected to 90 m resolution geodetic coordinates prior to the RICorDE computation.

RICorDE is an algorithm originally developed for post-event analysis of fluvial flood events in Canada that produces gridded water depth estimates by incorporating Height Above Nearest Drainage (HAND) and cost distancing sub-routines to extrapolate edge values into an inundation region. By using the vertical distance above the permanent water surface computed in the HAND routine, RICorDE pre-filters egregious flood extent predictions and assumes a water surface slope matching the permanent water surface (rather than the flat surface assumed by similar methods). The slower, more complex RICorDE algorithm has been shown to produce more accurate depths maps when compared to faster, more disaster response-focused solutions like the Floodwater Depth Estimation Tool (FwDET) (Bryant et al., 2022; Cohen et al., 2018).

While no data was available to validate the performance of the depths estimate, visual inspection suggests results are less accurate in areas with higher elevation (>20 m), especially where drainageways are of comparable width to the resolution of the JRC water extent layer. These false negatives in the JRC layer propagate as positive bias in the HAND routine, which leads to higher elevation water surface predictions and similar positive bias in the depth values (see white arrow in Figure S3a).

5.2.3 Combined flood depth product

The inland flood depth estimates from RICorDE are resampled from 3 arcsec to 9 arcsec, using the average resampling method (Rasterio library for Python), to match the resolution of the GeoClaw output. All flood depths are rounded to the nearest decimeter, their outline is cropped to the area of interest, and the final factual flood depth in each grid cell (shown in Figure 5.3a) is determined as the maximum of both products. This accounts for both potentially partly obscured satellite imagery by clouds and potential underestimation by the numerical model.

$$d_0 = \max\left(d_{c,0}, d_r\right) \qquad (1)$$

with d_0 referring to the factual flood depth, and indices *c* and *r* referring to the coastal flood model (GeoClaw) and to the remote sensing data translated into flood depth using RICorDE, respectively. To derive the counterfactual flood depth d_{cf}, we subtract the difference between modeled factual and counterfactual coastal flood depths from the combined factual flood depth:

$$d_{cf} = d_0 - (d_{c,0} - d_{c,cf}) \qquad (2)$$

5.2.4 Displacement

We use displacement data from the openly accessible *Global Internal Displacement Database* (IDMC, 2022). No granular information is available on the type of displacement, e.g., long-term displacement or temporary evacuation, nor on the proportion of displacement by hazard type. We assume that people exposed to flood levels greater or equal than 100 cm are affected by the flooding and thus prone to displacement, following previous studies (Custer and Nishijima, 2015; Kam et al., 2021). However, we also test the sensitivity of our results to this threshold choice by evaluating alternative water level thresholds of 10 cm and 50 cm.

We first determine the flood extent with depths greater than the selected water level threshold and overlay it with population data to estimate the number of people affected. We use gridded population data from GHS-POP (Schiavina et al., 2019) for the year 2015, on 9 arcsec resolution. Population growth in Mozambique was 1.12 % between 2015 and 2019 (The World Bank, 2022); we hence multiplied all population grid cells with this factor, assuming a spatially equal population growth.

We then calculate the ratio between the number of observed displacements, and the number of affected people from the factual flood estimate. This ratio, which may be thought of as an event-specific displacement vulnerability factor, is different for every tide assumption, reflecting the uncertainty about the actual flood extent and depth. We compute for every impact level threshold *i* and tide assumption *h* a displacement vulnerability factor $v_{i,h}$ by dividing the number of observed displacements D_o by the total number of affected people of the factual scenario $A_{i,h,o}$:

$$v_{i,h} = \frac{D_0}{A_{i,h,0}} \qquad (3)$$

Multiplying the specific displacement vulnerabilities with the counterfactual numbers of affected people, we derive the number of people at risk of displacement in a world without

climate change. This means that the difference between factual and counterfactual displacement estimates comes only from differences in the flood hazard, while exposure and vulnerability factors are held fixed. We achieve this by multiplying $v_{i,t}$ with the number of affected people of the counterfactuals $A_{i,h,cf}$, and estimate the expected number of displacements for each counterfactual scenario $D_{i,h,cf}$:

$$D_{i,h,cf} = v_{i,h} * A_{i,h,cf} \quad (4)$$

5.2.5 High wind speed-induced displacements

Even though disaster reports for TC Idai suggest flooding to be the main driver of displacement, high wind speeds may have locally intensified the impact of TC Idai (Figure S4) and be partially responsible for the observed displacements. We conduct an additional analysis where we assume that people affected by either flooding or wind (or both) were at risk of displacement with an equal vulnerability factor. We use a wind speed threshold of 96 kn (50 m s^{-1}) for population exposure (Geiger et al., 2018), corresponding to the Saffir–Simpson scale classification 3 (major hurricane). The resulting wind field is overlaid with gridded population data to compute the number of affected people, excluding those who are already affected by flooding.

5.3 Results

5.3.1 Counterfactuals

Constructing counterfactuals for sea level and TC intensity requires estimating the effect of historical climate change on these quantities. Total global mean sea level has risen by approximately 23 cm since the turn of the 20th century (Church and White, 2011); at a rate that has increased over time (Dangendorf Sönke et al., 2017). According to the IPCC, it is very likely that the rate of global mean SLR was 1.5 (1.1 to 1.9) mm yr^{-1} between 1902 and 2010, and 3.6 (3.1 to 4.1) mm yr^{-1} between 2006 and 2015 (Gulev et al., 2021). Nonetheless, regional changes in sea level may differ substantially from the global average due to shifting surface winds, the differential expansion of warming ocean water, and the addition of melting ice, which can alter the ocean circulation (Fox-Kemper et al., 2021). Additionally, increases in the amount of water stored on land (due to construction of dams and reservoirs), as well as

land subsidence, have also affected total sea level, with their relative effects varying geographically (Church et al., 2004; Strauss et al., 2021).

Long-term in-situ observational records of SLR are scarce in the Indian Ocean (Han et al., 2010), hampering a precise detection of changes in sea level. For example, no active tide gauge stations can be found on the coast of Beira (Beal et al., 2019), with the nearest station located in Inhambane, Mozambique, 448 km south of Beira. However, regional historical SLR rates for Mozambique, derived from satellite imagery or models, are close to global mean estimates. IPCC rates of change in sea surface height (geocentric sea level) derived from satellite altimetry show regional SLR off the coast of Mozambique at around 4.0 mm yr^{-1} for the period 1993–2012 (Church et al., 2013). Climate-induced SLR at the South-Eastern African coastline (1993 - 2015) is estimated at ~3.5 mm yr^{-1} using a coastal-length weighted approach (Nicholls et al., 2021). Reconstructed sea level fields using global tide gauge data suggests global-averaged SLR at 1.8 ± 0.3 mm yr^{-1} over the 1950-2000 period, with regional SLR off the coast of Mozambique at around 1.5 mm yr^{-1} (Church et al., 2004). Han and colleagues (Han et al., 2010) estimate regional Mozambican SLR at approximately 1.2 mm yr^{-1} between 1961-2008.

Given that these regional estimates are close to the global mean estimate by the IPCC, we assume that total SLR near Beira is the same as the global mean, a comparable approach as by Irish and colleagues (Irish et al., 2014). In order to exclude trends induced by natural variability, particularly in sea level contributions from glaciers and ice sheets, we use estimates of global mean sea level rise attributable to anthropogenic climate change for 1900–2012 from Strauss and colleagues (Strauss et al., 2021).Their ensemble estimate is 6.6 to 17.1 cm, which we use to define counterfactual sea level parameters for the coastal flood model. This also implies assuming no substantial local effects of land subsidence and human-induced changes in land water storage through reservoir construction and groundwater extraction that would confound comparison with the global estimates. This is hard to verify, but can be motivated by findings that city subsidence occurs only in a small fraction of the world's coasts (Nicholls et al., 2021).

Tropical cyclones are projected to become more intense with rising temperatures (Knutson et al., 2015), which is in line with the theoretical understanding of the potential intensity theory by Emanuel (Emanuel, 1987). Observed TC wind speed data in the South Indian Ocean basin shows that the maximum 10-minute sustained wind speed has been increasing by about 0.3 kn (0.15 m s^{-1}) per year on average, over the period 1973-2019 (Figure 5.2). Prior to 1973, the rate of increase was likely smaller, though observational data is lacking. We make a conservative assumption corresponding to 50 years of increase at a rate of 0.2 kn (0.1 m s^{-1}) per year, resulting in a total difference in maximum wind speed of

approximately 10 kn (5.1 m s^{-1}). For the case of TC Idai with maximum observed 10-minute sustained wind speeds of 105 kn (54 m s^{-1}), this corresponds to a 10% reduction in maximum wind speed by removing climate change, which we adopt as a plausible assumption about a counterfactual TC de-intensification. This is a larger change than when adopting an earlier model-based estimate of 3.7% increase in maximum surface wind speed per 1 °C of sea surface temperature (SST) rise (Knutson and Tuleya, 2008). However, a trend analysis of global satellite data (1982–2009) finds an observed increase in maximum intensity by 1.7 m s^{-1} per decade (p = 0.06) in the south Indian Ocean (Kossin et al., 2013), yielding an increase by about 8.5% when extrapolating this rate of change over the 50 years prior to 2019; which is in closer agreement with our analysis.

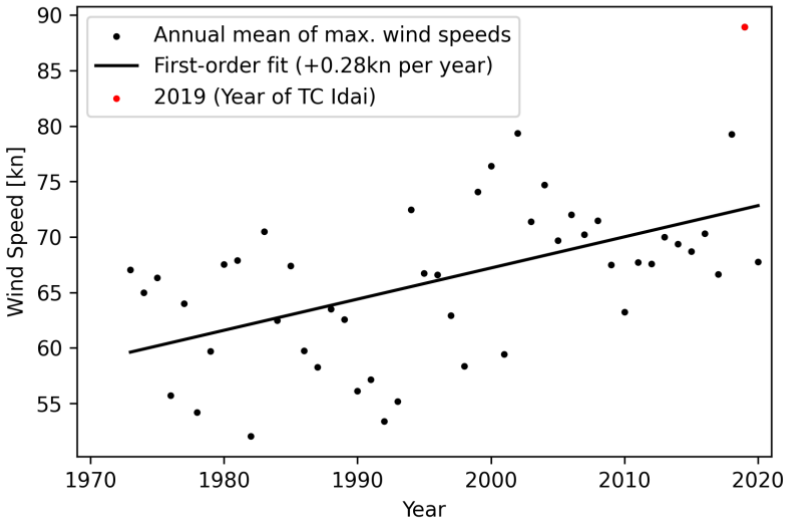

Figure 5.2: Annual means of maximum TC wind speeds in the South Indian Ocean (maximum 10-minute sustained wind speeds). Linear trend over the period 1973-2020; data from IBTrACS database (Knapp et al., 2010).

5.3.2 Simulated flooding

We calculate storm surge flood extent and depth for the factual (driven with observed wind speeds and sea levels) and counterfactual (reduced wind speeds and sea level) scenarios, using an open-source geophysical flow solver (see Sect. Methods). The contribution of tides to total sea water levels at the time of landfall is an important yet unknown model parameter. We test four different assumptions about astronomical tide levels, and find that the maximum astronomical tide shows the best agreement with simulated water levels from the Global Tide and Surge Model (Dullaart et al., 2021; Muis et al., 2020), followed by the monthly mean sea level from satellite altimetry without any tidal adjustment (Supplementary Figure S1).

Both factual and counterfactual coastal flooding are combined with inland flood depth estimates derived from satellite imagery in combination with an inundation depth estimation algorithm (Bryant et al., 2022), to obtain total inundation levels for Mozambique (Figure 5.3a). The difference between factual and counterfactual flooding is illustrated in the densely populated area of Beira (Figure 5.3b), the city where TC Idai made landfall and destroyed 90% of all houses according to some disaster reports (ReliefWeb, 2019). Differences in both flood extent and depth are observable between the factual (Figure 5.3c) and counterfactual scenario (Figure 5.3d). Notably, in a world without climate change, the area inundated by 100 cm or more is dramatically reduced.

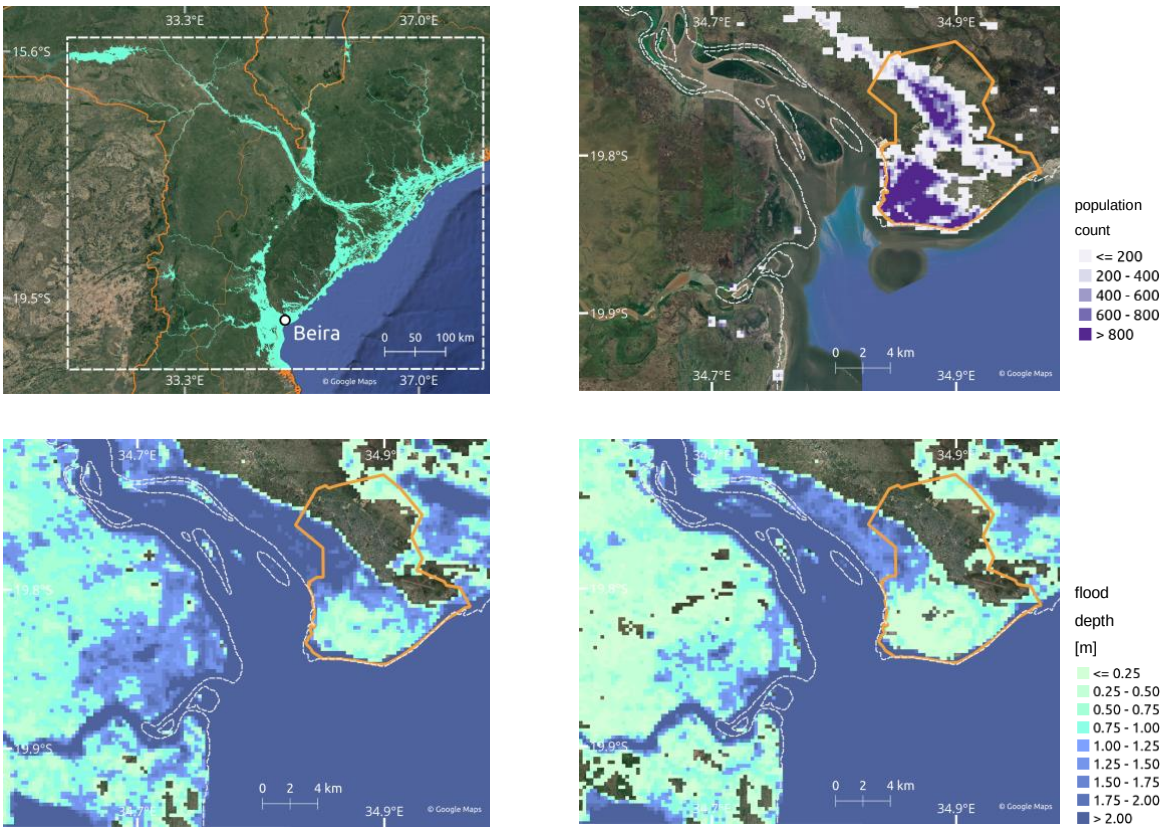

Figure 5.3: Simulated flood extent for Mozambique; population distribution and inundation levels for the greater area of Beira. (a) Combined factual estimate of inland and coastal flooding (binary; flood/no-flood). White dashed box shows the area of interest in which flood exposure is computed. (b) Population distribution for the greater area of Beira. Flood extent and levels for (c) the factual scenario, and (d) the "counterfactual TC intensity + sea level rise (10.5 cm)" scenario. City neighborhoods of Beira (HDX, 2019) are indicated by orange lines and shoreline (Wessel and Smith, 1996) is represented by dashed white lines in (b), (c), and (d); satellite image background by © Google Maps (Google Maps (b), 2022).

5.3.3 Displacement

In the next step, we investigate how the factual and counterfactual flood estimates translate into population at risk of displacement for the whole of Mozambique. Our analysis shows that the intensification of TC wind speeds leads to an increase in flood affected people and, consequently, in displacements by up to 3.6%, while counterfactuals regarding the sea level lead to only small changes (Figure 5.4). A combination of both counterfactuals only slightly exceeds the range as in contrast when considering the TC de-intensification alone. Despite the large uncertainty regarding SLR since 1900, the difference in the number of people affected (or displaced) is rather marginal; being less than 1% between the largest and the smallest SLR estimate. Our results highlight that the tide assumption plays a major role. The minimum and mean tide lead to marginal changes in affected/displaced people, in contrast to the maximum astronomical tide and monthly mean sea level from satellite altimetry, which show a median change in 3.1% and 3.5%, respectively. Given the high number of affected people, already small changes in the counterfactual scenarios lead to high changes in absolute numbers. The coupled effect of higher wind speeds and higher sea level increases the number of affected people and displacements by up to 43,300 and 16,500 (maximum tide) and 44,300 and 17,100 (monthly mean), respectively. Results regarding impact flood levels of 10 cm and 50 cm are displayed in the supplementary material (Figure S5 and S6), showing even higher changes for the counterfactual scenarios of up to 69,800 displacements (17.1%).

We assume that high wind speed caused only a marginal fraction of displacements, following disaster reports, media coverage and experience from other events; as an extreme example, wind by Hurricane Sandy caused less than 0.01% of the overall damage (Strauss et al., 2021). Nonetheless, in an additional sensitivity analysis, we also account for the number of people affected by high TC wind speeds of 50 m s^{-1} or above (Sect. Methods). Our analysis reveals that the number of people affected not by flooding (maximum tide assumption, 100 cm impact threshold) but by high wind speeds ranges between 354,400 to 357,400 in the factual simulation. In the counterfactual, even the maximum wind speed attained in any grid cell outside the flooded area drops from 51.5 m s^{-1} to 46.3 m s^{-1}, i.e. below the above-mentioned threshold; thus, no people are counted as affected. If the displacement vulnerability factor to high wind speed had been the same as to flooding, then the counterfactual would imply 109,200 to 111,500 displacements, or 22.8 to 23.3% of the total displacement, attributable to climate change.

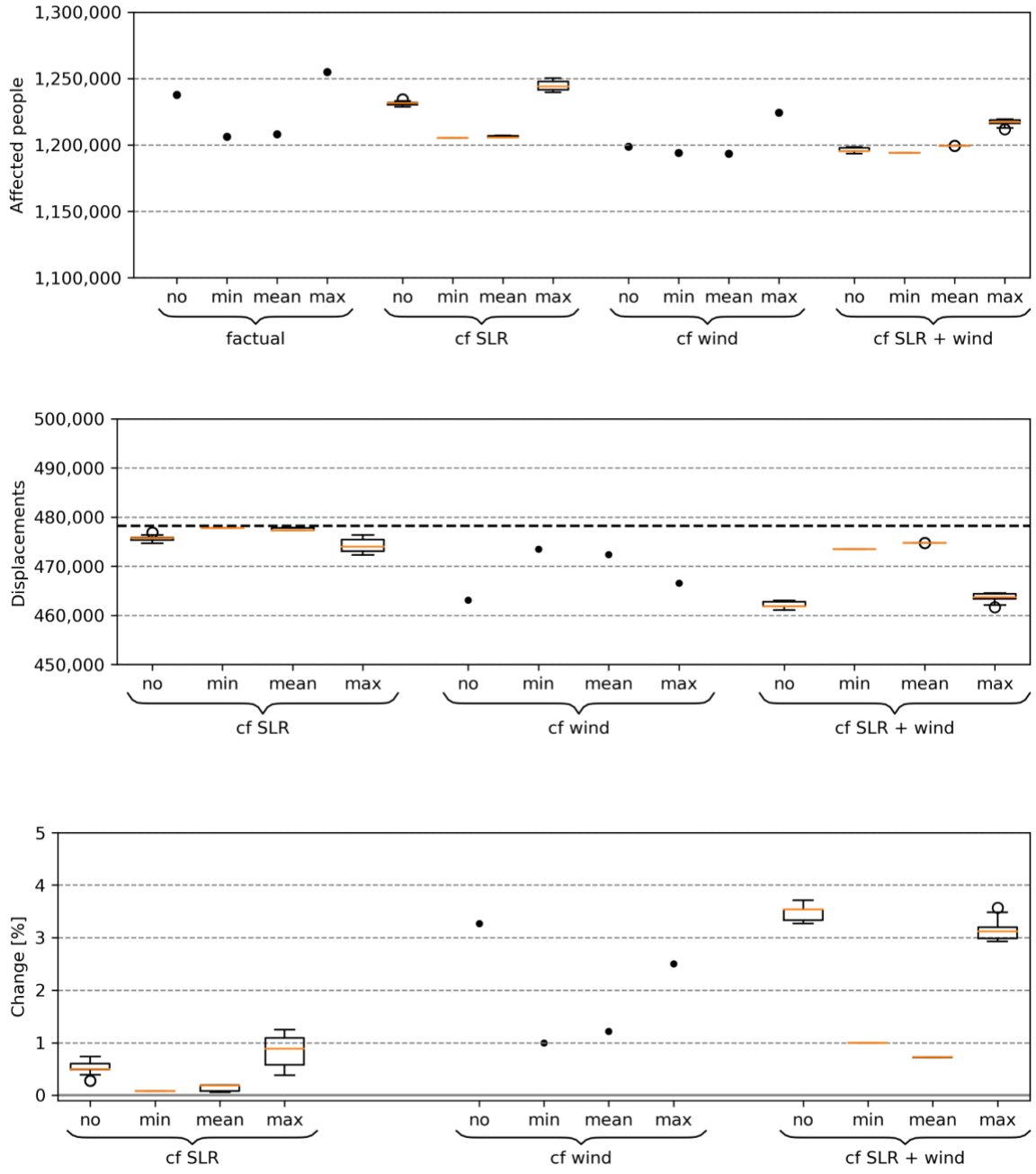

*Figure 5.4: Simulated affected people (top), displacements (middle) and percentile change (bottom) for the 100 cm impact threshold. Three counterfactual scenarios are shown: lower sea level ("cf SLR")), de-intensification ("cf wind"), and a combination of both ("cf SLR + wind"). Additionally, a variety of counterfactual sea levels as well as a set of astronomical tides is presented, covering minimum ("min"), mean ("mean"), and maximum ("max") as well as monthly mean sea level from satellite altimetry ("no"). Bold dashed line in the middle panel shows the number of observed displacements. Percentile changes in affected people and displacements are the same. The second quartile Q2 (median) of the box plot is shown in orange, "whiskers" are placed at ±1.5 * interquartile range (Q3-Q1).*

5.4 Discussion and conclusions

With more than one degree of global warming, most, if not all, extreme weather events now can be assumed to bear some imprint of climate change. By extension, this is also true for the humanitarian crises induced by catastrophic storms, floods, or droughts. However, while economic damages from climate change have been attributed both in case studies and global studies (Frame et al., 2020b, 2020a; Sauer et al., 2021; Strauss et al., 2021), little is known about the extent to which climate change has already exacerbated human displacement. Our modeling study of TC Idai suggests that climate change may have induced about 17,000 additional displacements from this one event. This is primarily due to the intensification of TC wind speed inducing a more powerful storm surge; and to a lesser extent due to sea level rise providing a higher baseline for the storm surge.

Our results likely underestimate the full contribution of climate change to displacement associated with TC Idai, because we solely addressed the effect of climate change on coastal flooding, neglecting changes in inland flooding. Between March 3 and 17, heavy precipitation between 200-400 mm was registered for Beira City and the region, with upstream sections of the Pungwe river basin exposed to more than 600 mm (Probst and Annunziato, 2019). With growing evidence that climate change not only affects precipitation intensity (Fowler et al., 2021; Guerreiro et al., 2018; Scherrer et al., 2016) but also continental-scale changes in fluvial flood discharge (Blöschl et al., 2019; Gudmundsson et al., 2021), it is likely that in a world without climate change, the river flood magnitude would have been smaller, and even less people would have been exposed than in our coastal-only counterfactual. Quantifying this additional effect would require a river flood model capable of reproducing the observed flood extent and associated inundation depths, and ideally coupled with a coastal flood model to capture the interaction between river flood and storm surge. Even though globally-applicable frameworks for compound flood hazard modeling are under construction, and have recently been tested for TC Idai (Eilander et al., 2022), evaluations of fluvial flood models reveal important shortcomings in data-scarce regions such as Mozambique (Bernhofen et al., 2018; Mester et al., 2021). Quantifying the role of river flooding in TC-induced displacement thus is a timely challenge.

Our main analysis also assumed no direct effect of high wind speeds on displacement, lacking clear evidence for substantial displacement due to high winds alone. Our additional sensitivity analysis suggests that changing this assumption could increase the number of displacements attributable to climate change considerably. Given this potentially large effect, and our limited understanding of the relative roles of different drivers of displacement in general, the specific vulnerability to displacement from different types of hazard should be the subject of future studies. Moreover, assuming that displacement can occur already at

inundation depths of less than 100 cm also leads to higher estimates of climate change-attributable displacement, according to our sensitivity analysis. Again, a better understanding of vulnerability beyond hard thresholds will be critical to refine risk assessments.

We did not change storm track or size in our counterfactual simulations. While storm tracks may be affected by climate change (Knutson et al., 2019), we assume that Beira has not become more or less likely as a landfall site. Mean storm size is found to increase systematically with the relative sea surface temperature (Chavas et al., 2016), although numerical simulations suggest that projected median sizes remain nearly constant globally (Knutson et al., 2015). Assuming increases in storm size due to climate change would again result in higher estimates of attributable displacements in our analysis. Furthermore, uncertainties regarding the population and observatory data, such as the satellite imagery, as well as the underlying digital elevation model (DEM), used for both the inland flood depth estimation and the coastal flood model, should not be neglected (Hawker et al., 2018).

By design, in our attribution study, we assumed a fixed population distribution in both factual and counterfactual simulations, as well as a fixed, empirically determined displacement vulnerability factor, and only investigated changes in displacement risk following from changes in the physical characteristics of TC Idai and its impacts. Assessments of future risks - or of past impacts - should not only take into account the intensification of physical hazards, but also increases in exposure (Kam et al., 2021); as well as potential changes in vulnerability due to social, economic, or technological developments. Changes in vulnerability have been studied with respect to economic damages and fatalities (Jongman et al., 2015; Sauer et al., 2021), but not for displacement.

Here, we have chosen a storyline approach for the impact attribution instead of a more traditional probabilistic attribution approach (Philip et al., 2020; Titley et al., 2016), as for instance previously employed to attribute heavy precipitation of Hurricane Harvey (Oldenborgh et al., 2017) to climate change. One reason is that for Mozambique neither the complete time series of rainfall nor the high station density required by a probabilistic approach (van Oldenborgh et al., 2021) are available. Reanalysis products for precipitation could be used as an alternative, however, their quality depends on geographic location, so the use of multiple reanalysis and/or observation products is recommended (Angélil et al., 2016). Further, in contrast to the probabilistic approach, the storyline approach allows us to investigate the driving factors involved, as well as their plausibility (Shepherd et al., 2018). Finally, framing the risk of tropical cyclones in the context of climate change in an extreme event-oriented rather than a probabilistic manner allows us to assign absolute numbers of attributable displacements, which raises risk awareness in a more tangible way.

Our study expands the scope of extreme event impact attribution to include displacement as a societal impact dimension. In general, due to the lack of calibrated regional models and gauge stations, only few attribution studies (Luu et al., 2021; Takayabu et al., 2015) focus on storms - or any extreme weather events, for that matter - in low-income countries. This not only limits our understanding of climate change effects on extreme events from a global perspective, but also biases geographically the amount of knowledge and information available to inform risk management and adaptation strategies (Otto et al., 2020). Mozambique, like many countries, is exposed not only to TCs but also other climate-related hazards, such as droughts, and at the same time facing socio-economic challenges, making it all the more important to understand and anticipate risks in a changing climate.

5.5 Code availability

The source code for this study is available from https://github.com/BenediktMester/TC_Idai_attribution.

5.6 Data availability

Satellite imagery is used with the permission of Atmospheric and Environmental Research & African Risk Capacity. Output of the flood depth algorithm, GeoClaw results, and TC Idai wind speed files can be accessed at https://zenodo.org/record/6907855 (Mester et al., 2022c). GHS gridded population data is available at https://data.jrc.ec.europa.eu/dataset/jrc-ghsl-ghs_pop_gpw4_globe_r2015a#dataaccess.

National borders of Mozambique were obtained from https://gadm.org/data.html. For the trendline analysis of annual means of maximum wind speeds we use IBTraCS Version 4 database, accessible at https://www.ncei.noaa.gov/data/international-best-track-archive-for-climate-stewardship-ibtracs/v04r00/access/netcdf/IBTrACS.ALL.v04r00.nc.

All data used for the figures are publicly available. Maps were generated with QGIS, which can be downloaded at https://www.qgis.org/. Satellite imagery background by © Google Maps can be accessed via http://mt0.google.com/vt/lyrs=s&hl=en&x={x}&y={y}&z={z}. We used IBTrACS Version 4 to extract the trajectory data of tropical cyclone Idai, availabe at https://www.ncei.noaa.gov/products/international-best-track-archive?name=ib-v4-access.

Mozambique admin level 4 shapefiles for Beira are available at https://data.humdata.org/dataset/mozambique-admin-level-4-beira-and-dondo-neighbourhood-boundaries. GSHHG shoreline data can be accessed via https://www.ngdc.noaa.gov/mgg/shorelines/data/gshhg/latest/.

5.7 Competing interests

The authors declare no competing interests.

5.8 Acknowledgments

This research received funding from the European Union's Horizon 2020 research and innovation programme under grant agreement No 820712 (RECEIPT).

Chapter 6 Discussion and recommendations

This thesis is motivated by the question on how flood-induced human displacement risk is affected by climate change and socio-economic change. In this chapter, the main findings, limitations, and uncertainties of this work are discussed and connected to the three **RQs**. The outcome is also placed in the context of the **Overarching Research Question** of this thesis. Each section is accompanied by an outlook on emerging challenges, expressed in **Future Research Questions (FRQs)**. Recommendations are made, if possible, on how to advance on these topics.

6.1 Improving the global flood modeling chain

Chapter 2 describes the evaluation of the global flood model CaMa-Flood in reproducing flood extent of historic flood events. A focus is set on the choice of two cascading data products of the global flood modeling chain, i.e., three climate reanalysis datasets and the output of 11 GHMs. Before this study, the sensitivity towards this choice was unknown. This chapter hence contributes to the improvement of global flood simulations (**RQ 1**) by guiding future applications of the input data products. Moreover, this work sheds light on general deficiencies in simulating historic flood events, and suggests several root causes for this model behavior. These insights are also relevant for overall topic of modeling flood-induced displacement, with the key findings of this chapter can be summarized as follows:

1. For most events, the simulated flood extent is rather insensitive to the choice of GHM and climate reanalysis dataset
2. Using a full suite of input products guarantees the robustness of the results as individual product combinations may lead to poor results for some events
3. Simulated flood extent is mostly overestimated (underestimated) when considering (neglecting) protection measures; translating most probably to great differences in affected people and estimated IDPs

Sensitivity to the choice of input product

Regarding the first key finding, the study addresses the need for investigating the role of climate forcing datasets and GHMs in simulating global flood hazard (Hoch and Trigg, 2019; Ward et al., 2013; Zhou et al., 2021). The GHM simulations are standardized and follow the same ISIMIP protocol. Before this study, it was unclear if the models are interchangeable or if some combinations of GHM and reanalysis data are to be favored. Chapter 2 highlights that generally no individual product or combination excels in all study regions. Rather, single GHMs lead to a poor performance in reproducing past flood extent for some events, while the other

GHMs are more or less equally performant. Similarly, differences among the climate reanalysis datasets are small in comparison with overall capacity in reproducing the correct flood extent. This implies for modeling global displacement risk that the choice of underlying input product is of comparatively low importance. Nonetheless, individual GHMs or reanalysis datasets or a combination of both lead to poor results; emphasizing the need for an ensemble of input products to account for individual deficiencies in some climatic regions or hydrological basin types. For example, the GHM MPI-HM in combination with the PGFv2 dataset produces one of the best results for a set of events, however, performs rather poorly for others, leading to a medium Median Region score. MPI-HM in combination with the GSWP3 reanalysis product is never the best GHM for single events, however, yields the best Median Region score of all GHMs. The findings of this chapter can be used to identify the most promising combination(s) of input products for individual hydrological basins or climatic zones. However, as laid out above, for continental- or global-scale analysis, this approach is not recommended. Emerging from this, other data products and processes, e.g., DEMs, routing schemes, downscaling, or intensity-impact functions, may require a similar sensitivity study to ensure robust estimations of affected people and IDPs. This also includes assumptions about flood protection measures in place which is discussed next.

Flood protection standards

Chapter 2 underpins the need for a detailed representation of flood protection levels. To this date, to the knowledge of the author, FLOPROS is the only existing global-scale river flood protection database. “openDELvE” provides global flood-protection levee data for river deltas (Nienhuis et al., 2022), however, this product is not used within the global flood modeling chain of this work. A comprehensive global overview on the actual standard of protection in place, or at least required policy regulations, is still missing. FLOPROS fills these gaps by modeling protection standards, mostly based on GDP per capita, for the majority of countries, especially the low-income ones (Scussolini et al., 2016). As highlighted in Chapter 2, assuming no flood protection leads to an overestimation of flood extent, on the other hand, the incorporation of the FLOPROS database produces an underestimation in flood extent. While the former one is to be anticipated, the latter one poses a critical challenge to overcome. This observation can be explained by potential deficiencies of FLOPROS in estimating the correct flood protection level, i.e. the assumptions are too high. Protection levels are on province-level (1st subnational administrative unit) and for most countries only derived from simulations mostly based on economic wealth (Scussolini et al., 2016), neglecting the high spatial heterogeneity in flood protection within countries and the influence of non-economic factors on structural defenses (Ward et al., 2017).

Flood frequency distribution

Another explanation for the underestimation in flood extent is the runoff and the respective return period of the flood simulated by the GHMs (Zhou et al., 2021). This source of error is backed by the observation that individual GHMs still reproduce flood extent even with the application of FLOPROS. If flooding of a given magnitude is modeled too frequently at a certain location, already low protection levels may lead to no inundation in the simulations. Contrarily, in some regions, e.g., Huainan in China, almost no flooding remains with any of the GHMs once FLOPROS is applied. This points to deficiencies in the river routing scheme by CaMa-Flood or the subsequent flood frequency analysis. The latter one was subject of a sensitivity study that suggested that the choice of variables for the flood frequency analysis and fitting distributions are less important than deviations in the runoff inputs (Zhou et al., 2021).

Outlook

High uncertainties in the simulated flood extent imply severe consequences for modeling flood events and associated risk of displacement. A core method in quantitative displacement modeling is to superimpose simulated flood extent and gridded population data to assess the number of people at risk of being displaced, as demonstrated in Chapter 4 and Chapter 5. An over- or underestimation of flood extent causes large deviations in the number of estimated IDPs, as similarly shown for population and economy exposure (Zhou et al., 2021). This error propagates down to hotspot identifications, disaster risk reduction measures, and management options to mitigate the adverse effects of displacement. To overcome this challenge, two new **FRQs** can be posed:

FRQ 1: How can estimates of global flood protection levels be improved and downscaled to more granular spatial units?

Despite the efforts of existing databases, such as FLOPROS, more detailed information on actual flood protection standards at a high spatial resolution (gridded; 2nd or 3rd subnational administrative unit level) is necessary as risk estimates are highly sensitive to this parameter (Ward et al., 2013). Artificial intelligence and machine learning, such as natural language processing, could be employed to gather fragments of empirical information on flood protection from the numerous scientific publications, government reports and other data sources (Bates et al., 2021). Other options cover the inclusion of dams and reservoirs and their respective amount of flood storage by the GRanD database (Lehner et al., 2011) or using multivariate methods to model flood protection levels (Scussolini et al., 2016). As an alternative to the GRanD database, which dates back to 2011, the automatic detection of dams, levees, dikes,

and other structural measures on satellite imagery could be used to build an updated inventory of mapped locations, dimensions, and possibly even estimates on protection capacities.

FRQ 2: How can the overestimation in simulated flood frequency within the global flood modeling chain be corrected?

Biases in the flood frequency distribution could be related to hydrological processes of the GHMs or to the river routing scheme of the hydraulic modeling part. Apart from improving the models directly, it might also be possible to correct the biases in the post processing phase of the modeling pathway. One option involves the comparison of simulated flood extent and corresponding return periods (on grid cell level) with observed flood extent for multiple events. One promising source for observatory data would be the GFD, as used in Chapter 3 and Chapter 4. For some events, it may be possible to determine the model return period that separates (observed) flooding from no-flooding. This threshold could be interpreted as a measure of bias in simulated flood frequency distribution and consequently be used for bias correction. Additionally, the threshold could also be interpreted as a local flood protection standard, and be compared with FLOPROS and other sources for plausibility, relating to FRQ 1.

Additional future work

Apart from answering these research questions, the global flood modeling chain can also be improved in several other ways, e.g., elaborating on the fine scale dynamics of floodplain inundation processes (Bates et al., 2021). Using the latest CaMa-Flood version 4.0 might refine the flow physics as it is based on an updated baseline topography (Yamazaki et al., 2019). Alternatively, increasing the spatial resolution could improve the accuracy of flood hazard modeling and allow for more rigorous comparison with observatory data. The evaluation exercise of Chapter 2 could also be repeated for other flood events. The availability of observed flood extent from satellite imagery has increased more recently; the GFD, for example, provides a set of 913 flood events. Further GFM evaluation and intercomparison studies could also include other hazard characteristics, such as inundation duration or flood depth, to enhance our understanding on the capabilities and limitations of global flood risk modeling.

6.2 Socio-economic drivers of vulnerability to displacement

Following the assessment of flood hazard modeling, Chapter 3 and Chapter 4 describe the creation of the new displacement data product FLODIS and its analysis regarding socio-economic drivers of vulnerability, respectively, which relate to **RQ 2**. The findings are discussed in more detail below and are divided into two sections according to the chapter structure, addressing FLODIS and the associated vulnerability analysis. The first part focuses on the underlying data and methods to derive FLODIS, including recommendations to increase the quality. The second part highlights how this new dataset can be used to investigate the socio-economic drivers of vulnerability to displacement. This analysis is a prerequisite in understanding how societal changes affect displacement risk both nowadays and in the future, referring to the **Overarching Research Question** of this thesis.

6.2.1 FLODIS

Matching satellite-derived flood hazard and spatially explicit displacement events yields the new disaster product FLODIS. Its development is motivated by the fact that, on the one hand, disaster impact inventories mostly only exhibit ambiguous information on the hazard, e.g., expressed by severity classes or disaster magnitude values. On the other hand, societal impacts are seldomly allocated to hazard archives or hydro-meteorological time series. FLODIS hence represents an unique repository of both detailed hazard and impact information for distinctive events. Less entries are available in comparison with other disaster databases due to, for example, the limited number of observed floods or failures in the geocoding process. FLODIS provides instead coupled hazard-impact information of high detail focusing on a rigorous matching process. Disaster entries are also extended with a set of subnational socio-economic characteristics of the event, such as demographic composition or GDP per capita. Such information is missing in other inventories, yet necessary for understanding the contextual drivers of flood vulnerability. Another novelty of this disaster dataset is the representation of flood hazard by observed flood footprints derived from satellite imagery products instead of GFMs. Despite recent model advancements, GFMs are still facing troublesome difficulties in reproducing flood extent in some catchments, as discussed in Chapter 2. This motivated to explore remote sensing products as an alternative to simulated flood extent. The key findings and achievements of this chapters can be summarized as:

1. Linking displacements, fatalities, and economic damages to remotely observed floods yields an unprecedented global inventory of both flood exposure and societal impact
2. Each FLODIS entry comprises sub-national socio-economic, demographic, environmental and other indicators

3. Using observed flood hazard from remote sensing poses a trustworthy alternative to GFMs; drawbacks include the lack of flood depths and the inability to simulate scenarios

Disadvantages of the usage of satellite-derived flood hazard and other limitations as well as points of improvements are discussed next.

Matching process

The matching procedure between displacement and flood hazard entries is subject to improvement. In the current setup, approximately 15% of all matches include two or more GFD floods. It is possible that the matched GIDD entries consist of sub-events, which could be allocated to individual GFD floods. However, some events are potentially matched in time and space with wrong flood extents. Double-or more matching is aimed to be avoided by using, for example, shorter temporal difference thresholds in such cases. However, more elaborated approaches could be applied to limit the matched GFD floods as much as possible. For example, the degree of spatial overlap in relation to the flood extent or matching all events by the shortest time difference are potential options.

Spatial distribution of IDPs

As only one number of IDPs per event is stated by GIDD, FLODIS assumes a spatial homogeneous distribution of IDPs. In most cases, this assumption is not correct since locally diverging levels of hazard intensity, population exposure, and vulnerability would lead to spatial differences in resulting IDPs after a flood event. In recent years, IDMC also records spatially more granular displacement information. Dividing a flood into several sub-floods and allocating displacement numbers according to their location would yield spatially more explicit insights. Another way to increase the quality of FLODIS would be the incorporation of lower levels of subnational administrative units, e.g. level 3 that includes municipalities and towns. Such information is partially already provided by GIDD and could be used to avoid an overestimation in flood exposure.

Necessity for updates

Between 2008 and 2018, 12.6% of all flood-induced displacement entries contain no event information, mostly in the early years of data recording. As information per entry has been increasing over time, the share of events that can be geocoded will increase in the future. The number, quality and resolution of sub-national socio-economic drivers will increase in the future as well. In this regard, FLODIS should also be regularly updated to incorporate the most recent events. This process depends also on the data availability of, for example, flood hazard

data from the GFD, which to this date ends in 2018. With a growing number of FLODIS entries, analysis results are expected to become more robust. Improving the geocoding algorithm would also yield more entries. Currently, 19.3 % of analyzed flood-induced displacement entries contain event information, yet, no geocoding is possible. This can be partially explained by not considering level-3 administrative units or an actual lack of geographical information, but also by deficiencies of the geocoding process.

Outlook

A couple of future applications arise from FLODIS. For example, the matching procedure is applicable to other disaster catalogs, e.g., Munich Re's NatCatSERVICE or Swiss Re's Sigma. The major recording work of IDMC started in 2008, making it difficult to reconstruct displacement events before. Yet, using vulnerability estimates and satellite imagery, or other hazard information, e.g. by GFMs, would allow drawing conclusions about displacement events before 2008 and eventually about the temporal evolution of flood-induced displacement impacts.

A major future task is the incorporation of flood depths within FLODIS, which is a necessary next step in the context of infrastructure vulnerability to displacement. Despite characteristics regarding the density of critical infrastructure, no information on the degree of housing and infrastructure exposed to critical flood depths is available in FLODIS. The destruction of housing is a major cause for displacement (Anzellini et al., 2017). Determining the number of buildings, or alternatively the population, exposed to high flood waters could improve displacement risk analysis. Similar to depth-damage functions which are often used for global-scale flood risk assessments (Ward et al., 2020), impact functions used in some studies on displacement (Anzellini et al., 2017; Kam et al., 2021), e.g. 1 m-step functions, can be used to estimate the number of IDPs once flood depth information is available. Furthermore, geocoded displacement events of other hazard categories may also be matched with hazard estimates. As 43 % of all weather-related displacements are caused by TCs and storms (IDMC, 2022), it would be worthwhile to extend FLODIS with this type of hazard category. Both challenges lead to the next two **FRQs**:

FRQ 3: How can flood depth estimations be incorporated into FLODIS?

Deriving flood depths estimates only requires the GFD flood extents and global DEM as input. The process itself, however, is not trivial, involving, for example, error correction of the flood extent, accounting for drainage network information, or the availability of high-resolution flood extent (Bryant et al., 2022). One option would be to automatically derive the flood depth for the whole set of GFD floods by employing existing flood depth estimation tools, such as FwDET or RICorDE (Bryant et al., 2022; Cohen et al., 2019). The RICorDE approach is already successfully applied using global data for the fluvial flooding by TC Idai in Chapter 5.

While several global DEM products at high spatial resolutions are available, such as the MERIT DEM at 90 m (Yamazaki et al., 2019), the flood depth estimation is limited by the GFD flood extent due to the coarser resolution of 250 m.

FRQ 4: How can tropical cyclones be integrated into FLODIS?

The GFD floods are only matched with IDMC entries related to “Flood”, not including “Storm”-related displacement events. Storms and TCs, as demonstrated with the example of TC Idai, may also lead to extensive coastal and inland flooding. The geocoding process of FLODIS covers all type of displacement events, including storms and TCs. The flood footprints and associated displacement impacts for storms are hence registered in the underlying data inventories of FLODIS, which can be used to extend FLODIS with this hazard category. In this context, it may be necessary to link high wind speed exposure to storm-induced displacement events to capture multivariate compound events (Zscheischler et al., 2020).

6.2.2 Analysis of vulnerability to displacement

Based on the new hazard-impact-dataset FLODIS, Chapter 4 exhibits the analysis of vulnerability to flood-induced displacement and its socio-economic drivers. Few global-scale studies exist that investigate displacement risk and only one of those, to the knowledge of the author, addresses the associated vulnerability (Kakinuma et al., 2020). Chapter 4 specifically targets the topic of vulnerability to displacement using a large set of observed flood extent derived from remote sensing to simulate flood hazard. A diverse set of contextual indicators are applied to describe the socio-economic, demographic, and other circumstances of the events. A machine learning framework investigates these features to reveal their importance in explaining the global variability of vulnerability. The following key findings can be distilled out of this work:

1. Displacement vulnerability is varying between and within continental regions by several orders of magnitude
2. The majority of development factors are positively correlated with lower levels of vulnerability
3. Non-economic predictors partially exhibit a higher explanatory power than GDP per capita
4. Important predictors include urbanization (growth), infant mortality rate, density of population and critical infrastructure

As the importance rankings and partial dependence plots of this study only depict how the model interacts with the provided FLODIS dataset, general conclusions on vulnerability to

flood-induced displacement are drawn with caution. Nonetheless, Chapter 4 addresses general assumptions, extends preliminary investigations, and provides new insights in the underlying processes that shape the vulnerability to displacement (**RQ 2**). The following sections discusses the vulnerability predictors and limitations in assessing their importance. In this context, it is laid out how these insights may be used in modeling global displacement risk and which next steps should be taken to refine vulnerability estimates.

Predictors of vulnerability

The common perception that the level of development is linked with (displacement) vulnerability is confirmed with this study. The strongest development predictors exhibit positive relations with lower vulnerability levels, i.e. the wealthier, more equal, and more secure, the less likely to be displaced. Vulnerability varies substantially between countries and by several orders of magnitude, which is in line with other modeled vulnerability studies at the global scale (Kakinuma et al., 2020). The national median vulnerability values differ somewhat from poverty maps and other quantitative approaches to categorize the flood risk of countries into “low” and “high”. This is to be anticipated as displacement risk is a complex phenomenon, differing from mortality and loss mechanisms, and going beyond societal assessments that are often only economically based. In fact, GDP per capita is only a predictor of medium relevance for both the national and sub-national analysis in this work. In addition, no distinctive two or three “best predictors” can be singled out, rather most predictors explain vulnerability to at least some degree. This confirms the demand for broad societal background information to characterize flood events, as provided by FLODIS. Nonetheless, urbanization (growth), infant mortality rate, density of population and critical infrastructure are identified as the major predictors of vulnerability in this study. This information provides evidence for humanitarian and disaster relief organizations that a diverse set of indicators is necessary to target groups especially vulnerable to displacement (Ward et al., 2020). These elaborated characteristics cover not only poverty and other economic shortages but also reflect that the settlement composition, societal inequality, or access to infrastructure also shape vulnerability.

Modeling limitations

In this study vulnerability can only be explained to some degree, characterized by, for example, missing data for some countries, ambiguous partial dependence plots, or a maximum R2 of 0.3. Even though the latter one is only one metric to assess the performance of a model, the results call for caution in drawing universal conclusions from this work. First, the underlying dataset FLODIS exhibits several deficiencies, e.g., regarding the matching process, geocoding, flood hazard data, population count, or the socio-economic indicators. Incorporating flood depths and more refined matching techniques would yield vulnerability estimates of higher accuracy for the analyzed events. The applied predictors also potentially

only represent a fraction of components that determine displacement vulnerability. Flood experience, for example, is computed in a simplistic approach for this study, neglecting the complex interactions and feedback loops between hydrological and social processes (Di Baldassarre et al., 2013). Furthermore, it is difficult, if not impossible, to display levels of early warning systems, holistic flood management or proactive governance consistently on a global scale. Another factor is the low number of entries in FLODIS, allowing only for limited insights into displacement vulnerability. Some countries only consist of one observation, while others have no FLODIS entry at all. This means that the findings of this study are predominantly based on a set of countries with many FLODIS entries, such as Indonesia, India or China. Future analysis should contain more data entries, especially in underrepresented world regions, e.g., Europe or the MENA-region, which is in line with the general need for regular updates of FLODIS. More data would also allow the usage of more complex models. This involves an extended set of predictors without the risk of overfitting or even more elaborated regression techniques, e.g., support vector machines or neural networks.

Fields of application

While it is not yet possible to express vulnerability to displacement through a universal formula or statistical model, this work provides the basis on how vulnerability should, and should not, be handled in future risk analysis studies. The results demonstrate that vulnerability varies by several orders of magnitude and a spatial distribution according to economic wealth alone is not advisable. The derived national median vulnerability values yield a first approximation, posing an alternative to other approaches assuming vulnerability is equally distributed around the world and displacement risk is only dependent on flood depth and extent. As vulnerability is also not fixed in time, future (sub-)national vulnerability levels may differ from current ones due to societal shifts. The constructed models of this work could incorporate such changes via changes in the underlying contextual predictors. For some predictors no projections are yet available, however, for others projections under the framework of shared socioeconomic pathways (SSPs) exist, e.g., urbanization (Chen et al., 2020), GDP (Murakami and Yamagata, 2019), or population density (Jones and O'Neill, 2016).

Outlook

Most global-scale studies employ GFMs to simulate flood hazard (Bates et al., 2021; Hirabayashi et al., 2013; Ward et al., 2013). This study shows that flood extent derived from a large set of remote sensing is a valid alternative to flood hazard simulated by GFMs, which is, to the knowledge of the author, another novelty in global-scale risk analysis of displacement. To test the sensitivity to the choice of hazard data, it is of interest to investigate the vulnerability derived from GFM simulations and compare it with the results of this work. Additionally, changes in exposure are responsible for major shifts in flood risk (Ceola et al., 2014; Di

Baldassarre et al., 2010). It is hence advisable to complement the displacement risk equation and address the **Overarching Research Question** by also investigating the role of exposure. This challenge leads to the next **FRQ**:

FRQ 5: In what ways do changes in exposure affect the flood-induced displacement risk?

Increases in historic flood risk can be partially explained by changes in the exposure to flooding (Ceola et al., 2014; Di Baldassarre et al., 2010), in particular by intensive and unplanned urbanization in hazardous floodplains (Andreadis et al., 2022). Including changes in population size will increase flood risk in the future even more (Swain et al., 2020), with marginalized communities being disproportionately impacted (Wing et al., 2022). The important role of population projections is also demonstrated for displacement risk (Kam et al., 2021). Future research should hence also focus more in detail on population projection trajectories as well as individual data sources for exposure; covering, for example, sensitivity tests to the choice of population data, as similarly performed by Bernhofen et al. (2021) and Smith et al. (2019). FLODIS provides affected people estimates on two population datasets, of which only one was used in the vulnerability analysis. Additionally, as housing quality shapes the disaster vulnerability (Flanagan et al., 2011), exposure estimates could also differentiate between different types of housing (building code, age, flood-proof, etc.) to explore how displacement risk is dependent on settlement characteristics.

6.3 Attribution of displacement to climate change

Following the examination of contextual vulnerability drivers, Chapter 5 addresses the **RQ 3** on how recent climate change has potentially affected the number of flood-induced displacements for the example of coastal flooding and high wind speeds by TC Idai. The applied storyline approach helps to understand why TC Idai unfolded the way it did, focusing on SLR and wind speed intensification due to global warming. The outcome of this study are absolute numbers of IDPs attributable to climate change. Even though these estimated numbers are based on simulations and should be taken with caution due to several limitations, this study conveys the risk of TCs under global warming in a tangible way. The impact attribution of TC Idai hence provides a starting position for adaptation planning, raises awareness on the immediacy of climate change, and calls for stronger mitigation measures. The key findings of this study are:

1. Climate change led a simulated increase in displacement risk by approximately 3.1 to 3.5%, corresponding to 16,000 - 17,000 additional IDPs
2. TC intensification causes the major share of additional IDPs in comparison with SLR
3. The effect of climate change on TC high wind speeds is high, but subject to large uncertainties
4. The effect of climate change on fluvial flooding is not included, which could drive the increase in displacement risk even more

Only few attribution studies (e.g., Takayabu et al. (2015)) focus on events taking place in low-income countries due to the lack of calibrated regional models and low-density networks of gauge stations. This limits not only our understanding of climate change effects on extreme events from a global perspective, but also excludes local communities from potentially useful information about risk management and adaptation strategies. Additionally, impact attribution studies often focus on economic dimensions. Hence, there is a need for impact attribution studies focusing on low-income countries and non-economic impacts (Otto et al., 2020; Thalheimer et al., 2022). This study on displacement risk in Mozambique ties in with this call, yet, the work presented also exhibits several simplifications and assumptions, which are discussed more in detail below. A focus is set on the general limitations of attributing TCs to climate change, the applied concept of vulnerability and future displacement risk due to TCs.

The effect of climate change on tropical cyclones

In this study, the effect of SLR is assessed to be marginal for coastal flooding induced by TC Idai; local SLR varies, however, substantially (Fox-Kemper et al., 2021) which may alter, if used instead of global estimates, its role for this event. A lot of debate exists about how climate

change has affected the wind-speed intensity of TCs (Knutson et al., 2019). One the one hand, changes in intensity have been observed for some basins, including the South Indian Ocean, however, these should be treated with high caution as long and consistent data records are missing (Knutson et al., 2019; Kossin et al., 2013, 2007; Webster et al., 2005). On the other hand, even no increase was detected for individual TCs, e.g., hurricanes Katrina, Irma and Maria (Patricola and Wehner, 2018). Additionally, multi-decadal or interannual climate variability, such as the Atlantic Multidecadal Oscillation or the El Niño–Southern Oscillation, respectively, may obscure the effects of climate change on TCs (Patricola and Wehner, 2018). Nonetheless, the presented analysis of the South Indian Ocean basin shows a steady increase in extreme wind speeds, indicating that an intensification of TCs is indeed present in this region. This hence underpins the need for high quality as well as consistent, long-term recording of TCs in all basins around the globe to refine TC-induced displacement risk analysis.

Vulnerability

It is very difficult, if not nearly impossible, to exactly reconstruct how TC Idai would have evolved in the absence of climate change, as changes in size and trajectory or socio-economic shifts, such as those related to vulnerability, would have to be additionally accounted for, to name just a few examples. The applied vulnerability to displacement is fixed in this study and derived empirically by dividing observed displacements by the number of affected people of the factual scenario. In a world without climate change, vulnerability would be probably different to what it was for the observed conditions. Economic growth is positively linked with the capacity of dealing with climate extremes (Bowen et al., 2012), which in turn affects productivity levels and productivity growth (Kalkuhl and Wenz, 2020), with some evidence of negative impacts of historic climate change on economic growth for some African countries (Abidoye and Odusola, 2015). In addition, vulnerability is also shaped by non-economic factors, as outlined in Chapter 4, which may likewise be altered by climate change. Changes in vulnerability are likely to be small, however, accounting for socio-economic perturbations, compounding with changes in hazard intensity, would potentially accumulate to an even higher displacement risk. In this context, the study investigates also the sensitivity of displacement risk to the choice of critical flood depth threshold (0.1 m, 0.5 m, and 1.0 m), relating to vulnerability to infrastructure. As the number of attributable IDPs varies between these simplified thresholds, more refined, empirically derived impact functions for flood-induced displacement are required.

Future tropical cyclone risk

The storyline approach targets specific events, thus this study is not allowing for generalizations about climate change, TCs, and related IDPs. Nonetheless, the overall TC

intensity is projected to increase under future global warming (Knutson et al., 2020). According to the IPCC AR6 projections, an additional global increase in SLR and surface temperature of 0.39 m / 0.7°C (SSP1-2.6) and 0.72 m / 3.3°C (SSP5-8.5) is estimated by the end of the century (Chen et al., 2021). These increases in drivers of coastal flooding could also non-linearly scale with societal impacts, e.g., due to the underlying bathymetry, low-lying settlements or insufficient protection levels. This suggests that TCs of similar magnitude as TC Idai would be more devastating under future climate change, resulting in more IDPs and a greater need for humanitarian aid.

Outlook

In the light of these uncertainties and an average of 9.1 million TC-induced IDPs every year (IDMC, 2022), attributing IDPs to climate change is a challenging, but necessary task. This study investigates coastal flooding and, partially, wind extremes by TC Idai, however, inland flooding due to heavy rain is not considered. Fluvial flooding is assumed to be constant throughout all scenarios, including the counterfactual runs. However, inland flooding due to heavy rain associated with TCs is also affected by global warming in various ways (Knutson et al., 2019; Seneviratne et al., 2021), posing another driver of displacement risk. The next **FRQ** addresses this gap:

FRQ 6: To what extent was fluvial flooding and associated displacement due to TC Idai affected by climate change?

As laid out in section 1.2.3, it is possible to attribute extreme precipitation to climate change using the CC relationship. The rate of 7% precipitation increase per 1° of warming is potentially even higher for tropical cyclones (Oldenborgh et al., 2017; Patricola and Wehner, 2018). This provides a direct physical basis for attributing fluvial flooding and associated impacts by TC Idai partially to climate change (Shepherd, 2016). The storyline approach could be used to establish factual (climate change) and counterfactual (no climate change) scenarios using observed precipitation reanalysis data and, e.g., detrended precipitation data derived by the CC relationship, respectively. Similar to the storyline approach on coastal modeling presented in Chapter 5, both datasets could be fed into GFMs to generate factual and counterfactual inland flooding. Differences between the simulated flood extent and depth together with estimated IDPs could be used to assess the role of fluvial flooding on displacement in the light of global warming. Despite some challenges regarding, e.g., the coupling of pluvial, fluvial, and coastal flooding (Eilander et al., 2023) or on how changes in precipitation translate to changes in stream discharge (see section 1.2.3 for further discussion), such an impact attribution study would complement our view on how TC Idai was potentially influenced by climate change.

Additionally future work may encompass a refined analysis of TC high wind speed-induced IDPs. It would be also of interest to investigate a large set of TCs using the storyline approach and counterfactual climate datasets, such as ATTRICI (Mengel et al., 2021), to deepen our knowledge on TC-induced displacement attributable to climate change.

Chapter 7 Conclusion

Former UN Secretary-General Kofi Annan once noted that "[i]nternal displacement is the great tragedy of our time. The internally displaced people are among the most vulnerable of the human family" (OCHA, 2004). Despite millions of displacements every year, global warming being on the rise, and societal shifts transforming the resilience of our communities, only little is known about the effect of global climate change and socioeconomic change on flood-induced displacement risk (Hoffmann et al., 2021; IDMC, 2022; Seneviratne et al., 2021). This lack of knowledge is facing a growing public interest as well as heated debates around the topic of climate-related mobility (Ayeb-Karlsson et al., 2022; Clement et al., 2021). A deeper insight is limited by insufficient data on the circumstances of displacement events, such as the socio-economic contextualization, or detailed information on the underlying hazard characteristics that may be already influenced by climate change (Hoffmann et al., 2021, 2020). Several severe implications emerge from this, e.g., disaster relief funds cannot be directed to regions especially prone to displacement risk or humanitarian aid cannot effectively reduce the vulnerability to displacement. This thesis addresses these caveats in a number of ways, from improving the flood hazard modeling chain, investigating the socio-economic drivers that shape the vulnerability of being displaced, and down to the attribution of displacement risk to climate change.

To gain a better understanding on the ability of GFMs in reproducing flood extent, the global hydraulic model CaMa-Flood and its input products are evaluated against satellite imagery for eight historic events. Spatial performance metrics reveal that for most events the GFM is relatively insensitive to the choice of climate reanalysis dataset and GHM. Some reanalysis-GHM combinations, however, lead to poor results, reflecting the need for a full suite of input products and ensemble simulations to guarantee the robustness of the flood hazard modeling. Furthermore, this study reveals that, regardless of the input products, the simulated flood extent is often overestimated; incorporating protection levels according to the FLOPROS database yields the tendency of underestimating flood extent. The latter one is especially problematic and can be partially explained by deficiencies in reproducing the correct return periods within the modeling chain as well as an overestimation of FLOPROS protection levels. To overcome this caveat, it is recommended to apply a bias correction scheme on the flood frequency distribution using a large set of observed floods from the GFD. Protection level estimates could be improved by screening of relevant literature based on advanced machine learning techniques, multivariate modeling or the incorporation of satellite imagery to assess location and retention capacities of structural protection measures.

Following the evaluation of the flood hazard modeling chain, this thesis addresses the vulnerability to displacement by two studies. The first work comprises the development of the new disaster dataset FLODIS that can be used to investigate the contextual characteristics that drive the vulnerability of being displaced. FLODIS links human displacements, fatalities, and economic damages to remotely observed floods from the GFD, yielding an unprecedented

global inventory of both flood exposure and societal impact. This new dataset addresses the challenge that displacement entries are often completely missing any information on the associated flood magnitude, hampering the comparison of flood exposure or vulnerability between events. FLODIS entries encompass a full set of socio-economic, demographic and other indicators to characterize the societal and environmental context of each event. A special feature is that the flood hazard is estimated from observed flood extent based on satellite imagery, avoiding the challenges that GFMs are still facing, as described above. Next versions of FLODIS should incorporate flood depth estimates to improve risk assessments as well as displacement events related to coastal flooding and extreme wind speeds caused by TCs.

In the next step, the vulnerability to flood-induced displacement and its underlying drivers are investigated using FLODIS and machine learning methods. Multivariate regression using a random forest model shows that vulnerability is heterogeneously distributed around the world, not following general expectations according to economic prosperity. Other development indicators, such as infant mortality rate, urbanization or the density of population and critical infrastructure, exhibit a stronger power in explaining vulnerability than GDP per capita. While the majority of development indicators are positively and non-linearly correlated with lower levels of vulnerability, the role of some predictors is still unclear. This calls for larger training data to improve modeling capacities as well as a comparison with vulnerability analysis based on GFM hazard simulations. In this context, future research should also investigate the uncertainty related to the choice of exposure datasets in displacement risk analysis.

Next to the role of socioeconomic change, this thesis also examines the link between historic displacements and climate change. Global warming is one of the greatest intensifiers of future displacement risk (Clement et al., 2021; Kam et al., 2021), yet it is unclear to what degree increased temperatures have already influenced extreme flooding and associated mobility in the past. This interaction is investigated for the example of TC Idai and associated coastal flood-induced displacement. Coastal flood modeling in combination with fluvial flood hazard derived from satellite imagery allows to simulate TC Idai under observed, factual conditions as well as under counterfactual scenarios without the effect of global warming. A simulated increase in displacement risk by approximately 3.1 to 3.5%, corresponding to 16,000 - 17,000 additional IDPs, suggests that climate change has already intensified the associated humanitarian crisis. These numbers should not be taken at face value, as it is an almost impossible task to reconstruct how TC Idai would have evolved in the absence of climate change. Nonetheless, the applied storyline approach improves our process understanding on the amplification of coastal flooding and associated displacement risk due to climate change, indicating that the intensification of TC wind speeds lead to a stronger storm surge than the effect of SLR. Including the effect of climate change on extreme wind-induced and fluvial flood-induced displacement in future studies would complement the multivariate compound character of TCs and provide a full picture of amplified displacement risk.

This thesis contributes to the overall understanding on how global climate change and socioeconomic change affect flood-induced displacement risk. Given the IPCC projections of global warming, even under a low-emission scenario, the cost of adaptation could push especially low-income countries to the brink of financial collapse (Fankhauser, 2010; Seneviratne et al., 2021; Willner et al., 2018); forcing unprotected individuals to leave their homes due to unprecedented climate and weather extremes (Cissé et al., 2022). In this work, the potential of remote sensing in the context of global disaster research is explored; with satellite imagery serving as a benchmark for GFMs, an estimate of flood hazard in the absence of modeling results or even directly as a source of flood exposure for a large number of events. The presented work demonstrates how modeled estimates and projections of displacement risk under current and future climate change become more robust by improving our understanding of the flood hazard simulations. The newly developed disaster dataset FLODIS provides meaningful insights in how the vulnerability to displacement is shaped and offers vast possibilities of future research topics. The conducted attribution study is one of the first to investigate the role of climate change for a displacement event in a low-income country. The outcomes of this work may serve as a scientific basis for identifying regions of high displacement risk, improving the targeting of humanitarian aid, or even providing the basis of financial funding for flood protection measures. In the light of these advancements, this thesis successfully demonstrates that modeling the effects of climate change and socioeconomic change on displacement risk enhances our understanding of climate related mobility.

References

Abidoye, B.O., Odusola, A.F., 2015. Climate Change and Economic Growth in Africa: An Econometric Analysis. J. Afr. Econ. 24, 277–301. https://doi.org/10.1093/jae/eju033

Alfieri, L., Bisselink, B., Dottori, F., Naumann, G., de Roo, A., Salamon, P., Wyser, K., Feyen, L., 2017. Global projections of river flood risk in a warmer world: RIVER FLOOD RISK IN A WARMER WORLD. Earths Future 5, 171–182. https://doi.org/10.1002/2016EF000485

Alfieri, L., Cohen, S., Galantowicz, J., Schumann, G.J.-P., Trigg, M.A., Zsoter, E., Prudhomme, C., Kruczkiewicz, A., Coughlan de Perez, E., Flamig, Z., Rudari, R., Wu, H., Adler, R.F., Brakenridge, R.G., Kettner, A., Weerts, A., Matgen, P., Islam, S.A.K.M., de Groeve, T., Salamon, P., 2018. A global network for operational flood risk reduction. Environ. Sci. Policy 84, 149–158. https://doi.org/10.1016/j.envsci.2018.03.014

Amatulli, G., Domisch, S., Tuanmu, M.-N., Parmentier, B., Ranipeta, A., Malczyk, J., Jetz, W., 2018. A suite of global, cross-scale topographic variables for environmental and biodiversity modeling. Sci. Data 5, 180040. https://doi.org/10.1038/sdata.2018.40

Andreadis, K.M., Wing, O.E.J., Colven, E., Gleason, C.J., Bates, P.D., Brown, C.M., 2022. Urbanizing the floodplain: global changes of imperviousness in flood-prone areas. Environ. Res. Lett. 17, 104024. https://doi.org/10.1088/1748-9326/ac9197

Angélil, O., Perkins-Kirkpatrick, S., Alexander, L.V., Stone, D., Donat, M.G., Wehner, M., Shiogama, H., Ciavarella, A., Christidis, N., 2016. Comparing regional precipitation and temperature extremes in climate model and reanalysis products. Weather Clim. Extrem. 13, 35–43. https://doi.org/10.1016/j.wace.2016.07.001

Anzellini, V., Desai, B., Fung, V., Ginnetti, J., Milano, L., Montandon, R., Ponserre, S., 2017. Global disaster displacement risk - a baseline for future work. IDMC.

Aronica, G., Bates, P.D., Horritt, M.S., 2002. Assessing the uncertainty in distributed model predictions using observed binary pattern information within GLUE. Hydrol. Process. 16, 2001–2016. https://doi.org/10.1002/hyp.398

Atmospheric and Environmental Research & African Risk Capacity, 2022. Flood depictions: AER AFED v05r01.

Ayeb-Karlsson, S., Baldwin, A.W., Kniveton, D., 2022. Who is the climate-induced trapped figure? WIREs Clim. Change 13, e803. https://doi.org/10.1002/wcc.803

Bates, P.D., De Roo, A.P.J., 2000. A simple raster-based model for flood inundation simulation. J. Hydrol. 236, 54–77. https://doi.org/10.1016/S0022-1694(00)00278-X

Bates, P.D., Neal, J., Sampson, C., Smith, A., Trigg, M., 2018. Chapter 9 - Progress Toward Hyperresolution Models of Global Flood Hazard, in: Michel, G. (Ed.), Risk Modeling for Hazards and Disasters. Elsevier, pp. 211–232. https://doi.org/10.1016/B978-0-12-804071-3.00009-4

Bates, P.D., Quinn, N., Sampson, C., Smith, A., Wing, O., Sosa, J., Savage, J., Olcese, G., Neal, J., Schumann, G., Giustarini, L., Coxon, G., Porter, J.R., Amodeo, M.F., Chu, Z., Lewis-Gruss, S., Freeman, N.B., Houser, T., Delgado, M., Hamidi, A., Bolliger, I., E. McCusker, K., Emanuel, K., Ferreira, C.M., Khalid, A., Haigh, I.D., Couasnon, A., E. Kopp, R., Hsiang, S., Krajewski, W.F., 2021. Combined Modeling of US Fluvial, Pluvial, and Coastal Flood Hazard Under Current and Future Climates. Water Resour. Res. 57, e2020WR028673. https://doi.org/10.1029/2020WR028673

Beal, L.M., Vialard, J., Roxy, M.K., lead authors, 2019. IndOOS-2: A roadmap to sustained observations of the Indian Ocean for 2020-203 CLIVAR-4/2019, GOOS-237, 206 pp., 218.

Berghuijs, W.R., Aalbers, E.E., Larsen, J.R., Trancoso, R., Woods, R.A., 2017. Recent changes in extreme floods across multiple continents. Environ. Res. Lett. 12, 114035. https://doi.org/10.1088/1748-9326/aa8847

Bernhofen, M.V., Trigg, M.A., Sleigh, P.A., Sampson, C.C., Smith, A.M., 2021. Global flood exposure from different sized rivers. Nat. Hazards Earth Syst. Sci. 21, 2829–2847. https://doi.org/10.5194/nhess-21-2829-2021

Bernhofen, M.V., Whyman, C., Trigg, M.A., Sleigh, P.A., Smith, A.M., Sampson, C.C., Yamazaki, D., Ward, P.J., Rudari, R., Pappenberger, F., Dottori, F., Salamon, P., Winsemius, H.C., 2018. A first collective validation of global fluvial flood models for major floods in Nigeria and Mozambique. Environ. Res. Lett. 13, 104007. https://doi.org/10.1088/1748-9326/aae014

Best, M.J., Pryor, M., Clark, D.B., Rooney, G.G., Essery, R.. L.H., Ménard, C.B., Edwards, J.M., Hendry, M.A., Porson, A., Gedney, N., Mercado, L.M., Sitch, S., Blyth, E., Boucher, O., Cox, P.M., Grimmond, C.S.B., Harding, R.J., 2011. The Joint UK Land Environment Simulator (JULES), model description – Part 1: Energy and water fluxes. Geosci. Model Dev. 4, 677–699. https://doi.org/10.5194/gmd-4-677-2011

Biau, G., Scornet, E., 2016. A random forest guided tour. TEST 25, 197–227. https://doi.org/10.1007/s11749-016-0481-7

Bishop-Royse, J., Lange-Maia, B., Murray, L., Shah, R.C., DeMaio, F., 2021. Structural racism, socio-economic marginalization, and infant mortality. Public Health 190, 55–61. https://doi.org/10.1016/j.puhe.2020.10.027

Black, R., Adger, W.N., Arnell, N.W., Dercon, S., Geddes, A., Thomas, D., 2011. The effect of environmental change on human migration. Glob. Environ. Change, Migration and Global Environmental Change – Review of Drivers of Migration 21, S3–S11. https://doi.org/10.1016/j.gloenvcha.2011.10.001

Black, R., Arnell, N.W., Adger, W.N., Thomas, D., Geddes, A., 2013. Migration, immobility and displacement outcomes following extreme events. Environ. Sci. Policy, Global environmental change, extreme environmental events and “environmental migration”: exploring the connections 27, S32–S43. https://doi.org/10.1016/j.envsci.2012.09.001

Blöschl, G., Hall, J., Parajka, J., Perdigão, R.A.P., Merz, B., Arheimer, B., Aronica, G.T., Bilibashi, A., Bonacci, O., Borga, M., Čanjevac, I., Castellarin, A., Chirico, G.B., Claps, P., Fiala, K., Frolova, N., Gorbachova, L., Gül, A., Hannaford, J., Harrigan, S., Kireeva, M., Kiss, A., Kjeldsen, T.R., Kohnová, S., Koskela, J.J., Ledvinka, O., Macdonald, N., Mavrova-Guirguinova, M., Mediero, L., Merz, R., Molnar, P., Montanari, A., Murphy, C., Osuch, M., Ovcharuk, V., Radevski, I., Rogger, M., Salinas, J.L., Sauquet, E., Šraj, M., Szolgay, J., Viglione, A., Volpi, E., Wilson, D., Zaimi, K., Živković, N., 2017. Changing climate shifts timing of European floods. Science 357, 588–590. https://doi.org/10.1126/science.aan2506

Blöschl, G., Hall, J., Viglione, A., Perdigão, R.A.P., Parajka, J., Merz, B., Lun, D., Arheimer, B., Aronica, G.T., Bilibashi, A., Boháč, M., Bonacci, O., Borga, M., Čanjevac, I., Castellarin, A., Chirico, G.B., Claps, P., Frolova, N., Ganora, D., Gorbachova, L., Gül, A., Hannaford, J., Harrigan, S., Kireeva, M., Kiss, A., Kjeldsen, T.R., Kohnová, S., Koskela, J.J., Ledvinka, O., Macdonald, N., Mavrova-Guirguinova, M., Mediero, L., Merz, R., Molnar, P., Montanari, A., Murphy, C., Osuch, M., Ovcharuk, V., Radevski, I., Salinas, J.L., Sauquet, E., Šraj, M., Szolgay, J., Volpi, E., Wilson, D., Zaimi, K., Živković, N., 2019. Changing climate both increases and decreases European river floods. Nature 573, 108–111. https://doi.org/10.1038/s41586-019-1495-6

Blöschl, G., Kiss, A., Viglione, A., Barriendos, M., Böhm, O., Brázdil, R., Coeur, D., Demarée, G., Llasat, M.C., Macdonald, N., Retsö, D., Roald, L., Schmocker-Fackel, P., Amorim, I., Bělínová, M., Benito, G., Bertolin, C., Camuffo, D., Cornel, D., Doktor, R., Elleder, L., Enzi, S., Garcia, J.C., Glaser, R., Hall, J., Haslinger, K., Hofstätter, M., Komma, J., Limanówka, D., Lun, D., Panin, A., Parajka, J., Petrić, H., Rodrigo, F.S., Rohr, C., Schönbein, J., Schulte, L., Silva, L.P., Toonen, W.H.J., Valent, P., Waser,

J., Wetter, O., 2020. Current European flood-rich period exceptional compared with past 500 years. Nature 583, 560–566. https://doi.org/10.1038/s41586-020-2478-3
Boas, I., Farbotko, C., Adams, H., Sterly, H., Bush, S., van der Geest, K., Wiegel, H., Ashraf, H., Baldwin, A., Bettini, G., Blondin, S., de Bruijn, M., Durand-Delacre, D., Fröhlich, C., Gioli, G., Guaita, L., Hut, E., Jarawura, F.X., Lamers, M., Lietaer, S., Nash, S.L., Piguet, E., Rothe, D., Sakdapolrak, P., Smith, L., Tripathy Furlong, B., Turhan, E., Warner, J., Zickgraf, C., Black, R., Hulme, M., 2019. Climate migration myths. Nat. Clim. Change 9, 901–903. https://doi.org/10.1038/s41558-019-0633-3
Boulange, J., Hanasaki, N., Yamazaki, D., Pokhrel, Y., 2021. Role of dams in reducing global flood exposure under climate change. Nat. Commun. 12, 417–417. https://doi.org/10.1038/s41467-020-20704-0
Bowen, A., Cochrane, S., Fankhauser, S., 2012. Climate change, adaptation and economic growth. Clim. Change 113, 95–106. https://doi.org/10.1007/s10584-011-0346-8
Brakenridge, G.R., 2006. “Global Active Archive of Large Flood Events”, Dartmouth Flood Observatory, University of Colorado.
Breiman, L., 2001. Random Forests. Mach. Learn. 45, 5–32. https://doi.org/10.1023/A:1010933404324
Bryant, S., McGrath, H., Boudreault, M., 2022. Gridded flood depth estimates from satellite-derived inundations. Nat. Hazards Earth Syst. Sci. 22, 1437–1450. https://doi.org/10.5194/nhess-22-1437-2022
Canning, S., Walton, R., 2014. Western Downs Regional Council. 2014 Flood Study Reports - Dalby Flood Study Volume I. Detailed Technical Report Western Downs Regional Council (available at: https://www.wdrc.qld.gov.au/wp-content/uploads/2015/08/Dalby-Flood-Study-Volume-I-Detailed-Technical-Report-April-2014.pdf).
Cardona, O.-D., van Aalst, M.K., Birkmann, J., Fordham, M., McGregor, G., Perez, R., Pulwarty, R.S., Schipper, E.L.F., Sinh, B.T., Décamps, H., Keim, M., Davis, I., Ebi, K.L., Lavell, A., Mechler, R., Murray, V., Pelling, M., Pohl, J., Smith, A.-O., Thomalla, F., 2012. Determinants of Risk: Exposure and Vulnerability, in: Field, C.B., Dahe, Q., Stocker, T.F., Barros, V. (Eds.), Managing the Risks of Extreme Events and Disasters to Advance Climate Change Adaptation: Special Report of the Intergovernmental Panel on Climate Change. Cambridge University Press, Cambridge, pp. 65–108. https://doi.org/10.1017/CBO9781139177245.005
Carisi, F., Schröter, K., Domeneghetti, A., Kreibich, H., Castellarin, A., 2018. Development and assessment of uni- and multivariable flood loss models for Emilia-Romagna (Italy). Nat. Hazards Earth Syst. Sci. 18, 2057–2079. https://doi.org/10.5194/nhess-18-2057-2018
Carozza, D.A., Boudreault, M., 2021. A Global Flood Risk Modeling Framework Built With Climate Models and Machine Learning. J. Adv. Model. Earth Syst. 13, e2020MS002221. https://doi.org/10.1029/2020MS002221
Carroll, B., Balogh, R., Morbey, H., Araoz, G., 2010. Health and social impacts of a flood disaster: responding to needs and implications for practice. Disasters 34, 1045–1063. https://doi.org/10.1111/j.1467-7717.2010.01182.x
Cattaneo, C., Beine, M., Fröhlich, C.J., Kniveton, D., Martinez-Zarzoso, I., Mastrorillo, M., Millock, K., Piguet, E., Schraven, B., 2019. Human Migration in the Era of Climate Change. Rev. Environ. Econ. Policy 13, 189–206. https://doi.org/10.1093/reep/rez008
Ceola, S., Laio, F., Montanari, A., 2014. Satellite nighttime lights reveal increasing human exposure to floods worldwide. Geophys. Res. Lett. 41, 7184–7190. https://doi.org/10.1002/2014GL061859
Chavas, D.R., Lin, N., Dong, W., Lin, Y., 2016. Observed Tropical Cyclone Size Revisited. J. Clim. 29, 2923–2939. https://doi.org/10.1175/JCLI-D-15-0731.1
Chen, D., Rojas, M., Samset, B.H., Cobb, K., Diongue Niang, A., Edwards, P., Emori, S., Faria, S.H., Hawkins, E., Hope, P., Huybrechts, P., Meinshausen, M., Mustafa, S.K.,

Plattner, G.-K., Tréguier, A.-M., 2021. Framing, Context, and Methods. In Climate Change 2021: The Physical Science Basis. Contribution of Working Group I to the Sixth Assessment Report of the Intergovernmental Panel on Climate Change[Masson-Delmotte, V., P. Zhai, A. Pirani, S.L. Connors, C. Péan, S. Berger, N. Caud, Y. Chen, L. Goldfarb, M.I. Gomis, M. Huang, K. Leitzell, E. Lonnoy, J.B.R. Matthews, T.K. Maycock, T. Waterfield, O. Yelekçi, R. Yu, and B. Zhou (eds.)]. Cambridge University Press, Cambridge, United Kingdom and New York, NY, USA, pp. 147–286, doi:10.1017/9781009157896.003.

Chen, G., Li, X., Liu, X., Chen, Y., Liang, X., Leng, J., Xu, X., Liao, W., Qiu, Y., Wu, Q., Huang, K., 2020. Global projections of future urban land expansion under shared socioeconomic pathways. Nat. Commun. 11, 537. https://doi.org/10.1038/s41467-020-14386-x

Church, J.A., Clark, P.U., Cazenave, A., Gregory, J.M., Jevrejeva, S., Levermann, A., Merrifield, M.A., Milne, G.A., Nerem, R.S., Nunn, P.D., Payne, A.J., Pfeffer, W.T., Stammer, D., Unnikrishnan, A.S., 2013. Sea Level Change. In: Climate Change 2013: The Physical Science Basis. Contribution of Working Group I to the Fifth Assessment Report of the Intergovernmental Panel on Climate Change [Stocker, T.F., D. Qin, G.-K. Plattner, M. Tignor, S.K. Allen, J. Boschung, A. Nauels, Y. Xia, V. Bex and P.M. Midgley (eds.)]. Cambridge University Press, Cambridge, United Kingdom and New York, NY, USA, pp. 1137–1216.

Church, J.A., White, N.J., 2011. Sea-Level Rise from the Late 19th to the Early 21st Century. Surv. Geophys. 32, 585–602. https://doi.org/10.1007/s10712-011-9119-1

Church, J.A., White, N.J., Coleman, R., Lambeck, K., Mitrovica, J.X., 2004. Estimates of the Regional Distribution of Sea Level Rise over the 1950–2000 Period. J. Clim. 17, 2609–2625. https://doi.org/10.1175/1520-0442(2004)017<2609:EOTRDO>2.0.CO;2

CIESIN, 2018. Center for International Earth Science Information Network - CIESIN - Columbia University. Gridded Population of the World, Version 4 (GPWv4): Population Count, Revision 11.

CIESIN, 2018a. Center for International Earth Science Information Network - CIESIN - Columbia University. Gridded Population of the World, Version 4 (GPWv4): Population Count, Revision 11.

CIESIN, 2018b. Center for International Earth Science Information Network - CIESIN - Columbia University. Gridded Population of the World, Version 4 (GPWv4): Basic Demographic Characteristics, Revision 11.

Cissé, G., McLeman, R., Adams, H., Aldunce, P., Bowen, K., Campbell-Lendrum, D., Clayton, S., Ebi, K.L., Hess, J., Huang, C., Liu, Q., McGregor, G., Semenza, J., Tirado, M.C., 2022. Health, Wellbeing, and the Changing Structure of Communities. In: Climate Change 2022: Impacts, Adaptation, and Vulnerability. Contribution of Working Group II to the Sixth Assessment Report of the Intergovernmental Panel on Climate Change [H.-O. Pörtner, D.C. Roberts, M. Tignor, E.S. Poloczanska, K. Mintenbeck, A. Alegría, M. Craig, S. Langsdorf, S. Löschke, V. Möller, A. Okem, B. Rama (eds.)]. Cambridge University Press, Cambridge, UK and New York, NY, USA, pp. 1041-1170, doi:10.1017/9781009325844.009.

Clement, V., Rigaud, K.K., de Sherbinin, A., Jones, B., Adamo, S., Schewe, J., Sadiq, N., Shabahat, E., 2021. Groundswell Part 2: Acting on Internal Climate Migration. World Bank, Washington, DC.

CMEMS, 2021. Global ocean gridded L4 sea surface heights and derived variables reprocessed (1993-ongoing). E.U. Copernicus Marine Service (CMEMS). Downloaded 2021-08-02.

Cohen, S., Brakenridge, G.R., Kettner, A., Bates, B., Nelson, J., McDonald, R., Huang, Y.-F., Munasinghe, D., Zhang, J., 2018. Estimating Floodwater Depths from Flood Inundation Maps and Topography. JAWRA J. Am. Water Resour. Assoc. 54, 847–858. https://doi.org/10.1111/1752-1688.12609

Cohen, S., Raney, A., Munasinghe, D., Loftis, J.D., Molthan, A., Bell, J., Rogers, L., Galantowicz, J., Brakenridge, G.R., Kettner, A.J., Huang, Y.-F., Tsang, Y.-P., 2019. The Floodwater Depth Estimation Tool (FwDET v2.0) for improved remote sensing analysis of coastal flooding. Nat. Hazards Earth Syst. Sci. 19, 2053–2065. https://doi.org/10.5194/nhess-19-2053-2019

Coppedge, M., Gerring, J., Knutsen, C.H., Lindberg, S.I., Teorell, J., Alizada, N., Altman, D., Bernhard, M., Cornell, A., Fish, M.S., Gastaldi, L., Gjerløw, H., Glynn, A., Hicken, A., Hindle, G., Ilchenko, N., Krusell, J., Lührmann, A., Maerz, S.F., Marquardt, K.L., McMann, K., Mechkova, V., Medzihorsky, J., Paxton, P., Pemstein, D., Pernes, J., von Römer, J., Seim, B., Sigman, R., Skaaning, S.-E., Staton, J., Sundström, A., Tzelgov, E., Wang, Y., Wig, T., Wilson, S., Ziblatt, D., 2021. V-Dem Country-Year Dataset v11.1. https://doi.org/10.23696/vdemds21

Custer, R., Nishijima, K., 2015. Flood vulnerability assessment of residential buildings by explicit damage process modelling. Nat. Hazards 78, 461–496. https://doi.org/10.1007/s11069-015-1725-7

Cutler, D.R., Edwards Jr., T.C., Beard, K.H., Cutler, A., Hess, K.T., Gibson, J., Lawler, J.J., 2007. Random Forests for Classification in Ecology. Ecology 88, 2783–2792. https://doi.org/10.1890/07-0539.1

Dai, A., 2021. Hydroclimatic trends during 1950–2018 over global land. Clim. Dyn. 56, 4027–4049. https://doi.org/10.1007/s00382-021-05684-1

Daley, W.R., Brown, S., Archer, P., Kruger, E., Jordan, F., Batts, D., Mallonee, S., 2005. Risk of tornado-related death and injury in Oklahoma, May 3, 1999. Am. J. Epidemiol. 161, 1144–1150. https://doi.org/10.1093/aje/kwi142

Dangendorf Sönke, Marcos Marta, Wöppelmann Guy, Conrad Clinton P., Frederikse Thomas, Riva Riccardo, 2017. Reassessment of 20th century global mean sea level rise. Proc. Natl. Acad. Sci. 114, 5946–5951. https://doi.org/10.1073/pnas.1616007114

Dangendorf, S., Arns, A., Pinto, J.G., Ludwig, P., Jensen, J., 2016. The exceptional influence of storm 'Xaver' on design water levels in the German Bight. Environ. Res. Lett. 11, 054001. https://doi.org/10.1088/1748-9326/11/5/054001

Davis, B.M., 1987. Uses and abuses of cross-validation in geostatistics. Math. Geol. 19, 241–248. https://doi.org/10.1007/BF00897749

De Marchi, B., Scolobig, A., 2012. The views of experts and residents on social vulnerability to flash floods in an Alpine region of Italy. Disasters 36, 316–337. https://doi.org/10.1111/j.1467-7717.2011.01252.x

Desai, B., Bresch, D.N., Cazabat, C., Hochrainer-Stigler, S., Mechler, R., Ponserre, S., Schewe, J., 2021. Addressing the human cost in a changing climate. Science 372, 1284–1287. https://doi.org/10.1126/science.abh4283

Desai, B., Ginnetti, J., Sydney, C., 2018. No matter of choice: displacement in a changing climate. THEMATIC SERIES by the Internal Displacement Monitoring Centre.

Di Baldassarre, G., Montanari, A., Lins, H., Koutsoyiannis, D., Brandimarte, L., Blöschl, G., 2010. Flood fatalities in Africa: From diagnosis to mitigation. Geophys. Res. Lett. 37. https://doi.org/10.1029/2010GL045467

Di Baldassarre, G., Viglione, A., Carr, G., Kuil, L., Salinas, J.L., Blöschl, G., 2013. Socio-hydrology: conceptualising human-flood interactions. Hydrol. Earth Syst. Sci. 17, 3295–3303. https://doi.org/10.5194/hess-17-3295-2013

Di Baldassarre, G., Viglione, A., Carr, G., Kuil, L., Yan, K., Brandimarte, L., Blöschl, G., 2015. Debates-Perspectives on socio-hydrology: Capturing feedbacks between physical and social processes: A socio-hydrological approach to explore flood risk changes. Water Resour. Res. 51, 4770–4781. https://doi.org/10.1002/2014WR016416

Do, H.X., Gudmundsson, L., Leonard, M., Westra, S., 2018. The Global Streamflow Indices and Metadata Archive (GSIM) -- Part 1: The production of a daily \hack{\break}

streamflow archive and metadata. Earth Syst. Sci. Data 10, 765–785. https://doi.org/10.5194/essd-10-765-2018
Do, H.X., Mei, Y., Gronewold, A.D., 2020. To What Extent Are Changes in Flood Magnitude Related to Changes in Precipitation Extremes? Geophys. Res. Lett. 47, e2020GL088684. https://doi.org/10.1029/2020GL088684
Do, H.X., Westra, S., Leonard, M., 2017. A global-scale investigation of trends in annual maximum streamflow. J. Hydrol. 552, 28–43. https://doi.org/10.1016/j.jhydrol.2017.06.015
Dottori, F., Salamon, P., Bianchi, A., Alfieri, L., Hirpa, F.A., Feyen, L., 2016. Development and evaluation of a framework for global flood hazard mapping. Adv. Water Resour. 94, 87–102. https://doi.org/10.1016/j.advwatres.2016.05.002
Dottori, F., Szewczyk, W., Ciscar, J.-C., Zhao, F., Alfieri, L., Hirabayashi, Y., Bianchi, A., Mongelli, I., Frieler, K., Betts, R.A., Feyen, L., 2018. Increased human and economic losses from river flooding with anthropogenic warming. Nat. Clim. Change 8, 781–786. https://doi.org/10.1038/s41558-018-0257-z
Dullaart, J.C.M., Muis, S., Bloemendaal, N., Chertova, M.V., Couasnon, A., Aerts, J.C.J.H., 2021. Accounting for tropical cyclones more than doubles the global population exposed to low-probability coastal flooding. Commun. Earth Environ. 2, 135. https://doi.org/10.1038/s43247-021-00204-9
Dun, O.V., Gemenne, F., 2008. Defining “environmental migration.” Forced Migr. Rev. 31 Oct. 10-11.
Eilander, D., Couasnon, A., Leijnse, T., Ikeuchi, H., Yamazaki, D., Muis, S., Dullaart, J., Haag, A., Winsemius, H.C., Ward, P.J., 2023. A globally applicable framework for compound flood hazard modeling. Nat. Hazards Earth Syst. Sci. 23, 823–846. https://doi.org/10.5194/nhess-23-823-2023
Eilander, D., Couasnon, A., Leijnse, T., Ikeuchi, H., Yamazaki, D., Muis, S., Dullaart, J., Winsemius, H.C., Ward, P.J., 2022. A globally-applicable framework for compound flood hazard modeling. EGUsphere 2022, 1–40. https://doi.org/10.5194/egusphere-2022-149
EM-DAT, 2020. The OFDA/CRED international disaster database, University Catholic Louvain-Brussels, Belgium.
Emanuel, K.A., 1987. The dependence of hurricane intensity on climate. Nature 326, 483–485. https://doi.org/10.1038/326483a0
Essou, G.R.C., Brissette, F., Lucas-Picher, P., 2017. The Use of Reanalyses and Gridded Observations as Weather Input Data for a Hydrological Model: Comparison of Performances of Simulated River Flows Based on the Density of Weather Stations. J. Hydrometeorol. 18, 497–513. https://doi.org/10.1175/JHM-D-16-0088.1
Fankhauser, S., 2010. The costs of adaptation. WIREs Clim. Change 1, 23–30. https://doi.org/10.1002/wcc.14
Farr, T.G., Rosen, P.A., Caro, E., Crippen, R., Duren, R., Hensley, S., Kobrick, M., Paller, M., Rodriguez, E., Roth, L., Seal, D., Shaffer, S., Shimada, J., Umland, J., Werner, M., Oskin, M., Burbank, D., Alsdorf, D., 2007. The Shuttle Radar Topography Mission. Rev. Geophys. 45. https://doi.org/10.1029/2005RG000183
Few, R., Ramírez, V., Armijos, M.T., Hernández, L.A.Z., Marsh, H., 2021. Moving with risk: Forced displacement and vulnerability to hazards in Colombia. World Dev. 144, 105482. https://doi.org/10.1016/j.worlddev.2021.105482
Fielding, J.L., 2012. Inequalities in exposure and awareness of flood risk in England and Wales. Disasters 36, 477–494. https://doi.org/10.1111/j.1467-7717.2011.01270.x
Fischer, E.M., Knutti, R., 2016. Observed heavy precipitation increase confirms theory and early models. Nat. Clim. Change 6, 986–991. https://doi.org/10.1038/nclimate3110
Flanagan, B., Gregory, E., Hallisey, E., Heitgerd, J., Lewis, B., 2011. A Social Vulnerability Index for Disaster Management. J. Homel. Secur. Emerg. Manag. 8. https://doi.org/10.2202/1547-7355.1792

Floodlist, 2016. Floodlist [WWW Document]. URL http://floodlist.com/asia/china-july-2016-floods-cost-33-billion-dollars

Formetta, G., Feyen, L., 2019. Empirical evidence of declining global vulnerability to climate-related hazards. Glob. Environ. Change 57, 101920. https://doi.org/10.1016/j.gloenvcha.2019.05.004

Fowler, H.J., Lenderink, G., Prein, A.F., Westra, S., Allan, R.P., Ban, N., Barbero, R., Berg, P., Blenkinsop, S., Do, H.X., Guerreiro, S., Haerter, J.O., Kendon, E.J., Lewis, E., Schaer, C., Sharma, A., Villarini, G., Wasko, C., Zhang, X., 2021. Anthropogenic intensification of short-duration rainfall extremes. Nat. Rev. Earth Environ. 2, 107–122. https://doi.org/10.1038/s43017-020-00128-6

Fox-Kemper, B., Hewitt, H.T., Xiao, C., Aðalgeirsdóttir, G., Drijfhout, S.S., Edwards, T.L., Golledge, N.R., Hemer, M., Kopp, R.E., Krinner, G., Mix, A., Notz, D., Nowicki, S., Nurhati, I.S., Ruiz, L., Sallée, J.-B., Slangen, A.B.A., Yu, Y., 2021. Ocean, Cryosphere and Sea Level Change. In Climate Change 2021: The Physical Science Basis. Contribution of Working Group I to the Sixth Assessment Report of the Intergovernmental Panel on Climate Change [Masson-Delmotte, V., P. Zhai, A. Pirani, S.L. Connors, C. Péan, S. Berger, N. Caud, Y. Chen, L. Goldfarb, M.I. Gomis, M. Huang, K. Leitzell, E. Lonnoy, J.B.R. Matthews, T.K. Maycock, T. Waterfield, O. Yelekçi, R. Yu, and B. Zhou (eds.)]. Cambridge University Press, Cambridge, United Kingdom and New York, NY, USA, pp. 1211–1362.

Frame, D.J., Rosier, S.M., Noy, I., Harrington, L.J., Carey-Smith, T., Sparrow, S.N., Stone, D.A., Dean, S.M., 2020a. Climate change attribution and the economic costs of extreme weather events: a study on damages from extreme rainfall and drought. Clim. Change 162, 781–797. https://doi.org/10.1007/s10584-020-02729-y

Frame, D.J., Wehner, M.F., Noy, I., Rosier, S.M., 2020b. The economic costs of Hurricane Harvey attributable to climate change. Clim. Change 160, 271–281. https://doi.org/10.1007/s10584-020-02692-8

Friedman, J.H., 2001. Greedy function approximation: A gradient boosting machine. Ann. Stat. 29, 1189–1232. https://doi.org/10.1214/aos/1013203451

GADM, 2018. Database of Global Administrative Areas.

Galantowicz, J.F., Picton, J., 2021. Flood Mapping with Passive Microwave Remote Sensing: Current Capabilities and Directions for Future Development, in: Earth Observation for Flood Applications. Elsevier, p. 28.

Gannon, K.E., Conway, D., Pardoe, J., Ndiyoi, M., Batisani, N., Odada, E., Olago, D., Opere, A., Kgosietsile, S., Nyambe, M., Omukuti, J., Siderius, C., 2018. Business experience of floods and drought-related water and electricity supply disruption in three cities in sub-Saharan Africa during the 2015/2016 El Niño. Glob. Sustain. 1, e14. https://doi.org/10.1017/sus.2018.14

Garner Andra J., Mann Michael E., Emanuel Kerry A., Kopp Robert E., Lin Ning, Alley Richard B., Horton Benjamin P., DeConto Robert M., Donnelly Jeffrey P., Pollard David, 2017. Impact of climate change on New York City's coastal flood hazard: Increasing flood heights from the preindustrial to 2300 CE. Proc. Natl. Acad. Sci. 114, 11861–11866. https://doi.org/10.1073/pnas.1703568114

Geiger, T., Frieler, K., Bresch, D.N., 2018. A global historical data set of tropical cyclone exposure (TCE-DAT). Earth Syst. Sci. Data 10, 185–194. https://doi.org/10.5194/essd-10-185-2018

Gemenne, F., 2011. Why the numbers don't add up: A review of estimates and predictions of people displaced by environmental changes. Glob. Environ. Change, Migration and Global Environmental Change – Review of Drivers of Migration 21, S41–S49. https://doi.org/10.1016/j.gloenvcha.2011.09.005

Ghimire, R., Ferreira, S., Dorfman, J.H., 2015. Flood-Induced Displacement and Civil Conflict. World Dev. 66, 614–628. https://doi.org/10.1016/j.worlddev.2014.09.021

Goldewijk, C.G.M.K., 2016. A historical land use data set for the Holocene; HYDE 3.2 (replaced). https://doi.org/10.17026/dans-znk-cfy3

Google Maps (a), 2022. Mozambique. Satellite image. URL: http://mt0.google.com/vt/lyrs=s&hl=en&x={x}&y={y}&z={z}. Accessed on 2022-04-27.
Google Maps (b), 2022. Greater Area of Beira, Mozambique. Satellite image. URL: http://mt0.google.com/vt/lyrs=s&hl=en&x={x}&y={y}&z={z}. Accessed on 2022-04-27.
Groth, J., Ide, T., Sakdapolrak, P., Kassa, E., Hermans, K., 2020. Deciphering interwoven drivers of environment-related migration – A multisite case study from the Ethiopian highlands. Glob. Environ. Change 63, 102094. https://doi.org/10.1016/j.gloenvcha.2020.102094
Gudmundsson, L., Boulange, J., Do, H.X., Gosling, S.N., Grillakis, M.G., Koutroulis, A.G., Leonard, M., Liu, J., Müller Schmied, H., Papadimitriou, L., Pokhrel, Y., Seneviratne, S.I., Satoh, Y., Thiery, W., Westra, S., Zhang, X., Zhao, F., 2021. Globally observed trends in mean and extreme river flow attributed to climate change. Science 371, 1159–1162. https://doi.org/10.1126/science.aba3996
Gudmundsson, L., Do, H.X., Leonard, M., Westra, S., 2018. The Global Streamflow Indices and Metadata Archive (GSIM) -- Part 2: Quality control, time-series indices and homogeneity assessment. Earth Syst. Sci. Data 10, 787–804. https://doi.org/10.5194/essd-10-787-2018
Guerreiro, S.B., Fowler, H.J., Barbero, R., Westra, S., Lenderink, G., Blenkinsop, S., Lewis, E., Li, X.-F., 2018. Detection of continental-scale intensification of hourly rainfall extremes. Nat. Clim. Change 8, 803–807. https://doi.org/10.1038/s41558-018-0245-3
Guha-Sapir, D., Below, R., Hoyois, Ph., 2022. EM-DAT: The CRED/OFDA International Disaster Database. Université Catholique de Louvain-Brussels, Belgium.
Gulev, S.K., Thorne, P.W., Ahn, J., Dentener, F.J., Domingues, C.M., Gerland, S., Gong, D., Kaufman, D.S., Nnamchi, H.C., Quaas, J., Rivera, J.A., Sathyendranath, S., Smith, S.L., Trewin, B., von Schuckmann, K., Vose, R.S., 2021. Changing State of the Climate System. In Climate Change 2021: The Physical Science Basis. Contribution of Working Group I to the Sixth Assessment Report of the Intergovernmental Panel on Climate Change [Masson-Delmotte, V., P. Zhai, A. Pirani, S.L. Connors, C. Péan, S. Berger, N. Caud, Y. Chen, L. Goldfarb, M.I. Gomis, M. Huang, K. Leitzell, E. Lonnoy, J.B.R. Matthews, T.K. Maycock, T. Waterfield, O. Yelekçi, R. Yu, and B. Zhou (eds.)]. Cambridge University Press. In Press.
Haddeland, I., Clark, D.B., Franssen, W., Ludwig, F., Voß, F., Arnell, N.W., Bertrand, N., Best, M., Folwell, S., Gerten, D., Gomes, S., Gosling, S.N., Hagemann, S., Hanasaki, N., Harding, R., Heinke, J., Kabat, P., Koirala, S., Oki, T., Polcher, J., Stacke, T., Viterbo, P., Weedon, G.P., Yeh, P., 2011. Multimodel estimate of the global terrestrial water balance: Setup and first results. J. Hydrometeorol. 12, 869–884. https://doi.org/10.1175/2011JHM1324.1
Hajjem, A., Bellavance, F., Larocque, D., 2014. Mixed-effects random forest for clustered data. J. Stat. Comput. Simul. 84, 1313–1328. https://doi.org/10.1080/00949655.2012.741599
Han, W., Meehl, G.A., Rajagopalan, B., Fasullo, J.T., Hu, A., Lin, J., Large, W.G., Wang, J., Quan, X.-W., Trenary, L.L., Wallcraft, A., Shinoda, T., Yeager, S., 2010. Patterns of Indian Ocean sea-level change in a warming climate. Nat. Geosci. 3, 546–550. https://doi.org/10.1038/ngeo901
Hanasaki, N., Kanae, S., Oki, T., Masuda, K., Motoya, K., Shirakawa, N., Shen, Y., Tanaka, K., 2008. An integrated model for the assessment of global water resources - Part 1: Model description and input meteorological forcing. Hydrol. Earth Syst. Sci. 12, 1007–1025. https://doi.org/10.5194/hess-12-1007-2008
Hansen, M.C., Potapov, P.V., Moore, R., Hancher, M., Turubanova, S.A., Tyukavina, A., Thau, D., Stehman, S.V., Goetz, S.J., Loveland, T.R., Kommareddy, A., Egorov, A., Chini, L., Justice, C.O., Townshend, J.R.G., 2013. High-Resolution Global Maps of 21st-Century Forest Cover Change. Science 342, 850–853. https://doi.org/10.1126/science.1244693

Hartmann, B., 2010. Rethinking climate refugees and climate conflict: Rhetoric, reality and the politics of policy discourse. J. Int. Dev. 22, 233–246. https://doi.org/10.1002/jid.1676

Hastie, T., Tibshirani, R., Friedman, J., 2009. Elements of Statistical Learning: data mining, inference, and prediction. 2nd Edition., 2nd ed. Springer.

Hattermann, F.F., Krysanova, V., Gosling, S.N., Dankers, R., Daggupati, P., Donnelly, C., Flörke, M., Huang, S., Motovilov, Y., Buda, S., Yang, T., Müller, C., Leng, G., Tang, Q., Portmann, F.T., Hagemann, S., Gerten, D., Wada, Y., Masaki, Y., Alemayehu, T., Satoh, Y., Samaniego, L., 2017. Cross-scale intercomparison of climate change impacts simulated by regional and global hydrological models in eleven large river basins. Clim. Change 141, 561–576. https://doi.org/10.1007/s10584-016-1829-4

Hawker, L., Rougier, J., Neal, J., Bates, P., Archer, L., Yamazaki, D., 2018. Implications of Simulating Global Digital Elevation Models for Flood Inundation Studies. Water Resour. Res. 54, 7910–7928. https://doi.org/10.1029/2018WR023279

HDX, 2019. Mozambique admin level 4 - Beira and Dondo neighbourhood boundaries.

Heslin, A., Deckard, N.D., Oakes, R., Montero-Colbert, A., 2019. Displacement and Resettlement: Understanding the Role of Climate Change in Contemporary Migration, in: Mechler, R., Bouwer, L.M., Schinko, T., Surminski, S., Linnerooth-Bayer, J. (Eds.), Loss and Damage from Climate Change: Concepts, Methods and Policy Options, Climate Risk Management, Policy and Governance. Springer International Publishing, Cham, pp. 237–258. https://doi.org/10.1007/978-3-319-72026-5_10

Hirabayashi, Y., Mahendran, R., Koirala, S., Konoshima, L., Yamazaki, D., Watanabe, S., Kim, H., Kanae, S., 2013. Global flood risk under climate change. Nat. Clim. Change 3, 816–821. https://doi.org/10.1038/nclimate1911

Hoch, J.M., Trigg, M.A., 2019. Advancing global flood hazard simulations by improving comparability, benchmarking, and integration of global flood models. Environ. Res. Lett. 14, 034001. https://doi.org/10.1088/1748-9326/aaf3d3

Hodgkins, G.A., Whitfield, P.H., Burn, D.H., Hannaford, J., Renard, B., Stahl, K., Fleig, A.K., Madsen, H., Mediero, L., Korhonen, J., Murphy, C., Wilson, D., 2017. Climate-driven variability in the occurrence of major floods across North America and Europe. J. Hydrol. 552, 704–717. https://doi.org/10.1016/j.jhydrol.2017.07.027

Hoffmann, R., Dimitrova, A., Muttarak, R., Crespo Cuaresma, J., Peisker, J., 2020. A meta-analysis of country-level studies on environmental change and migration. Nat. Clim. Change 10, 904–912. https://doi.org/10.1038/s41558-020-0898-6

Hoffmann, R., Šedová, B., Vinke, K., 2021. Improving the evidence base: A methodological review of the quantitative climate migration literature. Glob. Environ. Change 71, 102367. https://doi.org/10.1016/j.gloenvcha.2021.102367

Holland, G.J., 1980. An Analytic Model of the Wind and Pressure Profiles in Hurricanes. Mon. Weather Rev. 108, 1212–1218. https://doi.org/10.1175/1520-0493(1980)108<1212:AAMOTW>2.0.CO;2

Hugo, G., 1996. Environmental Concerns and International Migration. Int. Migr. Rev. 30, 105–131. https://doi.org/10.1177/019791839603000110

Hurlbert, M.A., 2018. Adaptive Governance of Disaster - Drought and Flood in Rural Areas, 1st ed. Springer, Cham. https://doi.org/10.1007/978-3-319-57801-9

Hurtt, G.C., Chini, L., Sahajpal, R., Frolking, S., Bodirsky, B.L., Calvin, K., Doelman, J.C., Fisk, J., Fujimori, S., Klein Goldewijk, K., Hasegawa, T., Havlik, P., Heinimann, A., Humpenöder, F., Jungclaus, J., Kaplan, J.O., Kennedy, J., Krisztin, T., Lawrence, D., Lawrence, P., Ma, L., Mertz, O., Pongratz, J., Popp, A., Poulter, B., Riahi, K., Shevliakova, E., Stehfest, E., Thornton, P., Tubiello, F.N., van Vuuren, D.P., Zhang, X., 2020. Harmonization of global land use change and management for the period 850–2100 (LUH2) for CMIP6. Geosci. Model Dev. 13, 5425–5464. https://doi.org/10.5194/gmd-13-5425-2020

Hyungjun, K., 2014. Global Soil Wetness Project phase 3 forcing data set (GSWP3).

IDMC, 2019. IDMC Global Report on Internal Displacement 2019 Displacement Dataset. https://www.internal-displacement.org/database/displacement-data.
IDMC, 2021. Sudden-Onset Hazards and the Risk of Future Displacement in Fiji. The Internal Displacement Monitoring Centre.
IDMC, 2022. “IDMC Global Report on Internal Displacement 2022 Displacement Dataset.” https://www.internal-displacement.org/database/displacement-data.
IDMC, ADB, 2022. Disaster Displacement in Asia and the Pacific: A Business Case for Investment in Prevention and Solutions. Internal Displacement Monitoring Centre and Asian Development Bank. Asian Development Bank.
International Organization for Migration, 2019. Global compact for migration.
IPCC (Ed.), 2014. Long-term Climate Change: Projections, Commitments and Irreversibility Pages 1029 to 1076, in: Climate Change 2013 – The Physical Science Basis: Working Group I Contribution to the Fifth Assessment Report of the Intergovernmental Panel on Climate Change. Cambridge University Press, Cambridge, pp. 1029–1136. https://doi.org/10.1017/CBO9781107415324.024
IPCC, 1992. Climate Change: The 1990 and 1992 IPCC Assessments. IPCC First Assessment Report. Overview and Policymaker Summaries and 1992 IPPC Supplement.
IPCC, 2012. Managing the Risks of Extreme Events and Disasters to Advance Climate Change Adaptation: Special Report of the Intergovernmental Panel on Climate Change (No. 9781139177245). (eds. Field, C. B. et al.) Cambridge Univ. Press. https://doi.org/10.1017/CBO9781139177245.009
Irish, J.L., Sleath, A., Cialone, M.A., Knutson, T.R., Jensen, R.E., 2014. Simulations of Hurricane Katrina (2005) under sea level and climate conditions for 1900. Clim. Change 122, 635–649. https://doi.org/10.1007/s10584-013-1011-1
Jha, A.K., Bloch, R., Lamond, J., 2012. Cities and Flooding : A Guide to Integrated Urban Flood Risk Management for the 21st Century. World Bank. © World Bank. License: CC BY 3.0 IGO. https://doi.org/10.1061/(ASCE)1084-0699(2003)8:1(1)
Jones, B., O’Neill, B.C., 2016. Spatially explicit global population scenarios consistent with the Shared Socioeconomic Pathways. Environ. Res. Lett. 11, 084003. https://doi.org/10.1088/1748-9326/11/8/084003
Jongman, B., Ward, P.J., Aerts, J.C.J.H., 2012. Global exposure to river and coastal flooding: Long term trends and changes. Glob. Environ. Change 22, 823–835. https://doi.org/10.1016/j.gloenvcha.2012.07.004
Jongman, B., Winsemius, H.C., Aerts, J.C.J.H., Coughlan de Perez, E., van Aalst, M.K., Kron, W., Ward, P.J., 2015. Declining vulnerability to river floods and the global benefits of adaptation. Proc. Natl. Acad. Sci. 112, E2271–E2280. https://doi.org/10.1073/pnas.1414439112
Jonkman, S.N., 2005. Global Perspectives on Loss of Human Life Caused by Floods. Nat. Hazards 34, 151–175. https://doi.org/10.1007/s11069-004-8891-3
Jonkman, S.N., Maaskant, B., Boyd, E., Levitan, M.L., 2009. Loss of Life Caused by the Flooding of New Orleans After Hurricane Katrina: Analysis of the Relationship Between Flood Characteristics and Mortality. Risk Anal. 29, 676–698. https://doi.org/10.1111/j.1539-6924.2008.01190.x
Jurgilevich, A., Räsänen, A., Groundstroem, F., Juhola, S., 2017. A systematic review of dynamics in climate risk and vulnerability assessments. Environ. Res. Lett. 12, 013002. https://doi.org/10.1088/1748-9326/aa5508
Kakinuma, K., Puma, M.J., Hirabayashi, Y., Tanoue, M., Baptista, E.A., Kanae, S., 2020. Flood-induced population displacements in the world. Environ. Res. Lett. 15, 124029. https://doi.org/10.1088/1748-9326/abc586
Kalkuhl, M., Wenz, L., 2020. The impact of climate conditions on economic production. Evidence from a global panel of regions. J. Environ. Econ. Manag. 103, 102360. https://doi.org/10.1016/j.jeem.2020.102360

Kam, P.M., Aznar-Siguan, G., Schewe, J., Milano, L., Ginnetti, J., Willner, S., McCaughey, J.W., Bresch, D.N., 2021. Global warming and population change both heighten future risk of human displacement due to river floods. Environ. Res. Lett. 16, 044026. https://doi.org/10.1088/1748-9326/abd26c

Kim, H., Yeh, P.J.-F., Oki, T., Kanae, S., 2009. Role of rivers in the seasonal variations of terrestrial water storage over global basins. Geophys. Res. Lett. 36. https://doi.org/10.1029/2009GL039006

Knapp, K.R., Kruk, M.C., Levinson, D.H., Diamond, H.J., Neumann, C.J., 2010. The International Best Track Archive for Climate Stewardship (IBTrACS): Unifying Tropical Cyclone Data. Bulletin of the American Meteorological Society 91 (3): 363-76.

Knutson, T., Camargo, S.J., Chan, J.C.L., Emanuel, K., Ho, C.-H., Kossin, J., Mohapatra, M., Satoh, M., Sugi, M., Walsh, K., Wu, L., 2019. Tropical Cyclones and Climate Change Assessment: Part I: Detection and Attribution. Bull. Am. Meteorol. Soc. 100, 1987–2007. https://doi.org/10.1175/BAMS-D-18-0189.1

Knutson, T., Camargo, S.J., Chan, J.C.L., Emanuel, K., Ho, C.-H., Kossin, J., Mohapatra, M., Satoh, M., Sugi, M., Walsh, K., Wu, L., 2020. Tropical Cyclones and Climate Change Assessment: Part II: Projected Response to Anthropogenic Warming. Bull. Am. Meteorol. Soc. 101, E303–E322. https://doi.org/10.1175/BAMS-D-18-0194.1

Knutson, T.R., Sirutis, J.J., Zhao, M., Tuleya, R.E., Bender, M., Vecchi, G.A., Villarini, G., Chavas, D., 2015. Global Projections of Intense Tropical Cyclone Activity for the Late Twenty-First Century from Dynamical Downscaling of CMIP5/RCP4.5 Scenarios. J. Clim. 28, 7203–7224. https://doi.org/10.1175/JCLI-D-15-0129.1

Knutson, T.R., Tuleya, R.E., 2008. Tropical cyclones and climate change: revisiting recent studies at GFDL, in: Diaz, H.F., Murnane, R.J. (Eds.), Climate Extremes and Society. Cambridge University Press, Cambridge, pp. 120–144. https://doi.org/10.1017/CBO9780511535840.010

Kossin, J.P., Knapp, K.R., Vimont, D.J., Murnane, R.J., Harper, B.A., 2007. A globally consistent reanalysis of hurricane variability and trends. Geophys. Res. Lett. 34. https://doi.org/10.1029/2006GL028836

Kossin, J.P., Olander, T.L., Knapp, K.R., 2013. Trend Analysis with a New Global Record of Tropical Cyclone Intensity. J. Clim. 26, 9960–9976. https://doi.org/10.1175/JCLI-D-13-00262.1

Kulp, S.A., Strauss, B.H., 2018. CoastalDEM: A global coastal digital elevation model improved from SRTM using a neural network. Remote Sens. Environ. 206, 231–239. https://doi.org/10.1016/j.rse.2017.12.026

Kulp, S.A., Strauss, B.H., 2021. CoastalDEM v2.1: A high-accuracy and high-resolution global coastal elevation model trained on ICESat-2 satellite lidar. Climate Central Scientific Report 17.

Kummu, M., Taka, M., Guillaume, J.H.A., 2018. Gridded global datasets for Gross Domestic Product and Human Development Index over 1990–2015. Sci. Data 5, 180004. https://doi.org/10.1038/sdata.2018.4

Kundzewicz, Z.W., Kanae, S., Seneviratne, S.I., Handmer, J., Nicholls, N., Peduzzi, P., Mechler, R., Bouwer, L.M., Arnell, N., Mach, K., Muir-Wood, R., Brakenridge, G.R., Kron, W., Benito, G., Honda, Y., Takahashi, K., Sherstyukov, B., 2014. Flood risk and climate change: global and regional perspectives. Hydrol. Sci. J. 59, 1–28. https://doi.org/10.1080/02626667.2013.857411

Lange, S., Volkholz, J., Geiger, T., Zhao, F., Vega, I., Veldkamp, T., Reyer, C.P.O., Warszawski, L., Huber, V., Jägermeyr, J., Schewe, J., Bresch, D.N., Büchner, M., Chang, J., Ciais, P., Dury, M., Emanuel, K., Folberth, C., Gerten, D., Gosling, S.N., Grillakis, M., Hanasaki, N., Henrot, A.-J., Hickler, T., Honda, Y., Ito, A., Khabarov, N., Koutroulis, A., Liu, W., Müller, C., Nishina, K., Ostberg, S., Müller Schmied, H., Seneviratne, S.I., Stacke, T., Steinkamp, J., Thiery, W., Wada, Y., Willner, S., Yang, H., Yoshikawa, M., Yue, C., Frieler, K., 2020. Projecting Exposure to Extreme

Climate Impact Events Across Six Event Categories and Three Spatial Scales. Earths Future 8, e2020EF001616. https://doi.org/10.1029/2020EF001616
Lee, Sunmin, Kim, J.-C., Jung, H.-S., Lee, M.J., Lee, Saro, 2017. Spatial prediction of flood susceptibility using random-forest and boosted-tree models in Seoul metropolitan city, Korea. Geomat. Nat. Hazards Risk 8, 1185–1203. https://doi.org/10.1080/19475705.2017.1308971
Lehner, B., Liermann, C.R., Revenga, C., Vörösmarty, C., Fekete, B., Crouzet, P., Döll, P., Endejan, M., Frenken, K., Magome, J., Nilsson, C., Robertson, J.C., Rödel, R., Sindorf, N., Wisser, D., 2011. High-resolution mapping of the world's reservoirs and dams for sustainable river-flow management. Front. Ecol. Environ. 9, 494–502. https://doi.org/10.1890/100125
Lehner, B., Verdin, K., Jarvis, A., 2008. New Global Hydrography Derived From Spaceborne Elevation Data. Eos Trans. Am. Geophys. Union 89, 93–94. https://doi.org/10.1029/2008EO100001
Leng, G., Huang, M., Tang, Q., Leung, L.R., 2015. A modeling study of irrigation effects on global surface water and groundwater resources under a changing climate. J. Adv. Model. Earth Syst. 7, 1285–1304. https://doi.org/10.1002/2015MS000437
Li, X., Yan, D., Wang, K., Weng, B., Qin, T., Liu, S., 2019. Flood Risk Assessment of Global Watersheds Based on Multiple Machine Learning Models. Water 11, 1654. https://doi.org/10.3390/w11081654
Liang, X., Lettenmaier, D.P., Wood, E.F., Burges, S.J., 1994. A simple hydrologically based model of land surface water and energy fluxes for general circulation models. J. Geophys. Res. Atmospheres 99, 14415–14428. https://doi.org/10.1029/94JD00483
Lin, N., Emanuel, K., Oppenheimer, M., Vanmarcke, E., 2012. Physically based assessment of hurricane surge threat under climate change. Nat. Clim. Change 2, 462–467. https://doi.org/10.1038/nclimate1389
Lin, N., Kopp, R.E., Horton, B.P., Donnelly, J.P., 2016. Hurricane Sandy's flood frequency increasing from year 1800 to 2100. Proc. Natl. Acad. Sci. U. S. A. 113, 12071–12075. https://doi.org/10.1073/pnas.1604386113
Luu, L.N., Scussolini, P., Kew, S., Philip, S., Hariadi, M.H., Vautard, R., Van Mai, K., Van Vu, T., Truong, K.B., Otto, F., van der Schrier, G., van Aalst, M.K., van Oldenborgh, G.J., 2021. Attribution of typhoon-induced torrential precipitation in Central Vietnam, October 2020. Clim. Change 169, 24. https://doi.org/10.1007/s10584-021-03261-3
Lyard, F.H., Allain, D.J., Cancet, M., Carrère, L., Picot, N., 2021. FES2014 global ocean tide atlas: design and performance. Ocean Sci. 17, 615–649. https://doi.org/10.5194/os-17-615-2021
Mandli, K.T., Dawson, C.N., 2014. Adaptive mesh refinement for storm surge. Ocean Model. 75, 36–50. https://doi.org/10.1016/j.ocemod.2014.01.002
Marjanac, S., Patton, L., 2018. Extreme weather event attribution science and climate change litigation: an essential step in the causal chain? J. Energy Nat. Resour. Law 36, 265–298. https://doi.org/10.1080/02646811.2018.1451020
Masutomi, Y., Inui, Y., Takahashi, K., Matsuoka, Y., 2009. Development of highly accurate global polygonal drainage basin data. Hydrol. Process. 23, 572–584. https://doi.org/10.1002/hyp.7186
Mateo, C.M., Hanasaki, N., Komori, D., Tanaka, K., Kiguchi, M., Champathong, A., Sukhapunnaphan, T., Yamazaki, D., Oki, T., 2014. Assessing the impacts of reservoir operation to floodplain inundation by combining hydrological, reservoir management, and hydrodynamic models. Water Resour. Res. 50, 7245–7266. https://doi.org/10.1002/2013WR014845
McMichael, A.J., 2012. Insights from past millennia into climatic impacts on human health and survival. Proc. Natl. Acad. Sci. 109, 4730–4737. https://doi.org/10.1073/pnas.1120177109

Mechler, R., Bouwer, L.M., 2015. Understanding trends and projections of disaster losses and climate change: is vulnerability the missing link? Clim. Change 133, 23–35. https://doi.org/10.1007/s10584-014-1141-0

Mengel, M., Treu, S., Lange, S., Frieler, K., 2021. ATTRICI v1.1 – counterfactual climate for impact attribution. Geosci. Model Dev. 14, 5269–5284. https://doi.org/10.5194/gmd-14-5269-2021

Merz, B., Kreibich, H., Lall, U., 2013. Multi-variate flood damage assessment: a tree-based data-mining approach. Nat. Hazards Earth Syst. Sci. 13, 53–64. https://doi.org/10.5194/nhess-13-53-2013

Mester, B., Frieler, K., Schewe, J., 2022a. Human displacements, fatalities, and economic damages linked to remotely observed floods (FLODIS). Zenodo. [WWW Document]. URL https://doi.org/10.5281/zenodo.7306882

Mester, B., Frieler, K., Schewe, J., 2022b. Code for human displacements, fatalities, and economic damages linked to remotely observed floods (FLODIS). GitHub. [WWW Document]. URL https://github.com/BenediktMester/FLODIS

Mester, B., Frieler, K., Schewe, J., 2023a. Human displacements, fatalities, and economic damages linked to remotely observed floods (FLODIS). Under consideration for Scientific Data.

Mester, B., Vogt, T., Bryant, S., Otto, C., Frieler, K., Schewe, J., 2022c. TC Idai attribution study - data collection v1.1 (Version v1.1). doi: 10.5281/zenodo.6907855.

Mester, B., Vogt, T., Bryant, S., Otto, C., Frieler, K., Schewe, J., 2023b. Human displacements from tropical cyclone Idai attributable to climate change. Under consideration for Natural Hazards and Earth System Sciences. EGUsphere [preprint], https://doi.org/10.5194/egusphere-2022-1308, 2023.

Mester, B., Willner, S.N., Frieler, K., Schewe, J., 2021. Evaluation of river flood extent simulated with multiple global hydrological models and climate forcings. Environ. Res. Lett. 16, 094010. https://doi.org/10.1088/1748-9326/ac188d

Milly, P.C.D., Wetherald, R.T., Dunne, K.A., Delworth, T.L., 2002. Increasing risk of great floods in a changing climate. Nature 415, 514–517. https://doi.org/10.1038/415514a

Monfreda, C., Ramankutty, N., Foley, J., 2008. Farming the Planet: 2. Geographic Distribution of Crop Areas, Yields, Physiological Types, and Net Primary Production in the Year 2000. Glob. Biogeochem Cycles 22, GB1022. https://doi.org/10.1029/2007GB002947

Morrow, B.H., 1999. Identifying and mapping community vulnerability. Disasters 23, 1–18. https://doi.org/10.1111/1467-7717.00102

Muis, S., Apecechea, M.I., Dullaart, J., de Lima Rego, J., Madsen, K.S., Su, J., Yan, K., Verlaan, M., 2020. A High-Resolution Global Dataset of Extreme Sea Levels, Tides, and Storm Surges, Including Future Projections. Front. Mar. Sci. 7. https://doi.org/10.3389/fmars.2020.00263

Müller Schmied, H., Adam, L., Eisner, S., Fink, G., Flörke, M., Kim, H., Oki, T., Portmann, F.T., Reinecke, R., Riedel, C., Song, Q., Zhang, J., Döll, P., 2016. Variations of global and continental water balance components as impacted by climate forcing uncertainty and human water use. Hydrol. Earth Syst. Sci. 20, 2877–2898. https://doi.org/10.5194/hess-20-2877-2016

Munich Re, 2020. NatCatSERVICE Relevant flood / flash flood events worldwide 2010 - 2018.

Murakami, D., Yamagata, Y., 2019. Estimation of Gridded Population and GDP Scenarios with Spatially Explicit Statistical Downscaling. Sustainability 11, 2106. https://doi.org/10.3390/su11072106

Nicholls, R.J., Lincke, D., Hinkel, J., Brown, S., Vafeidis, A.T., Meyssignac, B., Hanson, S.E., Merkens, J.-L., Fang, J., 2021. A global analysis of subsidence, relative sea-level change and coastal flood exposure. Nat. Clim. Change 11, 338–342. https://doi.org/10.1038/s41558-021-00993-z

Nienhuis, J.H., Cox, J.R., O'Dell, J., Edmonds, D.A., Scussolini, P., 2022. A global open-source database of flood-protection levees on river deltas (openDELvE). Nat. Hazards Earth Syst. Sci. 22, 4087–4101. https://doi.org/10.5194/nhess-22-4087-2022

Nirandjan, S., Koks, E.E., Ward, P.J., Aerts, J.C.J.H., 2022. A spatially-explicit harmonized global dataset of critical infrastructure. Sci. Data 9, 150. https://doi.org/10.1038/s41597-022-01218-4

Noy, I., 2016. The socio-economics of cyclones. Nat. Clim. Change 6, 343–345. https://doi.org/10.1038/nclimate2975

O'Neill, B., van Aalst, M., Zaiton Ibrahim, Z., Berrang Ford, L., Bhadwal, S., Buhaug, H., Diaz, D., Frieler, K., Garschagen, M., Magnan, A., Midgley, G., Mirzabaev, A., Thomas, A., Warren, R., 2022. Key Risks Across Sectors and Regions. In: Climate Change 2022: Impacts, Adaptation, and Vulnerability. Contribution of Working Group II to the Sixth Assessment Report of the Intergovernmental Panel on Climate Change [H.-O. Pörtner, D.C. Roberts, M. Tignor, E.S. Poloczanska, K. Mintenbeck, A. Alegría, M. Craig, S. Langsdorf, S. Löschke, V. Möller, A. Okem, B. Rama (eds.)]. Cambridge University Press.

Oakes, R., Banerjee, S., Warner, K., 2019. Human mobility and adaptation to environmental change [WWW Document]. https://doi.org/10.18356/2a8d511f-en

Obokata, R., Veronis, L., McLeman, R., 2014. Empirical research on international environmental migration: a systematic review. Popul. Environ. 36, 111–135. https://doi.org/10.1007/s11111-014-0210-7

OCHA, 2004. Guiding Principles on Internal Displacement. https://reliefweb.int/report/world/guiding-principles-internal-displacement-2004

Oldenborgh, G.J. van, Wiel, K. van der, Sebastian, A., Singh, R., Arrighi, J., Otto, F., Haustein, K., Li, S., Vecchi, G., Cullen, H., 2017. Attribution of extreme rainfall from Hurricane Harvey, August 2017. Environ. Res. Lett. 12, 124009. https://doi.org/10.1088/1748-9326/aa9ef2

Oppenheimer, M., Campos, M., Warren, R., Birkmann, J., Luber, G., O'Neill, B., Takahashi, K., Brklacich, M., Semenov, S., Licker, R., Hsiang, S., 2014. Emergent Risks and Key Vulnerabilities, in: Climate Change 2014 Impacts, Adaptation and Vulnerability: Part A: Global and Sectoral Aspects, Contribution of Working Group II to the Fifth Assessment Report of the Intergovernmental Panel on Climate Change. pp. 1039–1100.

Otto, F.E.L., Harrington, L., Schmitt, K., Philip, S., Kew, S., Oldenborgh, G.J. van, Singh, R., Kimutai, J., Wolski, P., 2020. Challenges to Understanding Extreme Weather Changes in Lower Income Countries. Bull. Am. Meteorol. Soc. 101, E1851–E1860. https://doi.org/10.1175/BAMS-D-19-0317.1

Patricola, C.M., Wehner, M.F., 2018. Anthropogenic influences on major tropical cyclone events. Nature 563, 339–346. https://doi.org/10.1038/s41586-018-0673-2

Paul, B.K., 2009. Why relatively fewer people died? The case of Bangladesh's Cyclone Sidr. Nat. Hazards 50, 289–304. https://doi.org/10.1007/s11069-008-9340-5

Paul, S.K., Routray, J.K., 2011. Household response to cyclone and induced surge in coastal Bangladesh: coping strategies and explanatory variables. Nat. Hazards 57, 477–499. https://doi.org/10.1007/s11069-010-9631-5

Pedregosa, F., Varoquaux, G., Gramfort, A., Michel, V., Thirion, B., Grisel, O., Blondel, M., Prettenhofer, P., Weiss, R., Dubourg, V., Vanderplas, J., Passos, A., Cournapeau, D., Brucher, M., Perrot, M., Duchesnay, E., 2011. Scikit-learn: Machine Learning in Python. J. Mach. Learn. Res. 12, 2825–2830.

Peduzzi, P., Chatenoux, B., Dao, H., De Bono, A., Herold, C., Kossin, J., Mouton, F., Nordbeck, O., 2012. Global trends in tropical cyclone risk. Nat. Clim. Change 2, 289–294. https://doi.org/10.1038/nclimate1410

Peduzzi, P., Dao, H., Herold, C., Mouton, F., 2009. Assessing global exposure and vulnerability towards natural hazards: the Disaster Risk Index. Nat. Hazards Earth Syst. Sci. 9, 1149–1159. https://doi.org/10.5194/nhess-9-1149-2009

Peel, M.C., Finlayson, B.L., McMahon, T.A., 2007. Updated world map of the Köppen-Geiger climate classification. Hydrol. Earth Syst. Sci. 11, 1633–1644. https://doi.org/10.5194/hess-11-1633-2007

Pekel, J.-F., Cottam, A., Gorelick, N., Belward, A.S., 2016. High-resolution mapping of global surface water and its long-term changes. Nature 540, 418–422. https://doi.org/10.1038/nature20584

Philip, S., Kew, S., van Oldenborgh, G.J., Otto, F., Vautard, R., van der Wiel, K., King, A., Lott, F., Arrighi, J., Singh, R., van Aalst, M., 2020. A protocol for probabilistic extreme event attribution analyses. Adv. Stat. Climatol. Meteorol. Oceanogr. 6, 177–203. https://doi.org/10.5194/ascmo-6-177-2020

Pokhrel, Y.N., Koirala, S., Yeh, P.J.-F., Hanasaki, N., Longuevergne, L., Kanae, S., Oki, T., 2014. Incorporation of groundwater pumping in a global Land Surface Model with the representation of human impacts. Water Resour. Res. 51, 78–96. https://doi.org/10.1002/2014WR015602

Probst, P., Annunziato, A., 2019. Tropical Cyclone IDAI: analysis of the wind, rainfall and storm surge impact. Join Research Centre (EUROPEAN COMMISSION).

Raadgever, T., Hegger, D., 2018. Flood risk management strategies and governance. Springer.

Reidpath, D.D., Allotey, P., 2003. Infant mortality rate as an indicator of population health. J. Epidemiol. Community Health 57, 344–346. https://doi.org/10.1136/jech.57.5.344

ReliefWeb, 2019. 'The First City Completely Devastated by Climate Change' Tries to Rebuild after Cyclone Idai.

Reliefweb, 2019. Mozambique: Cyclone Idai & Floods Flash Update No. 10, 26 March 2019. URL: https://reliefweb.int/report/mozambique/southern-africa-cyclone-idai-snapshot-26-march- 2019. Accessed on 2021-10-29.

Renaud, F.G., Bogardi, J.J., Dun, O., Warner, K., 2007. Control, adapt or flee: how to face environmental migration? UNU- EHS.

Rentschler, J., Salhab, M., Jafino, B.A., 2022. Flood exposure and poverty in 188 countries. Nat. Commun. 13, 3527. https://doi.org/10.1038/s41467-022-30727-4

Resio, D.T., Irish, J.L., 2016. Tropical Cyclone Storm Surge Risk, in: Handbook of Coastal and Ocean Engineering. WORLD SCIENTIFIC, pp. 1405–1422. https://doi.org/10.1142/9789813204027_0049

Rosvold, E.L., Buhaug, H., 2021. GDIS, a global dataset of geocoded disaster locations. Sci. Data 8, 61. https://doi.org/10.1038/s41597-021-00846-6

Rubin, O., 2014. Social vulnerability to climate-induced natural disasters: Cross-provincial evidence from Vietnam. Asia Pac. Viewp. 55, 67–80. https://doi.org/10.1111/apv.12037

Rufat, S., Tate, E., Burton, C.G., Maroof, A.S., 2015. Social vulnerability to floods: Review of case studies and implications for measurement. Int. J. Disaster Risk Reduct. 14, 470–486. https://doi.org/10.1016/j.ijdrr.2015.09.013

Sampson, C.C., Smith, A.M., Bates, P.D., Neal, J.C., Alfieri, L., Freer, J.E., 2015. A high-resolution global flood hazard model. Water Resour. Res. 51, 7358–7381. https://doi.org/10.1002/2015WR016954

Sanders, B.F., Schubert, J.E., Kahl, D.T., Mach, K.J., Brady, D., AghaKouchak, A., Forman, F., Matthew, R.A., Ulibarri, N., Davis, S.J., 2023. Large and inequitable flood risks in Los Angeles, California. Nat. Sustain. 6, 47–57. https://doi.org/10.1038/s41893-022-00977-7

Sauer, I.J., Reese, R., Otto, C., Geiger, T., Willner, S.N., Guillod, B.P., Bresch, D.N., Frieler, K., 2021. Climate signals in river flood damages emerge under sound regional disaggregation. Nat. Commun. 12, 2128. https://doi.org/10.1038/s41467-021-22153-9

Scherrer, S.C., Fischer, E.M., Posselt, R., Liniger, M.A., Croci-Maspoli, M., Knutti, R., 2016. Emerging trends in heavy precipitation and hot temperature extremes in Switzerland. J. Geophys. Res. Atmospheres 121, 2626–2637. https://doi.org/10.1002/2015JD024634

Schiavina, M., Freire, S., MacManus, K., 2019. GHS population grid multitemporal (1975, 1990, 2000, 2015) R2019A. European Commission, Joint Research Centre (JRC). https://doi.org/10.2905/42E8BE89-54FF-464E-BE7B-BF9E64DA5218

Schoppa, L., Sieg, T., Vogel, K., Zöller, G., Kreibich, H., 2020. Probabilistic Flood Loss Models for Companies. Water Resour. Res. 56, e2020WR027649. https://doi.org/10.1029/2020WR027649

Schutte, S., Vestby, J., Carling, J., Buhaug, H., 2021. Climatic conditions are weak predictors of asylum migration. Nat. Commun. 12, 2067. https://doi.org/10.1038/s41467-021-22255-4

Scussolini, P., Aerts, J.C.J.H., Jongman, B., Bouwer, L.M., Winsemius, H.C., de Moel, H., Ward, P.J., 2016. FLOPROS: an evolving global database of flood protection standards. Nat. Hazards Earth Syst. Sci. 16, 1049–1061. https://doi.org/10.5194/nhess-16-1049-2016

Sedova, B., Kalkuhl, M., 2020. Who are the climate migrants and where do they go? Evidence from rural India. World Dev. 129, 104848. https://doi.org/10.1016/j.worlddev.2019.104848

Seneviratne, S.I., Nicholls, N., Easterling, D., Goodess, C.M., Kanae, S., Kossin, J., Luo, Y., Marengo, J., McInnes, K., Rahimi, M., Reichstein, M., Sorteberg, A., Vera, C., Zhang, X., Rusticucci, M., Semenov, V., Alexander, L.V., Allen, S., Benito, G., Cavazos, T., Clague, J., Conway, D., Della-Marta, P.M., Gerber, M., Gong, S., Goswami, B.N., Hemer, M., Huggel, C., van den Hurk, B., Kharin, V.V., Kitoh, A., Tank, A.M.G.K., Li, G., Mason, S., McGuire, W., van Oldenborgh, G.J., Orlowsky, B., Smith, S., Thiaw, W., Velegrakis, A., Yiou, P., Zhang, T., Zhou, T., Zwiers, F.W., 2012. Changes in Climate Extremes and their Impacts on the Natural Physical Environment, in: Field, C.B., Dahe, Q., Stocker, T.F., Barros, V. (Eds.), Managing the Risks of Extreme Events and Disasters to Advance Climate Change Adaptation: Special Report of the Intergovernmental Panel on Climate Change. Cambridge University Press, Cambridge, pp. 109–230. https://doi.org/10.1017/CBO9781139177245.006

Seneviratne, S.I., Zhang, X., Adnan, M., Badi, W., Dereczynski, C., Di Luca, A., Ghosh, S., Iskandar, I., Kossin, J., Lewis, S., Otto, F., Pinto, I., Satoh, M., Vicente-Serrano, S.M., Wehner, M., Zhou, B., 2021. Weather and Climate Extreme Events in a Changing Climate. In Climate Change 2021: The Physical Science Basis. Contribution of Working Group I to the Sixth Assessment Report of the Intergovernmental Panel on Climate Change[Masson-Delmotte, V., P. Zhai, A. Pirani, S.L. Connors, C. Péan, S. Berger, N. Caud, Y. Chen, L. Goldfarb, M.I. Gomis, M. Huang, K. Leitzell, E. Lonnoy, J.B.R. Matthews, T.K. Maycock, T. Waterfield, O. Yelekçi, R. Yu, and B. Zhou (eds.)]. Cambridge University Press, Cambridge, United Kingdom and New York, NY, USA. pp. 1513–1766.

Sharma, A., Wasko, C., Lettenmaier, D.P., 2018. If Precipitation Extremes Are Increasing, Why Aren't Floods? Water Resour. Res. 54, 8545–8551. https://doi.org/10.1029/2018WR023749

Sheffield, J., Goteti, G., Wood, E.F., 2006. Development of a 50-Year High-Resolution Global Dataset of Meteorological Forcings for Land Surface Modeling. J. Clim. 19, 3088–3111. https://doi.org/10.1175/JCLI3790.1

Shepherd, T.G., 2016. A Common Framework for Approaches to Extreme Event Attribution. Curr. Clim. Change Rep. 2, 28–38. https://doi.org/10.1007/s40641-016-0033-y

Shepherd, T.G., Boyd, E., Calel, R.A., Chapman, S.C., Dessai, S., Dima-West, I.M., Fowler, H.J., James, R., Maraun, D., Martius, O., Senior, C.A., Sobel, A.H., Stainforth, D.A., Tett, S.F.B., Trenberth, K.E., van den Hurk, B.J.J.M., Watkins, N.W., Wilby, R.L., Zenghelis, D.A., 2018. Storylines: an alternative approach to representing uncertainty

in physical aspects of climate change. Clim. Change 151, 555–571. https://doi.org/10.1007/s10584-018-2317-9
Sieg, T., Vogel, K., Merz, B., Kreibich, H., 2017. Tree-based flood damage modeling of companies: Damage processes and model performance. Water Resour. Res. 53, 6050–6068. https://doi.org/10.1002/2017WR020784
Siegrist, M., Gutscher, H., 2008. Natural Hazards and Motivation for Mitigation Behavior: People Cannot Predict the Affect Evoked by a Severe Flood. Risk Anal. 28, 771–778. https://doi.org/10.1111/j.1539-6924.2008.01049.x
Sitch, S., Smith, B., Prentice, I.C., Arneth, A., Bondeau, A., Cramer, W., Kaplan, J.O., Levis, S., Lucht, W., Sykes, M.T., Thonicke, K., Venevsky, S., 2003. Evaluation of ecosystem dynamics, plant geography and terrestrial carbon cycling in the LPJ dynamic global vegetation model. Glob. Change Biol. 9, 161–185. https://doi.org/10.1046/j.1365-2486.2003.00569.x
Smith, A., Bates, P.D., Wing, O., Sampson, C., Quinn, N., Neal, J., 2019. New estimates of flood exposure in developing countries using high-resolution population data. Nat. Commun. 10, 1814. https://doi.org/10.1038/s41467-019-09282-y
Stacke, T., Hagemann, S., 2012. Development and evaluation of a global dynamical wetlands extent scheme. Hydrol. Earth Syst. Sci. 16, 2915–2933. https://doi.org/10.5194/hess-16-2915-2012
Stephens, E., Schumann, G., Bates, P., 2014. Problems with binary pattern measures for flood model evaluation. Hydrol. Process. 28, 4928–4937. https://doi.org/10.1002/hyp.9979
Strauss, B.H., Orton, P.M., Bittermann, K., Buchanan, M.K., Gilford, D.M., Kopp, R.E., Kulp, S., Massey, C., Moel, H. de, Vinogradov, S., 2021. Economic damages from Hurricane Sandy attributable to sea level rise caused by anthropogenic climate change. Nat. Commun. 12, 2720. https://doi.org/10.1038/s41467-021-22838-1
Stuart-Smith, R.F., Otto, F.E.L., Saad, A.I., Lisi, G., Minnerop, P., Lauta, K.C., van Zwieten, K., Wetzer, T., 2021. Filling the evidentiary gap in climate litigation. Nat. Clim. Change 11, 651–655. https://doi.org/10.1038/s41558-021-01086-7
Sun, Q., Zhang, X., Zwiers, F., Westra, S., Alexander, L.V., 2021. A Global, Continental, and Regional Analysis of Changes in Extreme Precipitation. J. Clim. 34, 243–258. https://doi.org/10.1175/JCLI-D-19-0892.1
Swain, D.L., Wing, O.E.J., Bates, P.D., Done, J.M., Johnson, K.A., Cameron, D.R., 2020. Increased Flood Exposure Due to Climate Change and Population Growth in the United States. Earths Future 8, e2020EF001778. https://doi.org/10.1029/2020EF001778
Takayabu, I., Hibino, K., Sasaki, H., Shiogama, H., Mori, N., Shibutani, Y., Takemi, T., 2015. Climate change effects on the worst-case storm surge: a case study of Typhoon Haiyan. Environ. Res. Lett. 10, 064011. https://doi.org/10.1088/1748-9326/10/6/064011
Tang, Q., Oki, T., Kanae, S., Hu, H., 2007. The influence of precipitation variability and partial irrigation within grid cells on a hydrological simulation. J. Hydrometeorol. 8, 499–512. https://doi.org/10.1175/JHM589.1
Tanoue, M., Hirabayashi, Y., Ikeuchi, H., 2016. Global-scale river flood vulnerability in the last 50 years. Sci. Rep. 6. https://doi.org/10.1038/srep36021
Tellman, B., Sullivan, J.A., Kuhn, C., Kettner, A.J., Doyle, C.S., Brakenridge, G.R., Erickson, T.A., Slayback, D.A., 2021. Satellite imaging reveals increased proportion of population exposed to floods. Nature 596, 80–86. https://doi.org/10.1038/s41586-021-03695-w
Thalheimer, L., Heinrich, D., Haustein, K., Singh, R., 2022. Integrating a Disaster Displacement Dimension in Climate Change Attribution. Meteorology 1, 468–476. https://doi.org/10.3390/meteorology1040029
Thalheimer, L., Otto, F., Abele, S., 2021a. Deciphering Impacts and Human Responses to a Changing Climate in East Africa. Front. Clim. 3.

Thalheimer, L., Williams, D.S., van der Geest, K., Otto, F.E.L., 2021b. Advancing the Evidence Base of Future Warming Impacts on Human Mobility in African Drylands. Earths Future 9, e2020EF001958. https://doi.org/10.1029/2020EF001958

The Nansen Initiative, 2015. Agenda for the protection of cross-border displaced persons in the context of disaster and climate change. Volume 1. Platform on disaster displacement.

The World Bank, 2022. World Development Indicators. Population, total - Mozambique.

Titley, D., Gabriele Hegerl, K Jacobs, P. W. Mote, C. J. Paciorek, J. M. Shepherd, T. G. Shepherd, A. H. Sobel, J. Walsh, F. W. Zwiers, 2016. Attribution of Extreme Weather Events in the Context of Climate Change, National Academies of Sciences, Engineering, and Medicine. Washington, DC: The National Academies Press.

Tozer, B., Sandwell, D.T., Smith, W.H.F., Olson, C., Beale, J.R., Wessel, P., 2019. Global Bathymetry and Topography at 15 Arc Sec: SRTM15+. Earth Space Sci. 6, 1847–1864. https://doi.org/10.1029/2019EA000658

Traore, A.K., Ciais, P., Vuichard, N., Poulter, B., Viovy, N., Guimberteau, M., Jung, M., Myneni, R., Fisher, J.B., 2014. Evaluation of the ORCHIDEE ecosystem model over Africa against 25 years of satellite-based water and carbon measurements. J. Geophys. Res. Biogeosciences 119, 1554–1575. https://doi.org/10.1002/2014JG002638

Trenberth, K.E., Fasullo, J.T., Shepherd, T.G., 2015. Attribution of climate extreme events. Nat. Clim. Change 5, 725–730. https://doi.org/10.1038/nclimate2657

Trigg, M.A., Birch, C.E., Neal, J.C., Bates, P.D., Smith, A., Sampson, C.C., Yamazaki, D., Hirabayashi, Y., Pappenberger, F., Dutra, E., Ward, P.J., Winsemius, H.C., Salamon, P., Dottori, F., Rudari, R., Kappes, M.S., Simpson, A.L., Hadzilacos, G., Fewtrell, T.J., 2016. The credibility challenge for global fluvial flood risk analysis. Environ. Res. Lett. 11, 094014. https://doi.org/10.1088/1748-9326/11/9/094014

Trisos, C.H., Adelekan, I.O., Totin, E., Ayanlade, A., Efitre, J., Gemeda, A., Kalaba, K., Lennard, C., Masao, C., Mgaya, Y., Ngaruiya, G., Olago, D., Simpson, N.P., Zakieldeen, S., 2022. Chapter 9: Africa. In: Climate Change 2022: Impacts, Adaptation and Vulnerability. Contribution of Working Group II to the Sixth Assessment Report of the Intergovernmental Panel on Climate Change [H.-O. Pörtner, D.C. Roberts, M. Tignor, E.S. Poloczanska, K. Mintenbeck, A. Alegría, M. Craig, S. Langsdorf, S. Löschke, V. Möller, A. Okem, B. Rama (eds.)]. Cambridge University Press, Cambridge, UK and New York, NY, USA, pp. 1285–1455, doi:10.1017/9781009325844.011.

UK Government Office for Science, 2011. Foresight: Migration and Global Environmental Change (2011). Final Project Report [WWW Document]. GOV.UK. URL https://www.gov.uk/government/publications/migration-and-global-environmental-change-future-challenges-and-opportunities (accessed 1.4.23).

UN Habitat, 2010. State of the World's Cities 2010/2011.

UN, 1951. Convention relating to the status of refugees. U. N. Treaty Ser. Geneva 189, 137.

UN, 2022. The secretary-general's action agenda on internal displacement. Quote by António Guterres.

United Nations Office for Disaster Risk Reduction, 2015. Sendai framework for disaster risk reduction 2015–2030.

van Oldenborgh, G.J., van der Wiel, K., Kew, S., Philip, S., Otto, F., Vautard, R., King, A., Lott, F., Arrighi, J., Singh, R., van Aalst, M., 2021. Pathways and pitfalls in extreme event attribution. Clim. Change 166, 13. https://doi.org/10.1007/s10584-021-03071-7

Vogel, E., Donat, M.G., Alexander, L.V., Meinshausen, M., Ray, D.K., Karoly, D., Meinshausen, N., Frieler, K., 2019. The effects of climate extremes on global agricultural yields. Environ. Res. Lett. 14, 054010. https://doi.org/10.1088/1748-9326/ab154b

Vogt, T., Treu, S., Mengel, M., Frieler, K., Otto, C., 2022. Assessing the scope and limitations of a fully-open global TC surge model. Manuscript in preparation.

Wada, Y., Wisser, D., Bierkens, M.F.P., 2014. Global modeling of withdrawal, allocation and consumptive use of surface water and groundwater resources. Earth Syst. Dyn. 5, 15–40. https://doi.org/10.5194/esd-5-15-2014

Wagenaar, D., de Jong, J., Bouwer, L.M., 2017. Multi-variable flood damage modelling with limited data using supervised learning approaches. Nat. Hazards Earth Syst. Sci. 17, 1683–1696. https://doi.org/10.5194/nhess-17-1683-2017

Walsh, K.J.E., Camargo, S.J., Knutson, T.R., Kossin, J., Lee, T.-C., Murakami, H., Patricola, C., 2019. Tropical cyclones and climate change. Trop. Cyclone Res. Rev. 8, 240–250. https://doi.org/10.1016/j.tcrr.2020.01.004

Ward, P.J., Blauhut, V., Bloemendaal, N., Daniell, J.E., de Ruiter, M.C., Duncan, M.J., Emberson, R., Jenkins, S.F., Kirschbaum, D., Kunz, M., Mohr, S., Muis, S., Riddell, G.A., Schäfer, A., Stanley, T., Veldkamp, T.I.E., Winsemius, H.C., 2020. Review article: Natural hazard risk assessments at the global scale. Nat. Hazards Earth Syst. Sci. 20, 1069–1096. https://doi.org/10.5194/nhess-20-1069-2020

Ward, P.J., Jongman, B., Aerts, J.C.J.H., Bates, P.D., Botzen, W.J.W., Diaz Loaiza, A., Hallegatte, S., Kind, J.M., Kwadijk, J., Scussolini, P., Winsemius, H.C., 2017. A global framework for future costs and benefits of river-flood protection in urban areas. Nat. Clim. Change 7, 642–646. https://doi.org/10.1038/nclimate3350

Ward, P.J., Jongman, B., Salamon, P., Simpson, A., Bates, P., De Groeve, T., Muis, S., de Perez, E.C., Rudari, R., Trigg, M.A., Winsemius, H.C., 2015. Usefulness and limitations of global flood risk models. Nat. Clim. Change 5, 712–715. https://doi.org/10.1038/nclimate2742

Ward, P.J., Jongman, B., Weiland, F.S., Bouwman, A., van Beek, R., Bierkens, M.F.P., Ligtvoet, W., Winsemius, H.C., 2013. Assessing flood risk at the global scale: model setup, results, and sensitivity. Environ. Res. Lett. 8, 044019. https://doi.org/10.1088/1748-9326/8/4/044019

Warner, K., Hamza, M., Oliver-Smith, A., Renaud, F., Julca, A., 2010. Climate change, environmental degradation and migration. Nat. Hazards 55, 689–715. https://doi.org/10.1007/s11069-009-9419-7

Warren, M., 2019. Why Cyclone Idai is one of the Southern Hemisphere's most devastating storms. Nature. https://doi.org/10.1038/d41586-019-00981-6

WDI, 2022. World Development Indicators 2022 (World Bank) [WWW Document]. URL (accessed 2.22.22).

Webster, P.J., Holland, G.J., Curry, J.A., Chang, H.-R., 2005. Changes in Tropical Cyclone Number, Duration, and Intensity in a Warming Environment. Science 309, 1844–1846. https://doi.org/10.1126/science.1116448

Weedon, G.P., Balsamo, G., Bellouin, N., Gomes, S., Best, M.J., Viterbo, P., 2014. The WFDEI meteorological forcing data set: WATCH Forcing Data methodology applied to ERA-Interim reanalysis data. Water Resour. Res. 50, 7505–7514. https://doi.org/10.1002/2014WR015638

Weedon, G.P., Gomes, S., Viterbo, P., Shuttleworth, W.J., Blyth, E., Österle, H., Adam, J.C., Bellouin, N., Boucher, O., Best, M., 2011. Creation of the WATCH Forcing Data and Its Use to Assess Global and Regional Reference Crop Evaporation over Land during the Twentieth Century. J. Hydrometeorol. 12, 823–848. https://doi.org/10.1175/2011JHM1369.1

Werner, M.G.F., Hunter, N.M., Bates, P.D., 2005. Identifiability of distributed floodplain roughness values in flood extent estimation. J. Hydrol. 314, 139–157. https://doi.org/10.1016/j.jhydrol.2005.03.012

Wessel, P., Smith, W., 1996. A global, self-consistent, hierarchical, high-resolution shoreline database. J. Geophys. Res. 101, 8741–8743. https://doi.org/10.1029/96JB00104

Willner, S.N., Levermann, A., Zhao, F., Frieler, K., 2018a. Adaptation required to preserve future high-end river flood risk at present levels. Sci. Adv. 4, eaao1914. https://doi.org/10.1126/sciadv.aao1914

Willner, Sven Norman, Otto, C., Levermann, A., 2018b. Global economic response to river floods. Nat. Clim. Change 8, 594–598. https://doi.org/10.1038/s41558-018-0173-2
Wing, O.E.J., Lehman, W., Bates, P.D., Sampson, C.C., Quinn, N., Smith, A.M., Neal, J.C., Porter, J.R., Kousky, C., 2022. Inequitable patterns of US flood risk in the Anthropocene. Nat. Clim. Change 12, 156–162. https://doi.org/10.1038/s41558-021-01265-6
Winsemius, H.C., Aerts, J.C.J.H., van Beek, L.P.H., Bierkens, M.F.P., Bouwman, A., Jongman, B., Kwadijk, J.C.J., Ligtvoet, W., Lucas, P.L., van Vuuren, D.P., Ward, P.J., 2016. Global drivers of future river flood risk. Nat. Clim. Change 6, 381–385. https://doi.org/10.1038/nclimate2893
Winsemius, H.C., Jongman, B., Veldkamp, T.I.E., Hallegatte, S., Bangalore, M., Ward, P.J., 2018. Disaster risk, climate change, and poverty: assessing the global exposure of poor people to floods and droughts. Environ. Dev. Econ. 23, 328–348. https://doi.org/10.1017/S1355770X17000444
Woodruff, J.D., Irish, J.L., Camargo, S.J., 2013. Coastal flooding by tropical cyclones and sea-level rise. Nature 504, 44–52. https://doi.org/10.1038/nature12855
World Meteorological Organization, 2009. Integrated Flood Management Concept Paper.
Wulder, M.A., White, J.C., Loveland, T.R., Woodcock, C.E., Belward, A.S., Cohen, W.B., Fosnight, E.A., Shaw, J., Masek, J.G., Roy, D.P., 2016. The global Landsat archive: Status, consolidation, and direction. Remote Sens. Environ. 185, 271–283.
Yamazaki, D., Ikeshima, D., Sosa, J., Bates, P.D., Allen, G.H., Pavelsky, T.M., 2019. MERIT Hydro: A High-Resolution Global Hydrography Map Based on Latest Topography Dataset. Water Resour. Res. 55, 5053–5073. https://doi.org/10.1029/2019WR024873
Yamazaki, D., Kanae, S., Kim, H., Oki, T., 2011. A physically based description of floodplain inundation dynamics in a global river routing model: FLOODPLAIN INUNDATION DYNAMICS. Water Resour. Res. 47. https://doi.org/10.1029/2010WR009726
Yamazaki, D., Oki, T., Kanae, S., 2009. Deriving a global river network map and its sub-grid topographic characteristics from a fine-resolution flow direction map. Hydrol. Earth Syst. Sci. 13, 2241–2251. https://doi.org/10.5194/hess-13-2241-2009
Yamazaki, D., Sato, T., Kanae, S., Hirabayashi, Y., Bates, P.D., 2014. Regional flood dynamics in a bifurcating mega delta simulated in a global river model: SIMULATION OF RIVER MEGA DELTA FLOWS. Geophys. Res. Lett. 41, 3127–3135. https://doi.org/10.1002/2014GL059744
Ye, H., Fetzer, E.J., Wong, S., Lambrigtsen, B.H., 2017. Rapid decadal convective precipitation increase over Eurasia during the last three decades of the 20th century. Sci. Adv. 3, e1600944. https://doi.org/10.1126/sciadv.1600944
Zaherpour, J., Gosling, S.N., Mount, N., Schmied, H.M., Veldkamp, T.I.E., Dankers, R., Eisner, S., Gerten, D., Gudmundsson, L., Haddeland, I., Hanasaki, N., Kim, H., Leng, G., Liu, J., Masaki, Y., Oki, T., Pokhrel, Y., Satoh, Y., Schewe, J., Wada, Y., 2018. Worldwide evaluation of mean and extreme runoff from six global-scale hydrological models that account for human impacts. Environ. Res. Lett. 13, 65015–65015. https://doi.org/10.1088/1748-9326/aac547
Zhao, F., Veldkamp, T.I.E., Frieler, K., Schewe, J., Ostberg, S., Willner, S., Schauberger, B., Gosling, S.N., Schmied, H.M., Portmann, F.T., Leng, G., Huang, M., Liu, X., Tang, Q., Hanasaki, N., Biemans, H., Gerten, D., Satoh, Y., Pokhrel, Y., Stacke, T., Ciais, P., Chang, J., Ducharne, A., Guimberteau, M., Wada, Y., Kim, H., Yamazaki, D., 2017. The critical role of the routing scheme in simulating peak river discharge in global hydrological models. Environ. Res. Lett. 12, 075003. https://doi.org/10.1088/1748-9326/aa7250
Zhou, X., Ma, W., Echizenya, W., Yamazaki, D., 2021. The uncertainty of flood frequency analyses in hydrodynamic model simulations. Nat. Hazards Earth Syst. Sci. 21, 1071–1085. https://doi.org/10.5194/nhess-21-1071-2021
Zscheischler, J., Martius, O., Westra, S., Bevacqua, E., Raymond, C., Horton, R.M., van den Hurk, B., AghaKouchak, A., Jézéquel, A., Mahecha, M.D., Maraun, D., Ramos, A.M.,

Ridder, N.N., Thiery, W., Vignotto, E., 2020. A typology of compound weather and climate events. Nat. Rev. Earth Environ. 1, 333–347. https://doi.org/10.1038/s43017-020-0060-z

Appendix

Supplementary Material for Chapter 4 - A global-scale vulnerability assessment of flood-induced human displacement

List of Figures:

List of Tables:

1 Number of displacement events in sample

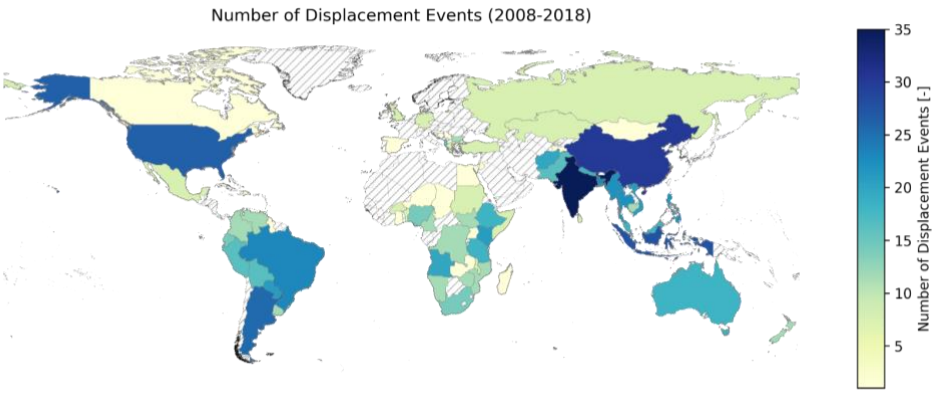

Figure S 1: Number of displacement events in sample

2 Correlation matrix and statistics

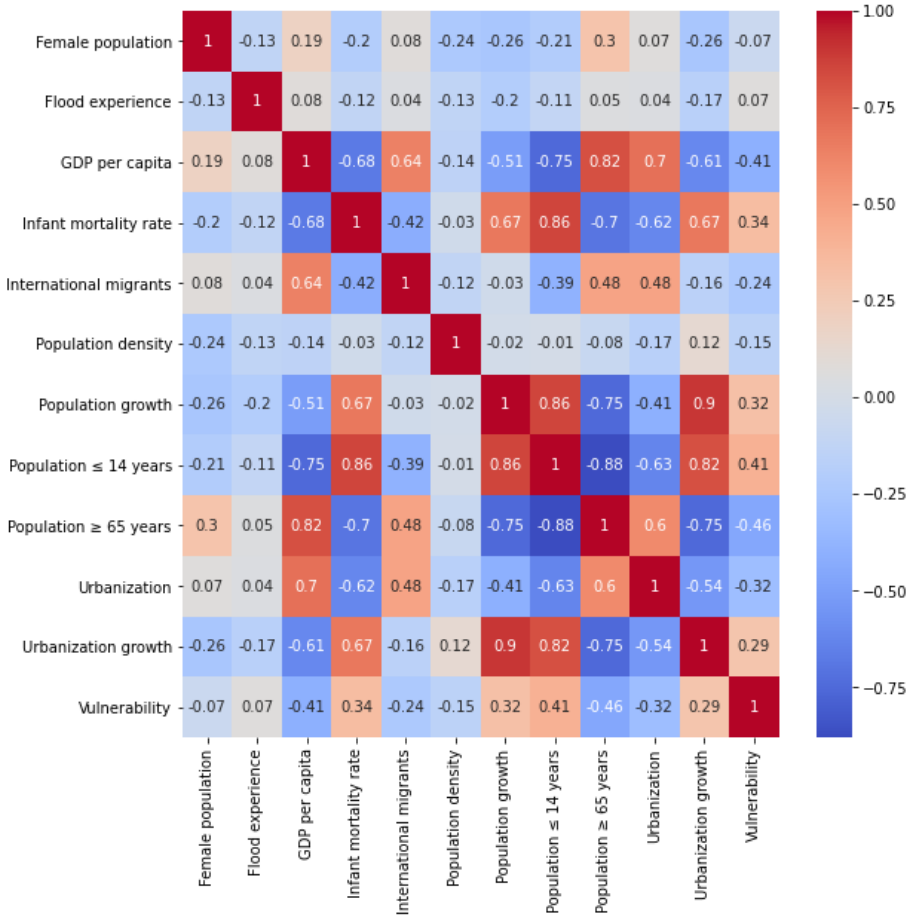

Figure S 2: Pearson correlation matrix of the predictors of the country-level data.

Table S 1: Pearson p-values and spearman p-values of country-level predictors for displacement vulnerability

predictor	pearson p-value	spearman p-value
Population density	0.201742	0.260986
GDP per capita	0.000406	0.000007
International migrants	0.042026	0.056390
Infant mortality rate	0.003044	0.000012
Population ≤ 14 years	0.000290	0.000005
Population ≥ 65 years	0.000054	0.000016
Female population	0.556897	0.125233
Population growth	0.005363	0.000687
Urbanization	0.005893	0.000211
Urbanization growth	0.014054	0.002194
Flood experience	0.551629	0.936218

Only up to one of the following predictors per list may be present in a country-level analysis:

list 1 = Infant mortality rate, Population ≤ 14 years, 'Population ≥ 65 years, Population growth

list 2 = Population growth, Urbanization growth

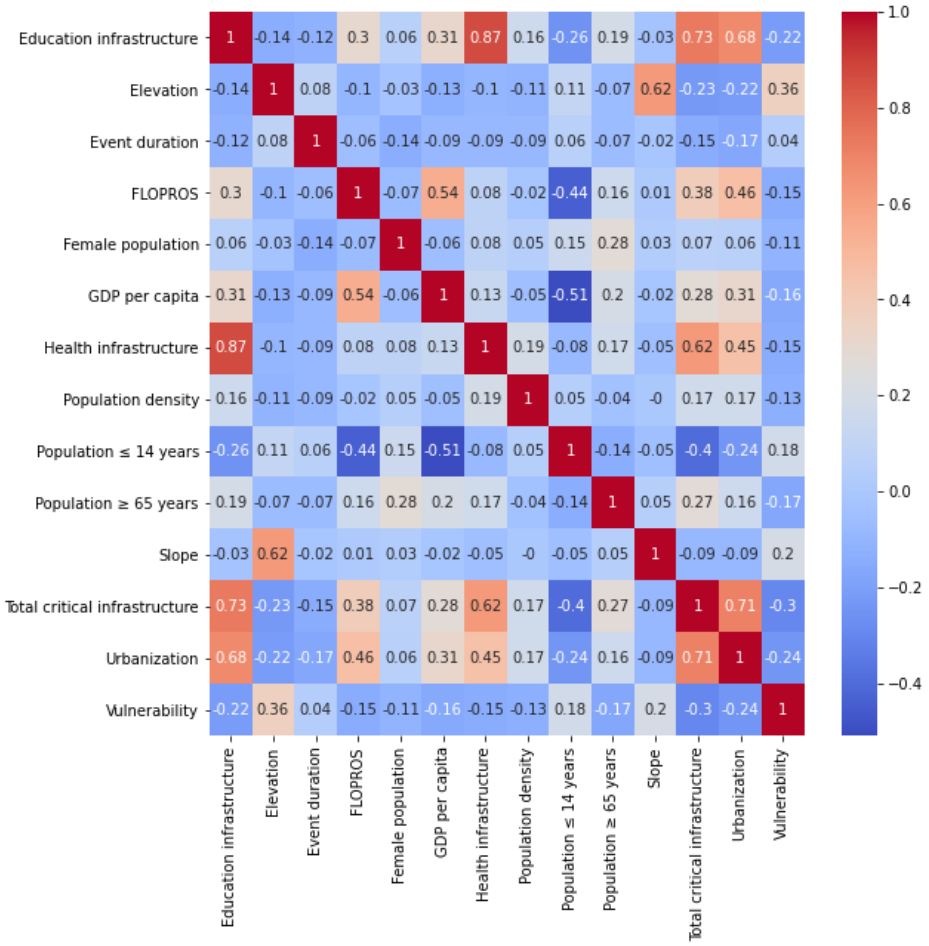

Figure S 3: Correlation matrix of the predictors of the event-level data.

Table S 2: Pearson p-values and spearman p-values of event-level predictors for displacement vulnerability

predictor	pearson p-value	spearman p-value
Education infrastructure	1.122650e-04	4.368879e-10
Health infrastructure	7.954636e-03	9.099458e-10
Total critical infrastructure	8.172624e-08	1.420093e-12
Urbanization	2.262749e-05	2.681697e-11
Elevation	1.055991e-10	1.893061e-08
Slope	4.412139e-04	4.985626e-01
Female population	6.025987e-02	1.539471e-03
Population ≤ 14 years	1.330337e-03	6.786888e-05
Population ≥ 65 years	2.057918e-03	1.713942e-03
FLOPROS	8.958934e-03	1.085546e-04
GDP per capita	5.123365e-03	2.414305e-05
Population density	1.956995e-02	9.510912e-09
Event duration	4.772010e-01	4.968906e-01

Only up to one of the following predictors per list may be present in an event-level analysis:

list 1 = Education infrastructure, Health infrastructure

3 Global displacement vulnerability over time

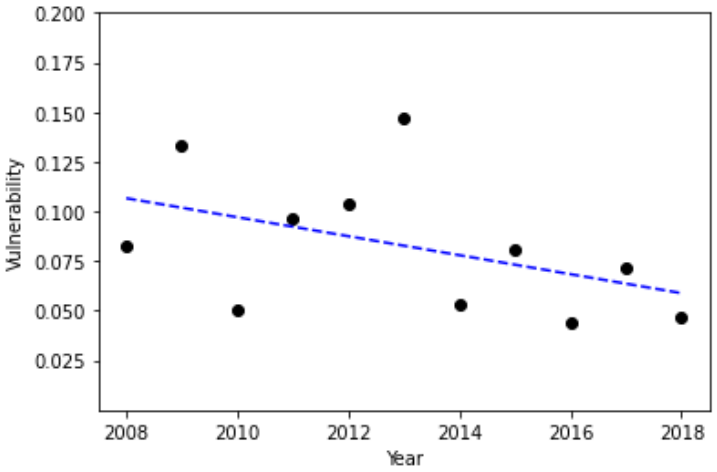

Figure S 4: Annual median of national median vulnerability to flood-induced displacement over time.

Mann-Kendall Trend Test:

trend= 'no trend'
h=False
p=0.16112494928905186
z=-1.4012980994907414
Tau=-0.34545454545454546
s=-19.0
var_s=165.0
slope=-0.004793508625701662
intercept=0.10517270667101386

4 Predictive power

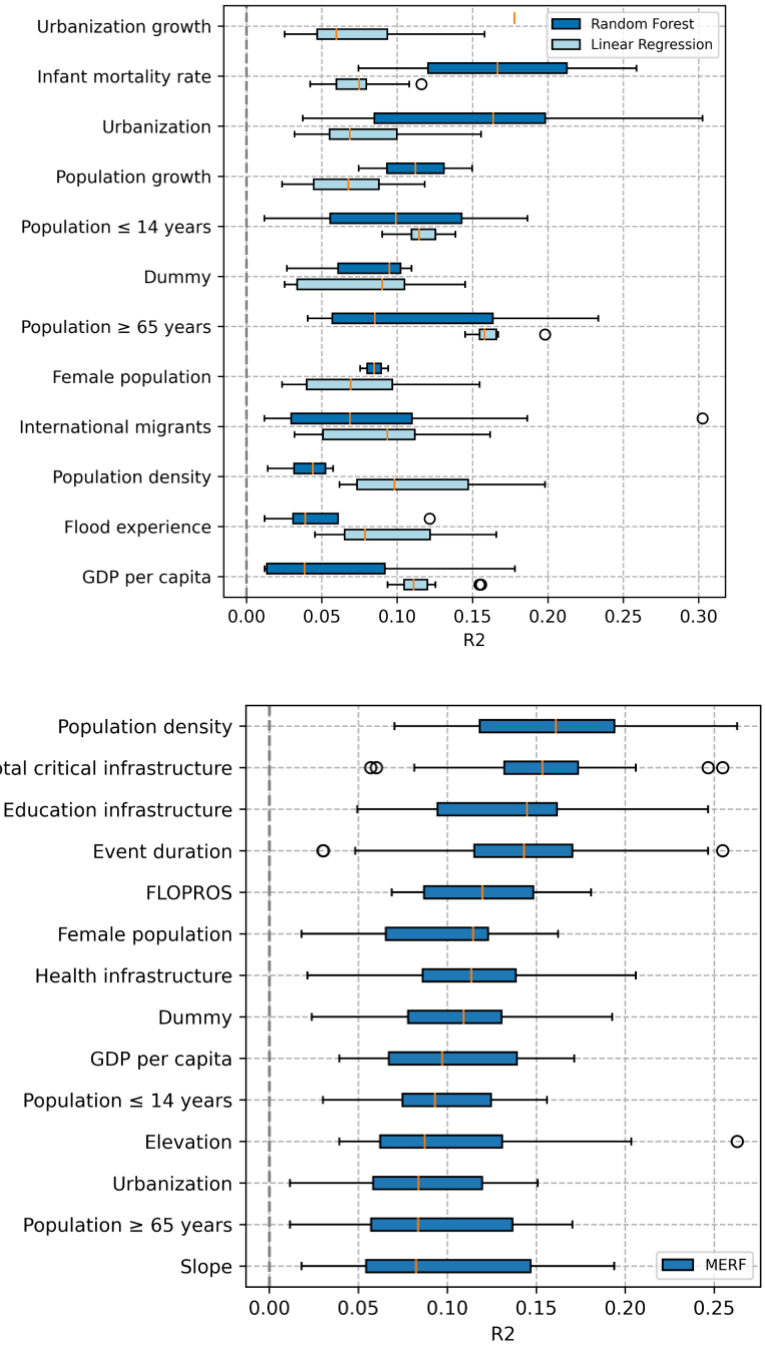

Figure S 5: Predictive power of vulnerability predictors of the country-level analysis (top) and the event-level analysis (bottom), ranked by R2s. Results relate to the test data using leave-one-out cross-validation. Each box plot represents all models using the predictor of interest; up to three predictors per model are chosen. Only models with R2s greater than 0.01 are displayed.

5 Partial dependence plots - event-level (non-log)

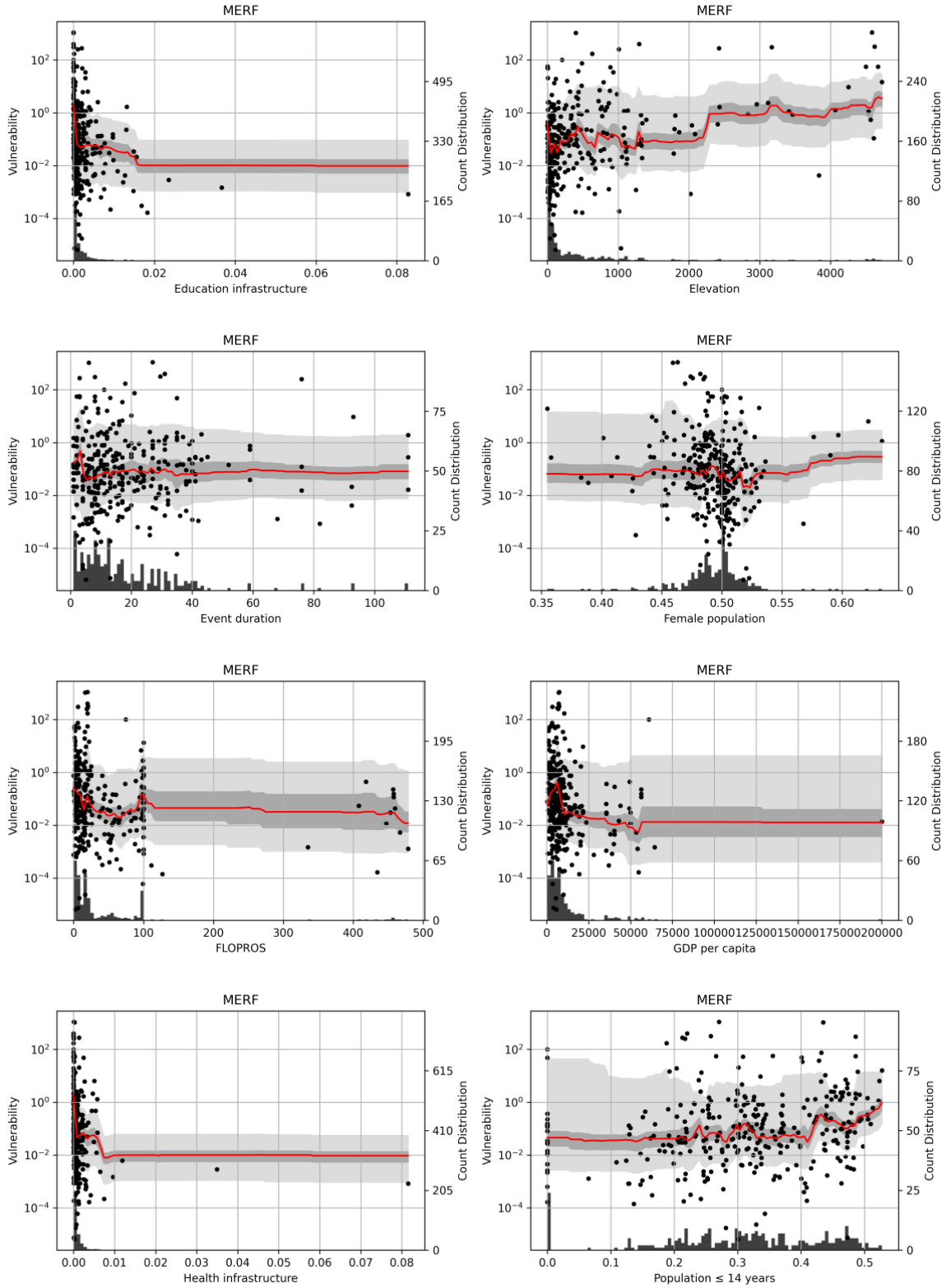

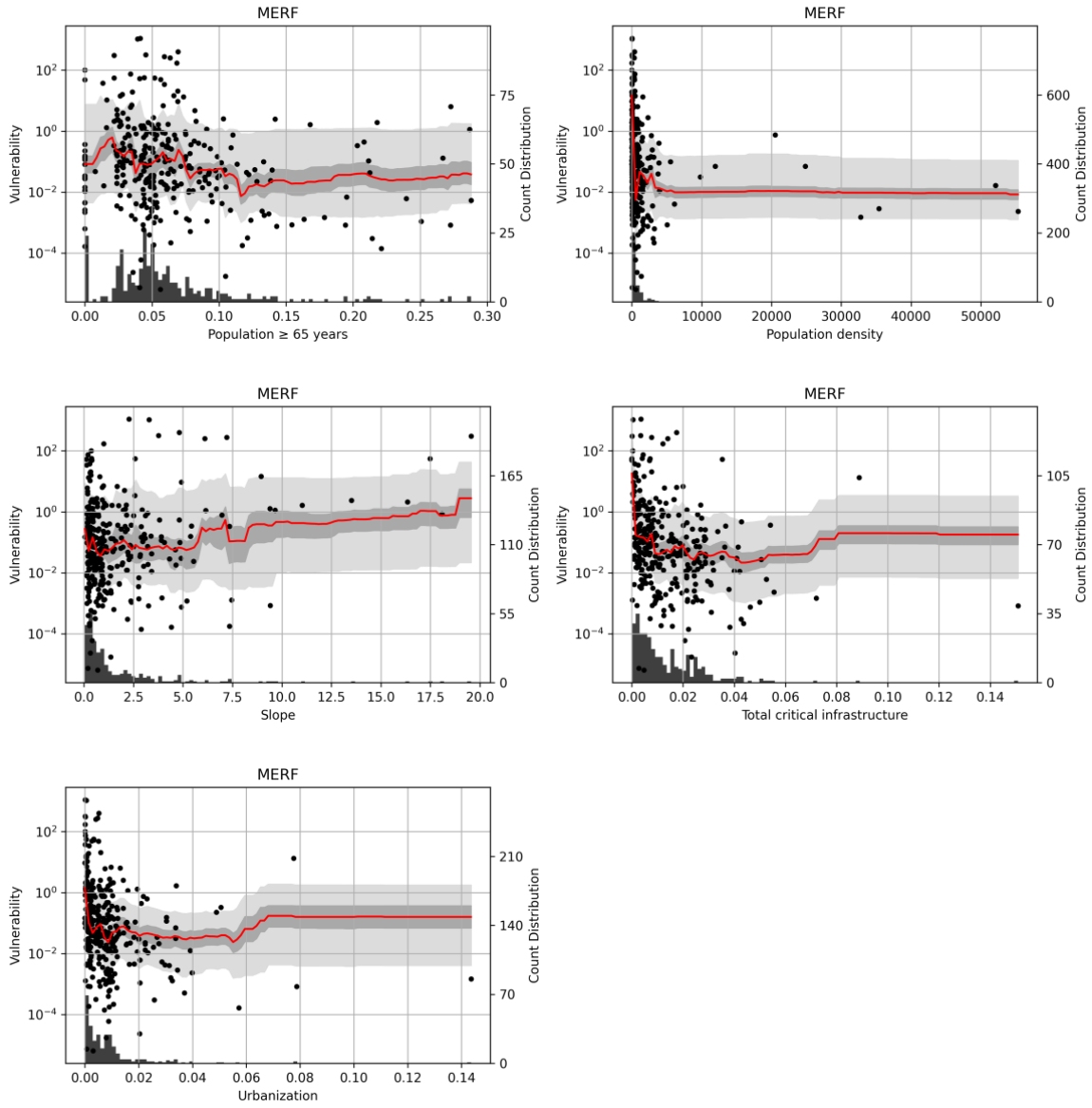

Figure S 6: PDPs of the MERF in non-log-scale. Each plot uses the best model involving the predictor of interest to compute the PDPs. The median vulnerability per predictor increment is indicated in red, uncertainty bands are displayed in light gray (5th/95th perc.) and dark gray (33th/66th perc.).